Multi-scale topography assessment for site-specific drought management in Sweden

Karl Knaebel

Independent project • 30 hp
Swedish University of Agricultural Sciences, SLU
Department of Soil and Environment
Soil, Water and Environment - Master's Programme
Skara 2021

Multi-scale topography assessment for site-specific drought management in Sweden

Karl Knaebel

Supervisor: Omran Alshihabi, Swedish University of Agricultural Sciences (SLU), Department of Soil and Environment
Assistant supervisor: Kristin Piikki, SLU, Department of Soil and Environment
Examiner: Johanna Wetterlind, SLU, Department of Soil and Environment

Credits: 30 hp
Level: Second cycle, A2E
Course title: Master thesis in Environmental science
Course code: EX0897
Programme/education: Soil, Water and Environment – Master´s Programme
Course coordinating dept: Department of Soil and Environment

Place of publication: Skara
Year of publication: 2021
Cover picture:
Title of series: Examensarbeten / Institutionen för mark och miljö SLU, (11656023)
Part number: 2021:14
ISSN:

Keywords: drought, topography, precision agriculture, Sentinel-2, DSS

Swedish University of Agricultural Sciences
Faculty of Natural Resources and Agricultural Sciences
Department of Soil and Environment

Publishing and archiving

Approved students' theses at SLU are published electronically. As a student, you have the copyright to your own work and need to approve the electronic publishing. If you check the box for **YES**, the full text (pdf file) and metadata will be visible and searchable online. If you check the box for **NO**, only the metadata and the abstract will be visible and searchable online. Nevertheless, when the document is uploaded it will still be archived as a digital file.

If you are more than one author you all need to agree on a decision. Read about SLU's publishing agreement here: https://www.slu.se/en/subweb/library/publish-and-analyse/register-and-publish/agreement-for-publishing/.

☒ YES, I/we hereby give permission to publish the present thesis in accordance with the SLU agreement regarding the transfer of the right to publish a work.

☐ NO, I/we do not give permission to publish the present work. The work will still be archived and its metadata and abstract will be visible and searchable.

Abstract

Globally, as well as in Sweden, the occurrence of droughts is expected to increase due to global warming. The drought summer of 2018 revealed the vulnerability of Sweden's agriculture – with cereal yield losses of up to 50 %. Subsequently, the development of more resilience crop production systems to mitigate future droughts is required. Precision agriculture practices (PAP), widely applied in Sweden, are promising to base such developments upon. Hence, the aim of this study was to investigate the potential usage of topography for site-specific decision support, to extend PAP for advanced drought management in Sweden. Therefore, the drought effect along the study period (between crop development stages DC31-DC75) on crop growth development and related to field topography was assessed in a dry year (2018) and compared to a non-dry year (2019). Two common cereals i.e., winter wheat and spring barely were selected to conduct this study. The study area was in the south-eastern region of Skåne in Sweden. The scale varied from the whole study area to within the field. Crop growth development was monitored using different vegetation and drought indices i.e., normalized difference vegetation index (NDVI), normalized difference red-edge index (NDRE), normalized difference water index (NDWI) and the normalized difference drought index (NDDI). Topography was analysed at and within the field using different topographic indices i.e., slope, relative height (RE) and the topographic wetness index (TWI). The data required to conduct this study was publicly available and consisted of a high-resolution digital elevation model, Sentinel-2 remote sensing data, weather data, field polygon as well as soil texture data.

Overall, the results clearly showed an average NDVI, NDRE and NDWI reduction over the study period in 2018 compared to 2019 for both cereals; this reduction was about 25 %, 32 % and 58 % for winter wheat and about 36 %, 43 % and 69 % for spring barley. Topographic related within-field crop growth variations were prominent under dry conditions in 2018 and not present under non-dry conditions in 2019. Within-field crop growth variation increased with an increase in average field slope under dry conditions. The TWI was the most promising index explaining within-field crop growth development. Further studies should include other site-specific field characteristics besides topography to better delineate within-field drought management zones for PAP.

Keywords: drought, topography, precision agriculture, Sentinel-2, DSS

Popular scientific summary

Title: Precision farming - a promising tool to better cope with droughts in the future?

What picture do you have in mind when you think about drought? I always think about this ancient story where no rain had fallen for several years. Where acres were bare, and food was scarce. If you just thought about one of these really hot summer days, that's also fine. However, if you live in Europe, you might remember the hot and dry summer of 2018. During that summer, massive yield losses with decreases of up to 50 % in cereals were observed in Sweden. At some places, farmers even needed to emergency slaughter their livestock since fodder was scarce. Although, the drought of 2018 was not directly noticeable for end-consumers in Swedish supermarkets, yet the economic impact for farmers was huge. One could now argue that droughts, as observed in 2018, are unlikely to occur every year and are just seldomly appearing extreme events - so why even bother? Researchers from around the globe elaborated, that extreme events, such as droughts, are more likely to occur in the future than they did in the past, due to global warming. Subsequently, new ways to better cope with droughts to counteract yield losses and to ensure food security in the future need to be developed. A promising concept to increase the overall farming efficiency is called precision agriculture. This form of agriculture intends to manage agricultural inputs, such as fertilizer, pesticides, or water site-specifically. In contrast, conventional farming methods homogenously manage these inputs in the field with constant input rates. Nevertheless, for precision agriculture to work, decision support systems providing information on optimal farming inputs at the field level are required. However, at the current state precision agriculture practices do not incorporate any decision support for advanced drought management in Sweden. Consequently, this study aimed to bridge this gap – elaborating ways on how to possibly use topographic data for advanced drought management. Several studies from around the world already investigated field topography in relation to yield variability under dry conditions. All these studies incorporated the basic idea that crop water stress and thus crop growth variability can potentially be linked to field topography. Predicting soil and crop water status by topography seems logical, if you think about the relation of water flow linked to earths gravitational field. However, for Sweden, no study of topography in relation to crop growth variability has been conducted yet. Therefore, in this study, non-drought (summer 2019) conditions were compared to drought conditions (summer 2018) by monitoring crop growth development of two common cereals cultivated in Sweden (i.e., winter wheat and spring barley) and in relation to field topography. Freely available data was used such as satellite remote as well as a high-resolution digital elevation model.

Overall, the results of this study showed an inhabited crop growth of winter wheat and spring barley during drought conditions in comparison to none-drought conditions. Winter wheat was less affected compared to spring barley – indicating a higher drought resilience of winter cultivars compared to spring cultivars. When speaking of topography linked to crop growth development, the results showed that topography is influential in explaining within-field crop growth variability. Within-field crop growth variations related to topography were only prominent under dry conditions in 2018 and not present under non-dry conditions in 2019. Overall, this study could show that topography is a major player in explaining within-field crop growth variability, especially under dry conditions. The results provided indications of topography potentially being useful in decision support systems for advanced drought management. Nevertheless, further research is needed to elaborate how to delineate within-field management zones in the best possible way to enable advanced within-field drought management.

Table of contents

List of tables

List of figures

Abbreviations

DC-Stage	Crop development Stage
DEM	Digital elevation model
DSMS	Digital soil map of Sweden
DSS(s)	Decision support system(s)
GeoTIFF	georeferenced TIFF file
LTA	Long-term 30-year average (1991 - 2020)
MoM	Mean of means
NDDI	Normalized difference drought index
NDRE	Normalized difference red-edge vegetation index
NDVI	Normalized difference vegetation index
NDWI	Normalized difference water index
PAP	Precision agriculture practices
RE	Relative height
RGB	Red-green-blue
SB	Spring barely
SLU	Swedish University of Agricultural Sciences
TWI	Topographic wetness index
WW	Winter wheat

1. Introduction

The frequency of droughts is expected to increase in the 21st century due to global warming (Cook et al. 2014). An increased drought probability in the upcoming decades is elaborated in IPCC's special report on global warming of 1.5 °C (IPCC 2018). In this context and linked to world population growth, global agriculture is pressured to ensure food security (Godfray et al. 2010; Wheeler & Braun 2013). At the same time the environmental impact of global food systems needs to be reduced, when considering earths planetary boundaries (Rockström et al. 2009; Campbell et al. 2017; Meier 2017). Hence, today's and tomorrow's agricultural systems are required to transform towards more resilient and resource efficient production systems, in order to adapt to present and future challenges (Howden et al. 2007; Lipper et al. 2014).

In 2018, Sweden was affected by an extremely warm summer (Sinclair et al. 2019; Wilcke et al. 2020). As mentioned by Wilcke et al. (2020) the probability for the occurrence of such a hot and dry summer, has increased compared to the pre-industrial era (1861–1890), as a consequence of global warming. Furthermore, the summer of 2018 revealed the vulnerability of Swedish agricultural systems to drought. Overall, 90 % of agricultural production area is rainfed in Sweden (Grusson et al. 2021). Subsequently, cereal production decreased by up to 50 % in 2018 when compared to the average yield data from 2013-2017 (SCB 2019). Under the circumstances of global warming an increased frequency and drought severity coming along with an increase in evapotranspiration and changes of regional precipitation patterns are expected in the future (SMHI 2019). Consequently, the necessity for measures and tools enabling an advanced drought management is outlined.

Precision agriculture is a promising technology to incorporate such measures. It has the potential capability to manage agricultural inputs (for example: water, fertilizer, pesticide etc.) site-specifically, respecting local field characteristics. Principally, precision agriculture aims to enhance crop growth while reducing environmental impacts by increasing its resource use efficiency via the optimization of returns in comparison to inputs (Pierce & Nowak 1999; Gebbers & Adamchuk 2010; Santos Valle & Kienzle 2020). Nonetheless, to counteract yield gaps in response to

agricultural drought using precision agriculture practices (PAP), decision support systems (DSSs) are required. Such DSSs provide site-specific information at the field level.

High resolution digital elevation models (DEM) are a valuable resource to be included in DSSs for PAP. A number of benefits of DEMs such as decision support for seeding, fertilizing, usage of pesticide or water management are mentioned in a study by Sugarbaker & Carswell, Jr. (2016). Several studies have been conducted linking yield variability to topography at the field level considering dry and non-dry conditions. These studies provided evidence that within-field yield variations can potentially be explained by topography. Most of these studies utilized within field yield data, which were linked to different topographic indices. Marques da Silva & Silva (2008) stated the influence of field topography influencing average maize yield considering elevation and slope. Kaspar et al. (2003) outlined the possibility for an site-specific management based on a negative correlation between corn yield and relative height/slope in years with less than average precipitation and a positive correlation in years with higher than average precipitation, during growing season. Kumhálová et al. (2011) found a significant link between field topography and crop yield as well as crop nutrient concentration. In another study, they found that the leverage of topography on yield variability was very low in wet years, while it was elevated in dry years (Kumhálová et al. 2011; Kumhálová & Moudrý 2014). In turn, this indicated a stronger relation of topography and crop yield under warm and dry conditions. The fact of topography being more influential on yield in dry years in comparison to wet years was confirmed by Chi et al. (2009) in a study on winter wheat in Canada. Maestrini & Basso (2018) investigated the within-field temporal yield variability in relation to field topography utilizing the topographic wetness index (TWI). They analysed high-resolution yield monitor data of 338 fields in the Midwest - US. As a result, the authors identified three different zones in terms of yield stability: zones with low and stable yields (low TWI, relatively dry zones), zones with high and stable yields (mid-high TWI) and zones with unstable yields, waterlogged in wet years (high TWI – field depressions). In a study from Sweden by Delin & Berglund (2005), soil electric conductivity and field topography was used to divide a field into management zones more or less vulnerable to drought or water logging. Iqbal et al. (2005) found a reduced cotton lint yield in areas with higher elevation, suffering from stress more often.

Overall, the above-mentioned studies elaborated topography as a site-specific characteristic, being capable in explaining within-field yield variability, especially under dry conditions. Additionally, some of these studies suggested potential opportunities to implement topography as a site-specific characteristic in PAP.

However, only few research has been conducted investigating a relation of topography under dry conditions on crop growth in Sweden. Yet no study elaborated how high resolution DEMs that are commonly available, could potentially be used in PAP in Sweden. Consequently, this study aimed to bridge this gap in knowledge. Therefore, the influence of a very dry year (2018) in comparison to a non-dry year (2019) on crop growth was investigated. To evaluate whether and how topography could potentially be utilized, the drought effect on crop growth was related to topography. Two prominent cereals cultivated in Sweden i.e., winter wheat (*Triticum aestivum L.*) and spring barley (*Hordeum vulgare L.*) were selected to conduct this study. Instead of relating topography to cereal yields as most of the before mentioned studies, in this study the crop growth development was monitored using different vegetation and drought stress indices. Subsequently, the following vegetation indices were utilized in this study: the normalized difference vegetation index (NDVI), the normalized difference red-edge index (NDRE), the normalized difference water index (NDWI) and the normalized difference drought index (NDDI). With the outputs gained, implementation options for precision agriculture were suggested in the discussion part of this study.

1.1. Aim

The aim of this study was to investigate a possible relation between topography, as a site-specific characteristic and crop growth of two typical field crops (i.e., winter wheat and spring barley) under dry and non-dry conditions in Sweden.

The aim of this study was achieved by:

1. Selection of one dry and one non-dry year out of the years 2017 – 2020, in comparison to the long-term 30-year average (LTA) of precipitation and temperature.
2. Topography (using relative height, slope, and TWI indices) and soil texture assessment of all arable fields within the study area.
3. Multi-scale assessment of the spatiotemporal crop growth development using different vegetation and drought indices, from within- field to all fields.
4. Discussion of opportunities on implementing topography as site-specific for PAP under Swedish conditions.

2. Background

2.1. Crop development stages of cereals

This study refers to the internationally accepted scale describing crop development of cereals proposed by Zadoks et al. (1974). The scale is based on a two-digit code system. The first digit code (as described in Tab. 1 below) divides the cereal crop development into nine main development stages. The second digit as outlined in the original paper describes temporal crop development with a higher level of detail (Zadoks et al. 1974). This study mainly focused on the crop development stages DC31–DC75 (stem elongation, booting, inflorescence emergence, anthesis and milk development), being most applicable for satellite-based vegetation sensing. Between DC31 – 75, the cereal matures and starts to turn yellow. Before DC31 satellite-based vegetation sensing is difficult since the vegetation canopy is not dense enough to be remotely detected and after DC75 it is not meaningful since the cereal naturally dries and turns yellow.

Tab. 1 The nine main crop development stages of cereals and there corresponding first digit code copied from the original paper by Zadoks et al. (1974).

1-digit code	Description
0	Germination
1	Seedling growth
2	Tillering
3	**Stem elongation**
4	**Booting**
5	**Inflorescence emergence**
6	**Anthesis**
7	**Milk development**
8	Dough development
9	Ripening

2.2. Sentinel-2

Remote sensing is wildly used for agriculture purposes such as land use monitoring, vegetation sensing, crop yield forecasting or crop stress monitoring (Segarra et al. 2020; Weiss et al. 2020). The Sentinel-2 mission launched by the European Space Agency (ESA) in 2015 is a fundamental source of high quality and publicly available remote sensing data (ESA 2021c). Two polar-orbiting satellites (S2A & S2B) are phased by 180 ° to each other, leading to a temporal resolution of five days at the equator (ESA 2021c). The temporal resolution is even higher (up to two days) closer to the poles due to overlapping orbits. Both satellites are carrying sensors which are capable to detect 13 different spectral bands in various resolutions 10 – 60 m (Tab. 2). For this study, the following bands were used: B4 (nominal red) and B8 (broad band near infra-red) in 10 m resolution and B5 (red edge), B7 (red edge), B8A (narrow near infrared), B11 (short wave infrared) in 20 m resolution.

*Tab. 2 Sentinel-2 spectral bands in nm. *near infrared (NIR); **shortwave infrared (SWIR) (ESA 2021a).*

Band	Resolution (m)	S2A - λ (nm)	S2A – width (nm)	S2B - λ (nm)	S2B – width (nm)
Band 1–Coastal aerosol	60	442.7	21	442.3	21
Band 2–Blue	10	492.4	66	492.1	66
Band 3–Green	10	559.8	36	559.0	36
Band 4–Red	10	664.6	31	665.0	31
Band 5–Vegetation red edge	20	704.1	15	703.8	16
Band 6–Vegetation red edge	20	740.5	15	739.1	15
Band 7–Vegetation red edge	20	782.8	20	779.7	20
Band 8–NIR*	10	832.8	106	833.0	106
Band 8A–Narrow NIR*	20	864.7	21	864.0	22
Band 9–Water vapour	60	945.1	20	943.2	21
Band 10–SWIR–Cirrus	60	1373.5	31	1376.9	30
Band 11–SWIR**	20	1613.7	91	1610.4	94
Band 12–SWIR**	20	2202.4	175	2185.7	185

2.3. Vegetation indices

Three different vegetation indices were calculated based on the spectral bands provided by the Sentinel-2 mission in this study i.e., NDVI, NDRE and NDWI. Furthermore, based on NDVI and NDWI the NDDI was calculated.

NDVI

The NDVI vegetation index is ranging from -1 – 1 and is calculated using near infra-red light reflectance (NIR) and red visible light reflectance (nominal red) (Kriegler et al. 1969). The NDVI is derived based on the fact that healthy vegetation absorbs red light in the process of photosynthesis (chlorophyll absorbance) but reflects almost all NIR radiation (0.7 – 1.3 µm) due to the internal leaf structure of crops (scattering at mesophyll and epidermis cells) (Knipling 1970). Under stress conditions NIR reflectance and red light absorbance alter, due to changes in the individual leaf structure, as well as due to reduction of the total leaf area (Knipling 1970). Thus, NIR reflectance decreases relatively more than red light absorbance (Knipling 1970). Hence, high values of NDVI are found in dense and healthy vegetation, whereas values close to zero are representative for bare land or vegetation suffering from drought possibly. NDVI was calculated (Rouse et al. 1974) using Sentinal-2 bands B8 and B4 (eq. 1 below).

$$NDVI = \frac{NIR - Nominal\ Red}{NIR + Nominal\ Red} = \frac{B8 - B4}{B8 + B4}$$

[eq. 1]

NDWI

The NDWI vegetation index is complementary to the NDVI and was first proposed by Gao (1996). This index was suggested for remote sensing of liquid water in vegetation (Gao 1996). The index is calculated using NIR reflectance and short-wave infrared reflectance (SWIR) of vegetation. Absorption of NIR due to vegetation liquid water is negligible, whereas weak SWIR absorption due to the presence of the vegetation water content occurs (Gao 1996). Negative values of NDWI are expected to be found in water-stressed vegetation and positive values in vegetation with good water status (Gao 1996). In the literature two different formulas were identified to calculate NDWI using the spectral bands provided by the Setninel-2 mission. Djamai & Fernandes (2018) estimated the NDWI using bands B12 and B8A; Zhang et al. (2017) are using B11 and B8A. In this study, the formula presented by Zhang et al. (2017) was used since the wavelength of B11 (see Tab. 1) is closer to the original paper by Gao than B12 (eq. 2).

$$NDWI = \frac{NIR - SWIR}{NIR + SWIR} = \frac{B8A - B11}{B8A + B11}$$

[eq. 2]

NDRE

The normalised difference red-edge vegetation index is similar to the NDVI, but uses red-edge bands instead of nominal red (Sims & Gamon 2002). There are several calculation options available for this index when it is based on Sentinal-2 spectral bands. Wolters et al. (2021) used NDRE85 (bands 8 and 5) and NDRE86 (bands 8 and 6), see Tab. 2. However, in this study NDRE75 (bands 7 and 5) was used based on the research by Söderström et al. (2021). The research of Söderström et al. (2021) showed that NDRE75 can potentially be used as a key index to model within-field yield variability of winter wheat. Comparing NDVI and NDRE, the NDRE has a higher chlorophyl content sensitivity and tends to gets saturated later in the season (Li et al. 2014; Thilakarathna & Raizada 2018).

$$NDRE75 = \frac{B7 - B5}{B7 + B5}$$

[eq. 3]

NDDI

The NDDI is calculated based on NDVI and NDWI, being a more sensitive indicator for drought (Gu et al. 2007). High NDDI values represent drought conditions, while low values (close to zero) represents non-drought conditions (Du et al. 2018). The NDDI combines the properties of NDVI (detecting vegetation health and density) and NDWI (sensitive to vegetation liquid water content) (Du et al. 2018).

$$NDDI = \frac{NDVI - NDWI}{NDVI + NDWI}$$

[eq. 4]

2.4. Topography and water availability

Soil water-content can vary within the field based on topography, since water flow is related to earths gravitational field (Murphy et al. 2009). Subsequently, the soil-water flow direction is downhill under saturated conditions. In hydrology, topography is widely used to predict water-flow or soil-water availability within a catchment (Beven 2011). TOPMODEL, a rainfall-runoff model, predicts soil water content based on TWI (Quinn et al. 1995). Other examples on how topography is used in hydrology range from catchment delineation to flow accumulation models. Digitally, topographic information is mostly available as a DEM, representing the surface topography (USGS 2021). As mentioned in the introduction, within-field yield variability can be, to some extent, explained by within-field variation of topography especially in the dry years. Overall, explaining within-field crop growth variations by topography assumes that within-field water availability can be related to within-field topography. Hence, in the context of this study topography dares to reflect upon the soil-water availability within the field. Therefore, three different topographic indices i.e., relative elevation (RE), slope (in %) and TWI were selected and derived from a high-resolution DEM (as shown below) to investigate within-field crop growth variability.

Relative elevation:

RE was calculated at the field level, by subtracting the lowest pixel elevation-value from all other pixel elevation-values as proposed by Kaspar et al. (2003).

Slope:

Slope in % was calculated at the pixel level using the "Zevenbergen & Thorne formula" for smooth landscapes in GDAL (GDAL/OGR contributors 2021).

Topographic wetness index:

TWI maps were generated at the field level using the r.topidx feature in GRASS GIS 7.8.5 (GRASS Development Team 2020). The TWI was first introduced by Quinn et al. (1995) and was estimated at the pixel level as described by Mattivi et al. (2019) using eq. 6 below.

$$TWI = \ln\left(\frac{SCA}{tan\beta}\right)$$

[eq. 5]
SCA = pixel specific catchment area
tanβ = slope angle

The TWI assumes that water flow is regulated by topography, implying that soil moisture can spatially be predicted by TWI (Schmidt & Persson 2003).

Subsequently, high TWI values occur in flat – converging terrain, while low TWI values are found in steep – diverging areas (Schmidt & Persson 2003)

2.5. Statistics

The statistical analysis in this study was carried on using the boxplot analysis developed by Spear (1952). A boxplot is a way of visualization any given set of data by its quartiles. The second quartile (Q2 or median) divides a dataset into two groups which are equal in size. The first quartile (Q1) divides the data in two groups were all values below Q1 and above Q1 represent 25 % and 75 % of the total dataset, respectively. The third quartile (Q3) divides the data into two groups were all values above Q3 and below Q3 represent 25 % and 75 % of the total dataset, respectively. The range between Q1 – Q3 is called interquartile range and represents 50 % of the data (Fig. 1 below).

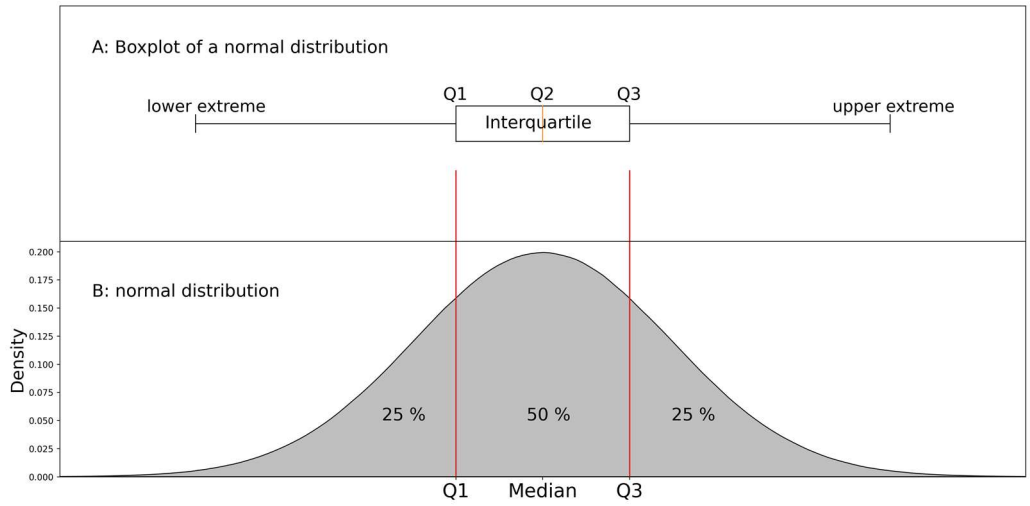

Fig. 1. A: Boxplot of the normal distribution shown in B without outliers. B: normal distribution with a standard deviation equal to one ($\mu = 1$).

3. Material and methods

This study consists of three main parts, as shown in Fig. 2. In the first part, the definition of the study boundaries (i.e., study area, crops, and timeframe) and the preparation of the required datasets were carried out. In the second part the main analysis was conducted (i.e., multi-scale assessment of crop growth in relation to drought and topography as well as to soil texture). In part three, the results were discussed to elaborate possible implementation options for in precision agriculture in Sweden.

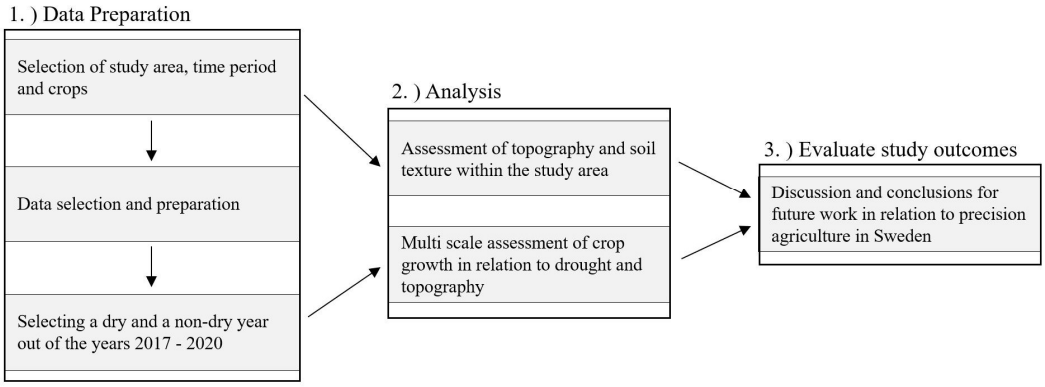

Fig. 2. Overview of the method of this study.

3.1. Study area and materials

3.1.1. Study area

The study area is located in Österlen in the very south-eastern part of Sweden in the province of Skåne (see Fig. 3). This area was chosen for several reasons: the intensive cultivation of cereals, the high topographical variation, and its high vulnerability to drought in the Swedish context. The area is enclosed within the following coordinates: 55°22'14.045" - 55°56'38.674" N; 13°48'55.222" - 14°21'39.703" E. The elevation ranges from sea level to 188 m in the study area.

The area size is about 1,246 km^2, of which 62 % (775 km^2) is arable land (Swedish Board of Agriculture 2018-2020).

Fig. 3. Study area enclosed in red boundaries (basemap: Wikimedia OSM).

3.1.2. Study period

The study period was chosen relevant to the crop development stages DC31–DC75. Hence, this period was ranging approximately from the end of April to the end of July for winter wheat and from the beginning of May to the beginning of July for spring barley. Two years i.e., 2018 and 2019 were selected, based on the drought feature analysis (section 3.3) out of the period 2017–2020, where Sentinel-2 data was available.

3.1.3. Crops

In Swedish agriculture, cereal production holds a dominant share, with around 40 % of all arable land utilized (Swedish Board of Agriculture 2009). In accordance with the Swedish Board of Agriculture about 44 % and 28 % of total cereal yield accounted for wheat and barley in 2007. Thus, two of the most grown cereals in Sweden i.e., winter wheat (WW) and spring barley (SB), were selected to conduct

this study. Photos representing the different growth stages of WW are shown in Fig. 4. Between 2018-2019 on average 18.2 % of all arable land within the study area was cultivated with WW, while on average 17.4 % was cultivated with SB (see Tab. 3 below).

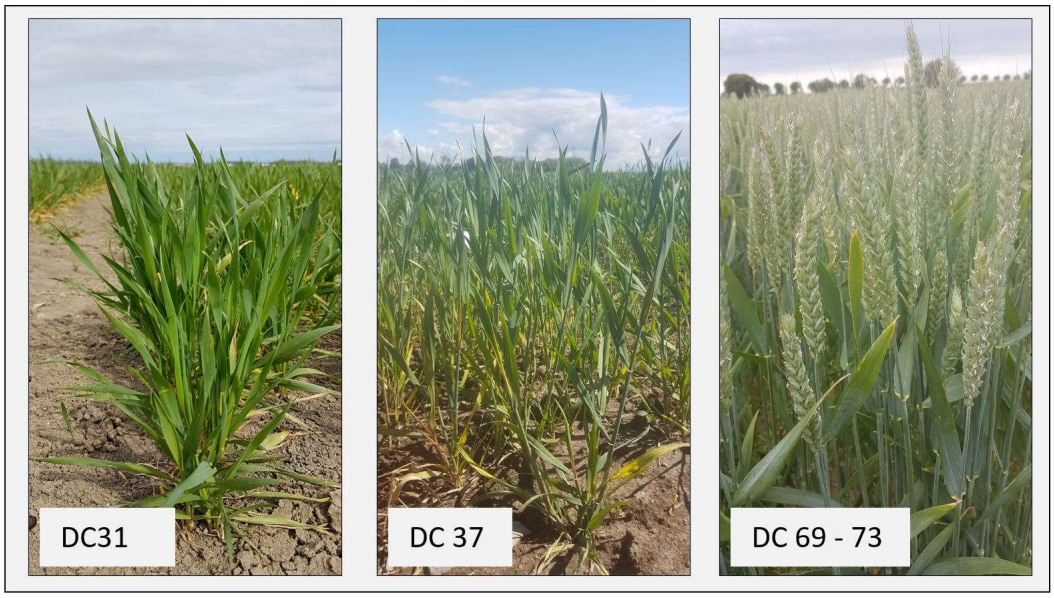

Fig. 4. Crop development stages of winter wheat (Triticum aestivum L.) between DC31–DC73 (photos by Kristin Piikki).

Tab. 3. Arable land in the study area used for winter wheat and spring barley production in 2018 and 2019 (Swedish Board of Agriculture 2018 - 2020).

Year	All fields (km^2)	Winter Wheat (km^2)	Spring Barley (km^2)
2018	774.2	128.7	156.5
2019	776.2	154.6	114.6

3.2. Data and data preparation

The data required to conduct this study is free of charge and included: a digital elevation model, meteorological data, satellite images, soil type data and field polygon data.

3.2.1. Weather data

Daily precipitation in mm (P) and daily mean Temperature in °C (T), were downloaded from the Swedish Meteorological and Hydrological Institute (SMHI 2020), for the years 2017–2020. In total eight P-Stations, having a full record for the years 2017–2020, were available within or close to the study area (Fig. 8). Daily

mean temperature data was obtained from two stations (Fig. 8). Historical precipitation data from 1991–2020 was available from four of the eight weather stations i.e., Lövstad, Tomelilla, Bollerup and Ystad.

3.2.2. Digital elevation model (DEM)

The digital elevation model used in this study was provided by Lantmäteriet. This dataset was originally derived from laser point data (Lidar) collected by airborne. The dataset is available for whole Sweden and is provided as tiles of 6.75 km^2 size. To work more efficiently, 253 single "GeoTIFF" tiles in total were merged into one big file which was then clipped using the study area boundary. The horizontal resolution of this dataset is 2 m; the vertical uncertainty is 0.1 m (Lantmäteriet 2021). Data was downloaded using SLU´s geo data extraction tool (GET 2021).

3.2.3. Satellite images

Satellite images were manually downloaded from the "Copernicus Open Access Hub" (https://scihub.copernicus.eu/) for the study period April-July in 2018 and 2019 from both satellites S2A & S2B (ESA 2021b). The chosen product was Level 2-A ("bottom of the atmosphere reflectance"). Images were downloaded independently of the cloud cover percentage (the chosen range was 0 to 90 % cloud cover). Clouds and cloud shadows were masked manually and then removed as shown in Fig. 5. Depending on the cloud cover magnitude, 0 – 93 % of the study area needed to be removed. In 2018, in total 15 images were available of which clouds needed to be removed from six; in 2019, five of 17 images were cloud-free. The actual Sentinal-2 coverage from April – July used for analysis are shown in Fig. 6.

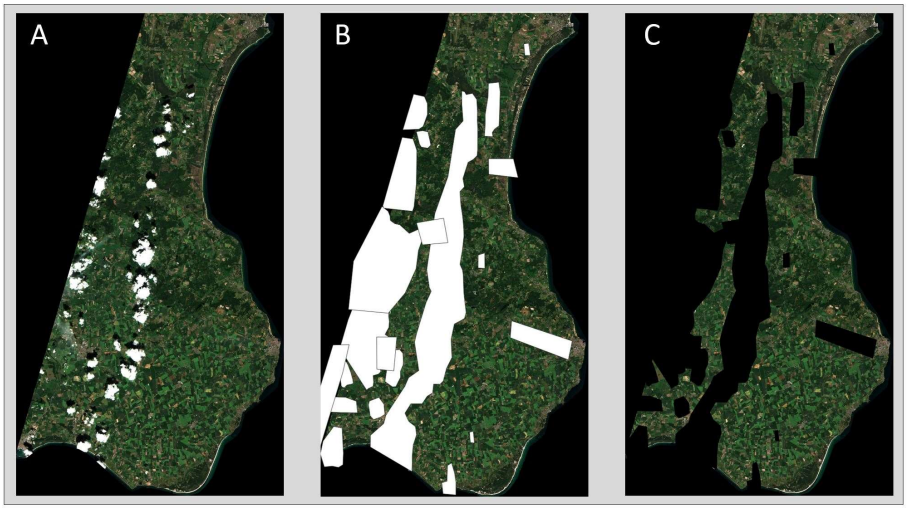

Fig. 5. Exemplary, process of cloud and cloud shadow masking and removal based on a RGB Sentinal-2 image (10 m resolution) captured at 26 of June 2019 for the area under study. A: original image. B: masked image. C: cloud and cloud shadow free image ready for further analysis.

Fig. 6. Sentinel-2 coverage after cloud and cloud-shadow removal in 2018 and 2019. The coloured areas (orange: 2018, blue: 2019) are showing the cloud free parts at the respective dates utilized for analysis.

3.2.4. Soil texture data

Soil texture data was extracted from the digital soil map of Sweden (DSMS). Raster files are available for clay, silt, and sand content (in %) with a resolution of 50 m. The cell size was downscaled from 50 to 5 m, to ensure smooth clipping at the field boundary. The uncertainty of this dataset is described in details in the original paper by Piikki & Söderström (2019). In summary, the error of this dataset is < 8 % clay and <13 % sand in 75 % of the validation samples. The density of the validation soil samples was one per 3 hectares (Piikki & Söderström 2019). Soil clay, sand, and silt content maps were generated at the field level (Fig. 7).

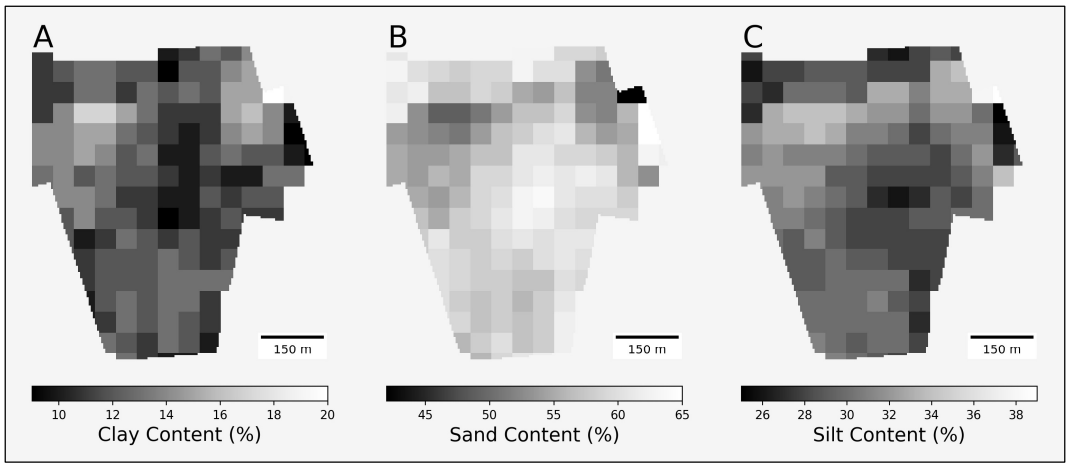

Fig. 7. Exemplary soil texture maps of sand (B), silt (C), and clay (A) content in % for one winter wheat field (ID 239).

3.2.5. Field polygons

Field polygons GIS layers, delineating all arable fields in the study area, were available from the Swedish Board of Agriculture (2018 - 2020). The dataset provides information about crop type, field size and the geographical location at the field level.

3.3. Drought feature analysis

The selection of the studied years was based on the drought feature analysis. Since this study focused on DC31– DC75 of WW and SB, the analysis of P and T from April – July was most relevant. The drought feature analysis was substructure as outlined below:

30-years climate average for P and T

In accordance with the recommendations of the World Meteorological Organization (WMO 2015), the LTA of T and P was computed based on the time period 1991–2020, to identify a dry and a non-dry year. The precipitation records of the four weather stations had some data-gaps throughout 1991–2020. Hence, the ordinary mean precipitation was calculated based on three stations for the years 1994, 1995, 2005, 2006, 2007 and 2015, while it was calculated based on four stations for the rest of the years respecting missing values. A complete temperature record was only available from Bollerup station. P and T values were aggregated annually and for the period April to July for all the years 1991 – 2021. Nonetheless, since the four stations are all located in the southern part of the study area. The LTA analysis is not representative for the total study area but provides approximative information on the climatic conditions in the region.

P and T analysis of the years 2018 - 2019

To gain a comprehensive understanding of P and T for the years 2018 – 2019, daily P and T data was analysed for each station separately. However, to summarize the results for the total study area the weighted average precipitation over the total study area was estimated based on the Thiessen polygon method. Thiessen polygons were automatically generated using the Voronoi Polygon feature in QGIS (QGIS Development Team 2021). Station weights were then calculated based on the fraction of the Thiessen polygon with respect to the total study area. The weighted average over the total study area was calculated using eq. 6 (Taesombat & Sriwongsitanon, 2009). Precipitation stations and their associated Thiessen polygon are presented in Fig. 8.

$$P_T = \sum_{i=1}^{n=8} T_i P_i$$

[eq. 6]

P_T = weighted average rainfall over the total study area

T_i = gauged rainfall of station i

P_i = station weight of station i

For T data the ordinary mean was calculated based on Skillinge and Bollerup station.

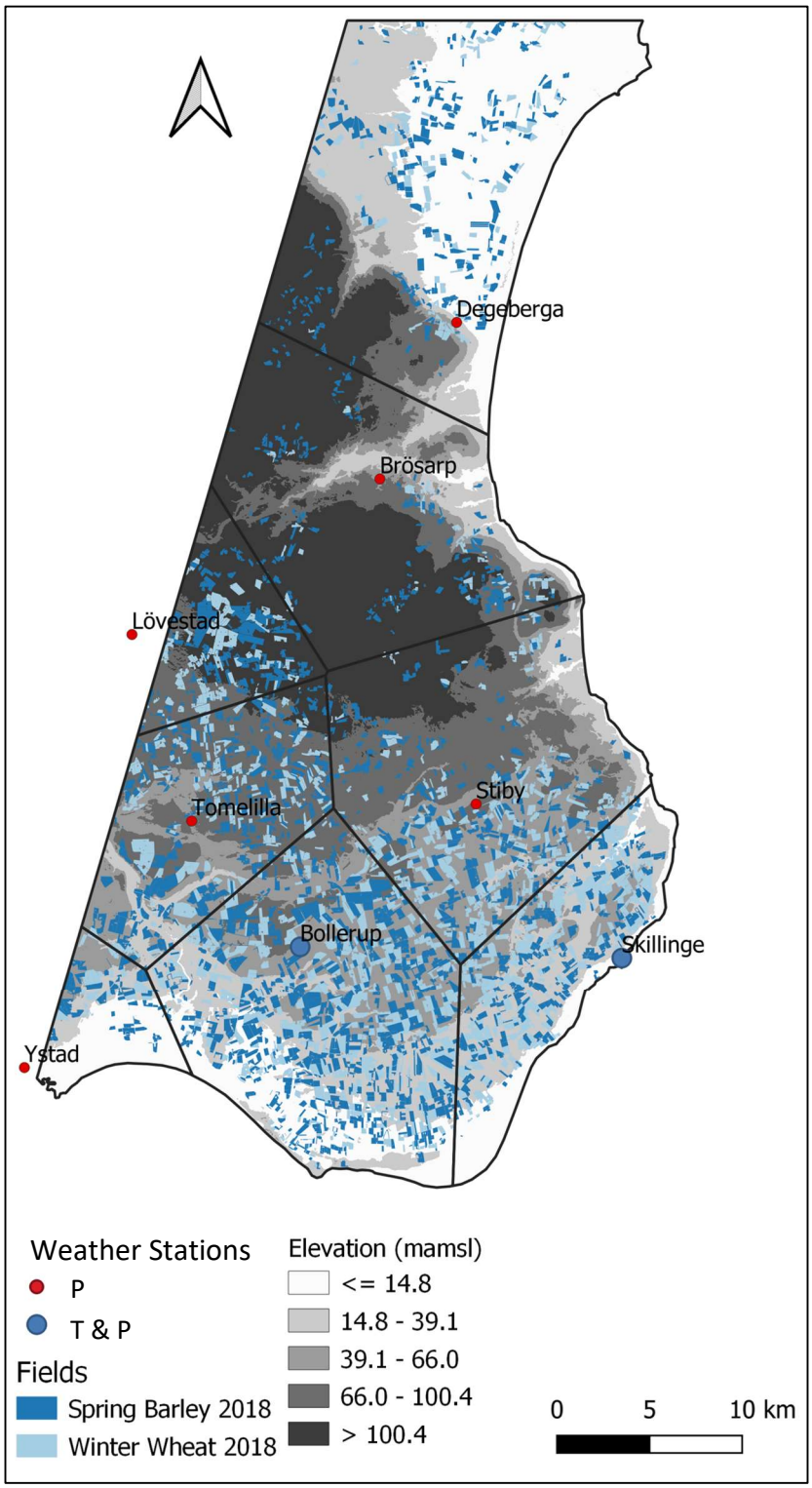

Fig. 8. Study area with Thiessen polygons for the drought feature analysis, weather stations, winter wheat and spring barley fields and elevation above sea level. Precipitation (P) and temperature (T) stations are shown as red and blue dotes.

3.4. Topography

The topography of all arable fields (n = 19,022) in the study area was assessed by generating slope maps (slope in %) derived from the DEM for each field separately. The mean field slope (in %) was then estimated for each field and the data was summarized using the boxplot framework. Furthermore, investigating within-field topography was crucial when evaluating the effect of drought within the field. Besides slope RE and the TWI field-maps were elaborated from the DEM. RE, Slope and TWI field-maps were then divided into three zones for each field separately, based on the quartiles of the relative pixel distribution (<=Q1, Q1-Q3, >Q3). Example maps of one field for all topographic indices are presented in Fig. 9.

3.5. Multi-scale crop growth development analysis

Assessing the effect of drought in relation to topography by comparing dry and non-dry conditions (2018 versus 2019) was a main objective of this study. Hence, the development of the different vegetation indices was investigated. Therefore, a time-series analysis of NDVI, NDRE, NDWI and NDDI from beginning of April to the end of July was conducted. The general approach of this analysis and how it is structured is presented in the flowchart shown in Fig. 10. The approach is divided into three main parts, and it is identical for WW and SB. In the first part, the crop growth development at the field, of all arable fields cultivated with WW and SB in 2018 and 2019 was analysed to evaluate the effect of the drought in 2018. The second part focused on linking crop growth development, at the field level to the average field slope. In the third part, crop growth development was analysed within the field and in relation to mean field slope topography. Generally, crop growth development was investigated at two different scales i.e., at the field and within the field, see Fig. 11 for further details. Furthermore, to display the spatiotemporal drought status at the field scale in an unbiased way, NDDI maps for WW and SB were generated. Throughout the analysis field polygons were buffered to the interior by 10 meters to reduce noise signals from streets, field-tracks, or buildings close to the field.

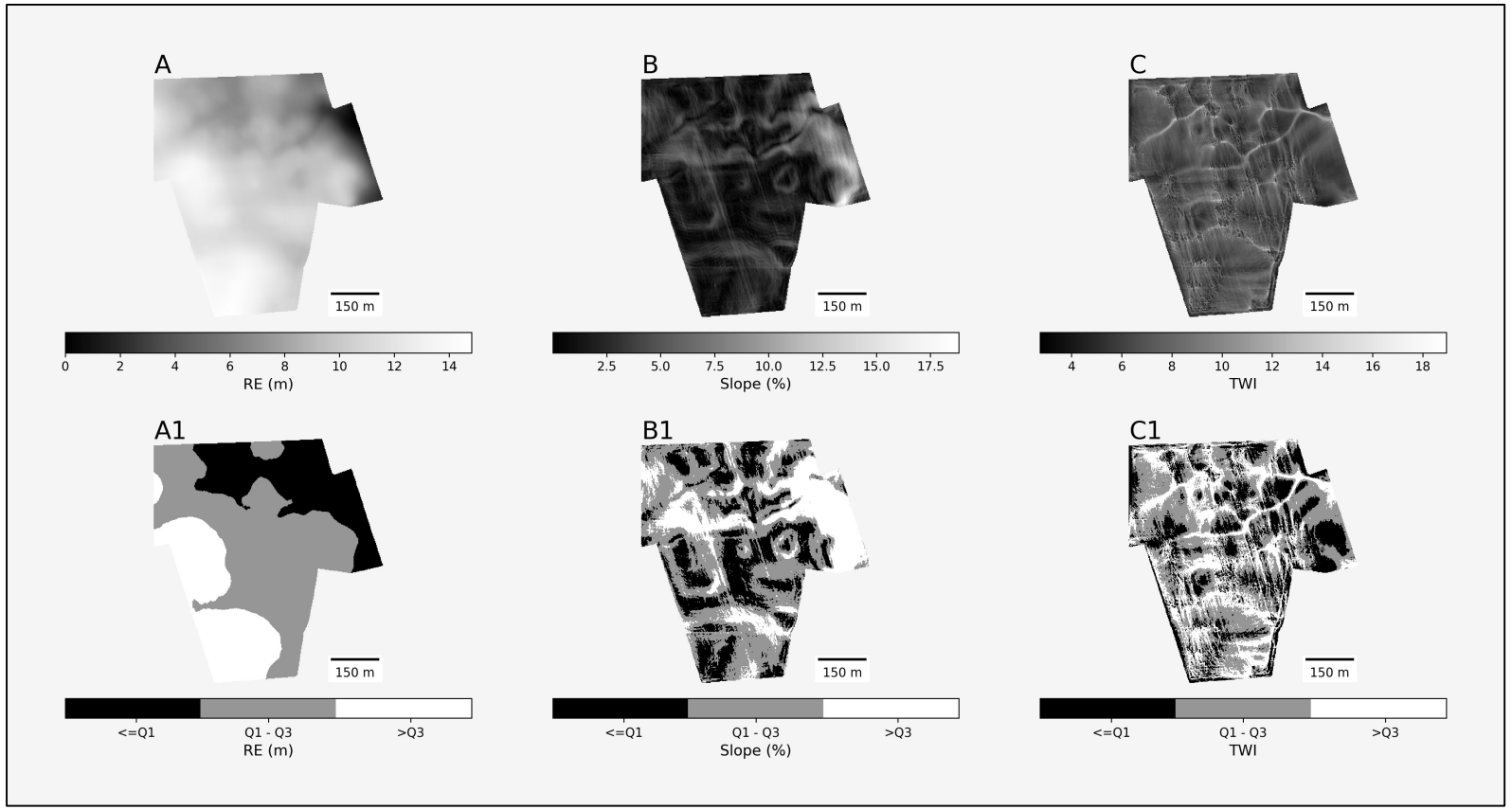

Fig. 9. Within-field topography for one winter wheat field (ID 239). RE raster (A) and RE divided into three zones (A1). Slope raster (B) and Slope divided into three zones (B1). TWI raster (C) and TWI divided into three zones (C1); zoning was based on the quartiles of the pixel distribution.

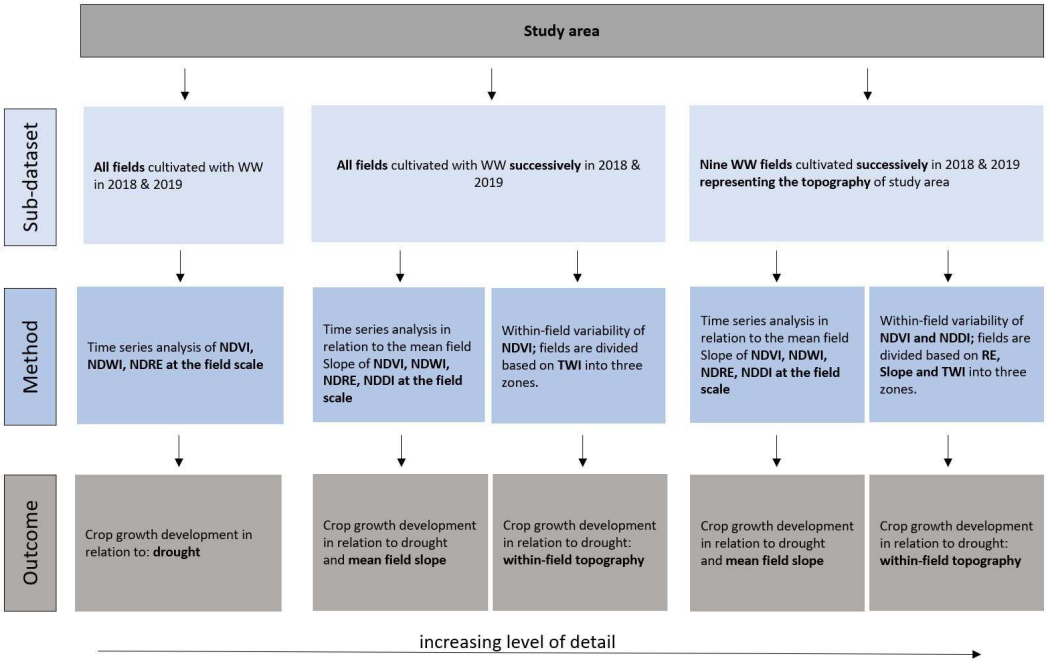

Fig. 10. Flow chart presenting the different parts of the crop growth development analysis in 2018 and 2019 of winter wheat and spring barley and how it is related to topography. The level of detail increases from left to right.

3.5.1. Crop growth development

To assess the effect of drought on crop growth development, a time series analysis of the mean values of NDVI, NDRE and NDWI was conducted at the field scale for WW and SB in the period April–July in both years 2018 and 2019. The respective number of fields available for this part of the analysis is presented in Tab. 4. Due to the variation in cloud coverage between the different satellite images, the number of fields at a certain day of observation varied: ranging from 596 – 1,230 fields in 2018 and 127 – 1,453 fields in 2019 for WW and 928 – 1,591 fields in 2018 and 129 – 1,135 fields in 2019 for SB. When analysing the different vegetation indices like for example NDVI, the mean NDVI value was calculated at the field scale at every date of observation and for all respective fields. Hence, this data was then visualized using the box plot framework. The average value of any such given dataset/boxplot is called mean of means (MoM). MoM values were calculated for each date in the study period as well as over the total study period.

Fig. 11. A: Field scale, NDVI, NDRE, NDWI and NDDI were calculated as mean values for the whole field. B: Within-field scale, NDVI, NDRE, NDWI and NDDI were calculated as mean values for each zone separately Zones were derived from topographic indices maps. The zones visible in map B are derived from TWI. Sentinal-2 image of spring barley field (ID 885) at 01.06.2021.

3.5.2. Crop growth development versus mean field slope

The crop growth development was assessed from a topographical perspective by investigating the influence of the mean field slope on the time series of the average values of the different vegetation indices (NDVI, NDRE, NDWI and NDDI) at the field level. The selected fields for this part were successively cultivated by the same crop in 2018 and 2019. The selected fields were divided into three slope categories based on the mean field slope distribution (<= Q1, Q1-Q3, >Q3). For this part of the analysis, an overall field size threshold of 3 hectare was chosen to avoid the usage of small narrow field strips cultivated in both years. In total, 363 fields successively cultivated with WW and 230 with SB, were used for this analysis (Tab. 4). Additionally, this analysis was conducted and is presented for nine. representative SB/WW fields separately. The location of the fields used in this part of the analysis are presented in Fig. 12.

Tab. 4. Total field area of winter wheat (WW) and spring barley (SB) fields as well as the number of field polygons (n) in 2018 and 2019.

Year	WW (n)	WW (km^2)	SB (n)	SB (km^2)
2018	1230	120.9	1591	141.6
2019	1453	145.2	1135	104.3
2018 - 2019	363	32.1	230	16.72

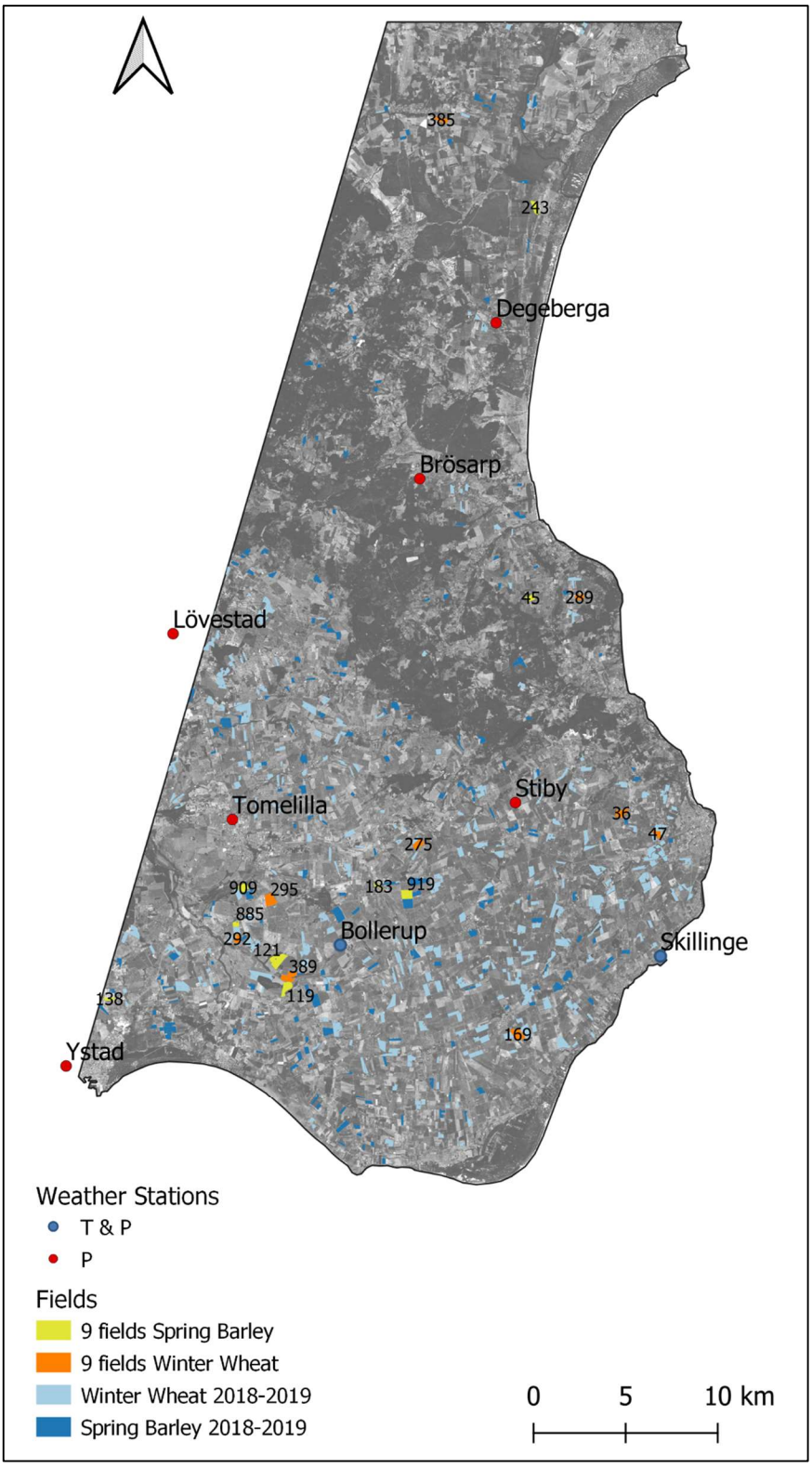

Fig. 12. Spatial location of all winter wheat and spring barley fields cultivated in both consecutive years 2018 and 2019 as well as nine winter wheat and spring barley fields. Precipitation (P) and temperature (T) stations are shown as red, and blue dotes.

3.5.3. Crop growth within-field development variability

To investigate within-field spatial variations of crop growth development in relation to within-field topography and drought, fields were divided into three zones (based on RE, Slope and TWI maps). These three zones represent the quartiles of the topographic maps at the pixel scale of the individual field under study (<= Q1, Q1 - Q3, >Q3). The average values of NDVI and the NDDI were calculated at zonal bases to track the crop growth development within the field separately (Fig. 13). This part of the analysis was conducted for nine fields cultivated successively with WW and nine fields cultivated successively with SB. The selected fields represent the slope categories of section 3.5.2 i.e., three fields out of every slope category. Furthermore, NDVI within field variation was analysed for all fields cultivated with WW/SB in both consecutive years 2018 and 2019, using the same approach as for the nine fields (Fig. 12) but only using TWI to divide the fields. Additionally, NDDI maps were generated to visualize the spatiotemporal drought status of WW/SB within the field unbiased.

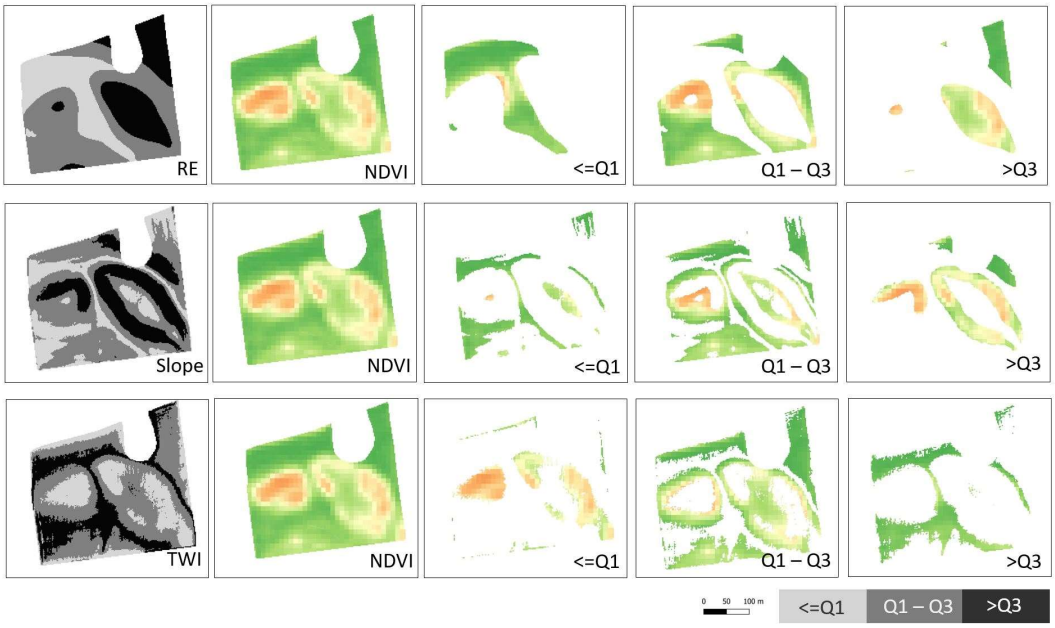

Fig. 13. Spatial NDVI distribution in one spring barley field (ID 885) at 24 of May 2019 with NDVI ranging from 0.2 (beige) to 1.0 (dark green). The field was divided into three zones based on RE (top), Slope (middle) and TWI (bottom) maps to investigate the within field topographic related NDVI variation.

3.6. Crop growth development versus other site-specifics

Furthermore, to investigate other possible factors affecting crop growth in response to drought, the following analysis was carried out at the field scale.
From the MoM NDVI time series of all fields cultivated with WW (n = 1,230) and SB (n = 1,142) in 2018 the maximum was selected. Two groups of fields for both crops were then drawn from the boxplot at the time series maximum i.e., the two extreme quartiles (fields with NDVI <= Q1 and >Q3). The selection date for the two groups was 24 of May and on 3rd of June for WW and SB respectively (as shown in Fig. 14). WW and SB fields of out of the two extremes were than linked to common site-specific characteristics such as slope (%), clay content (%), field size (ha) and spatial location.

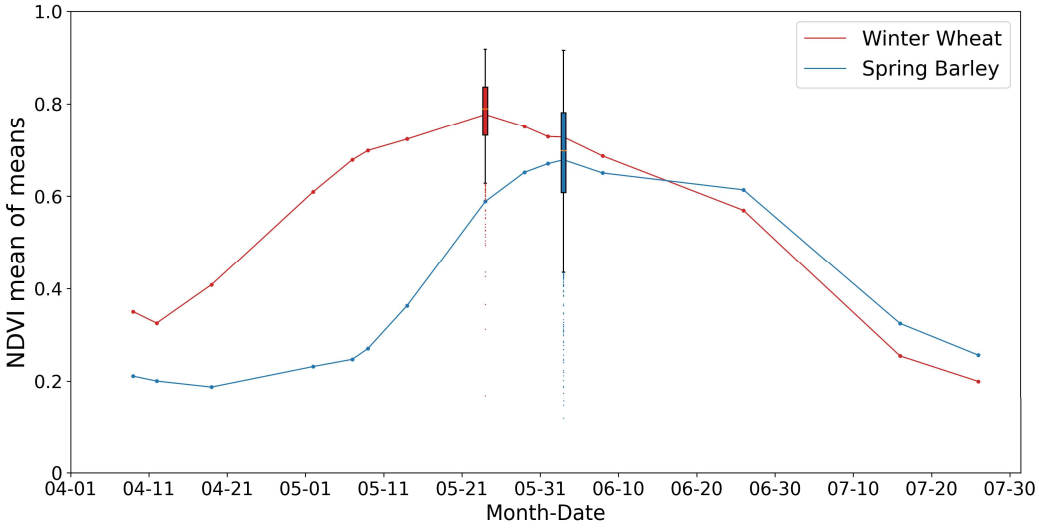

Fig. 14. Average NDVI time series of all winter wheat (red) and spring barley (blue) fields in 2018. The mean field NDVI distribution at the time series maximum of both crops is presented as a boxplot.

3.7. Software

Due to the huge number of satellite images, field polygons, vegetation indices and topographic indices, automatization was a crucial to conduct this work successfully. Therefore, the Python programming language and the various available libraries written in Python were utilized. To name only the most important libraries used for this work:

- Numpy, Pandas and Glob for data analysis
- GDAL, Geopandas and Rasterio for spatial data analysis
- Matplotlib and Seaborn for data visualization

Libraries were managed using the anaconda software distribution (Anaconda 2021) and the package installer for python (pip).

4. Results

The results of this study are presented in the following order: First, the results of the drought feature analysis, justifying the selection of the years 2018 and 2019 are presented. The second part focuses on crop growth development of SB and WW in 2018 and 2019 and the assessment of the drought effect. In the third part, the results of a possible relation between drought stress and field topography are presented.

4.1. Drought feature analysis

Out of the years 2017 – 2020 the year 2018 was the driest year both on an annual scale as well as for the study period (April to July). The years 2017 and 2019 were wet years of which 2019 was closer to the LTA. The year 2020 was dry and warm, with an average temperature close to the LTA during April–July. As the results of the drought feature analysis the year 2018 was selected as a dry year and the year 2019 as a non-dry year to conduct the crop growth development analysis in this study.

LTA precipitation and temperature

The LTA precipitation estimated on the period 1991 – 2020 based on Lövstad, Tomelilla, Bollerup and Ystad weather station was 705.9 ± 104.3 mm. The LTA temperature of this period was 8.6 ± 0.7 °C computed based on Bollerup station. For the period April–July, the LTA precipitation was 197.9 ± 63.9 mm and the LTA temperature was 12.7 ± 0.8 °C. The year 2017 was rather wet with 23 % more rainfall compared to the LTA. The years 2018 and 2020 were rather dry with 18 % and 12 % less rainfall compared to the LTA. In 2019, the annual rainfall was 6 % higher compared to the LTA. Annual P and T values and for the period April – July are presented in Tab. 5 below.

Tab. 5. Annual precipitation (P) and temperature (T), and for the period April–July (P: n = 4, T: n = 1).

Year	Annual P (°C)	April-July P (mm)	Annual T (°C)	April-July T (mm)
2017	868.7	267.4	8.8	12.4
2018	581.9	103.1	9.5	15.3
2019	753.0	230.4	9.6	13.3
2020	624.1	148.3	9.9	12.7

In 2018, the mean temperature between April–July was noticeable elevated by 3.25 standard deviations above the LTA. In keeping with that, 2018 was the driest year in the period 2017–2020, due to its low precipitation and high temperatures, especially between April–July. The year 2017 was a wet year with both annual and summer precipitation above the LTA. In 2019, both summer and annual precipitation were close to the LTA. However, in 2018, temperature was elevated on an annual basis and during summer when comparing it to the LTA by 11 % and 54 % respectively. The year 2020 was a dry year with reduced summer and annual precipitation. Nonetheless, the mean summer temperature between April – July was equal to the LTA in 2020. Thus, the year 2018 was selected as a dry year and the 2019 as a year close to the LTA. The precipitation and temperature time series from 1991–2020 are presented in Fig. 15.

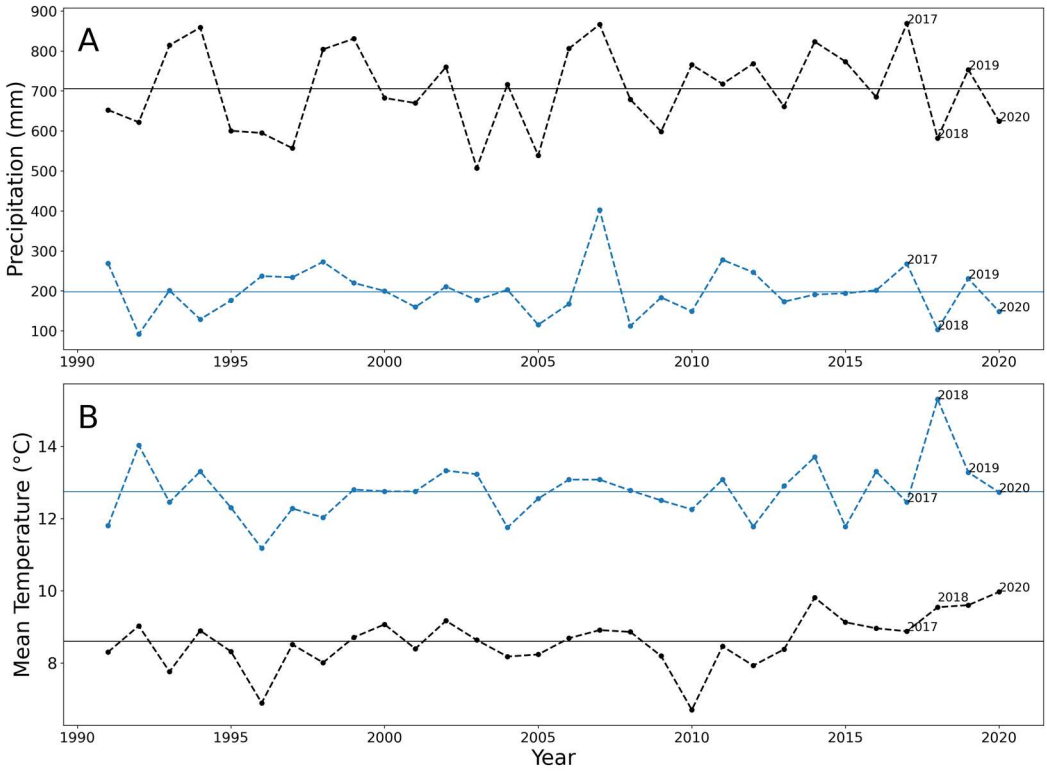

Fig. 15. A: Precipitation and temperature (Annual in black, April–July in blue) for the period 1991–2020. LTA's are displayed as horizontal lines.

Weighted average over the study area

In 2018, between April–July, about 99.4 mm (n stations = 8) of precipitation were fallen on average over the total study area. In comparison 2.2 times more rainfall (217.1 mm, n = 8) was gauged in 2019. The spatial rainfall variability between April to July in 2018 and 2019, is presented in Fig. 16 using the Thiessen polygon method.

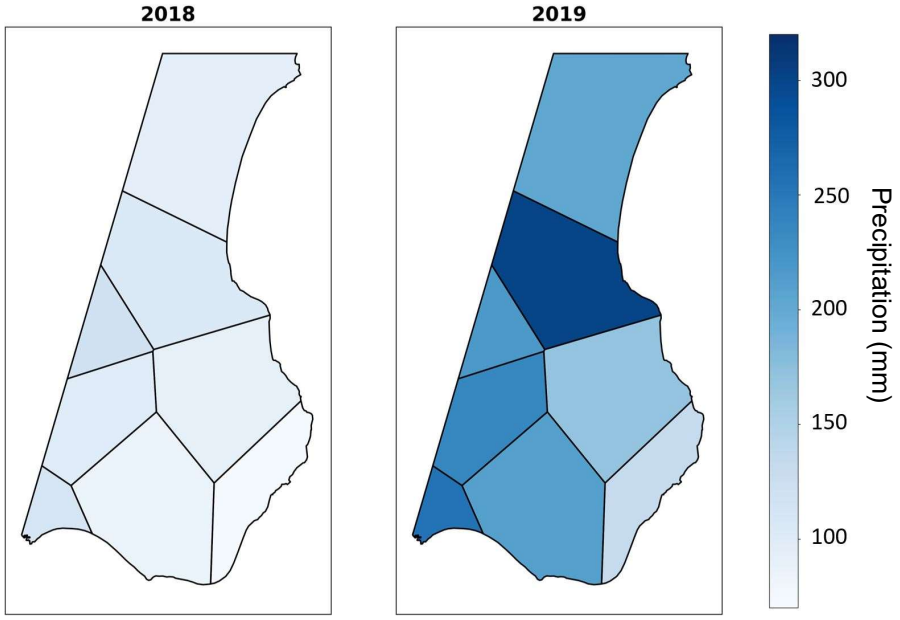

Fig. 16. Precipitation variability based on the Thiessen-polygon method within the study area for the years 2018 and 2019 between April – July.

Rainfall events analysis

In 2018, 15 rainfall events (> 1 mm) occurred, while in 2019 the number of rainfall events (> 1 mm) was 34, more than twice as high compared to 2018. The weighted average daily precipitation over the total study area is presented in Fig. 17.

When focusing on the study period of the year May–July, it was clearly noticeable that especially 2018 was very dry in comparison to 2019. In 2018, P was 93 % lower in May, 67 % lower in June and 54 % lower in July in comparison to 2019. Temperature was 37 % warmer in May and 18 % warmer in July in 2018 when compared to 2019. In June, the temperature difference was quite small. Further information for all months can be obtained from Fig. 18.

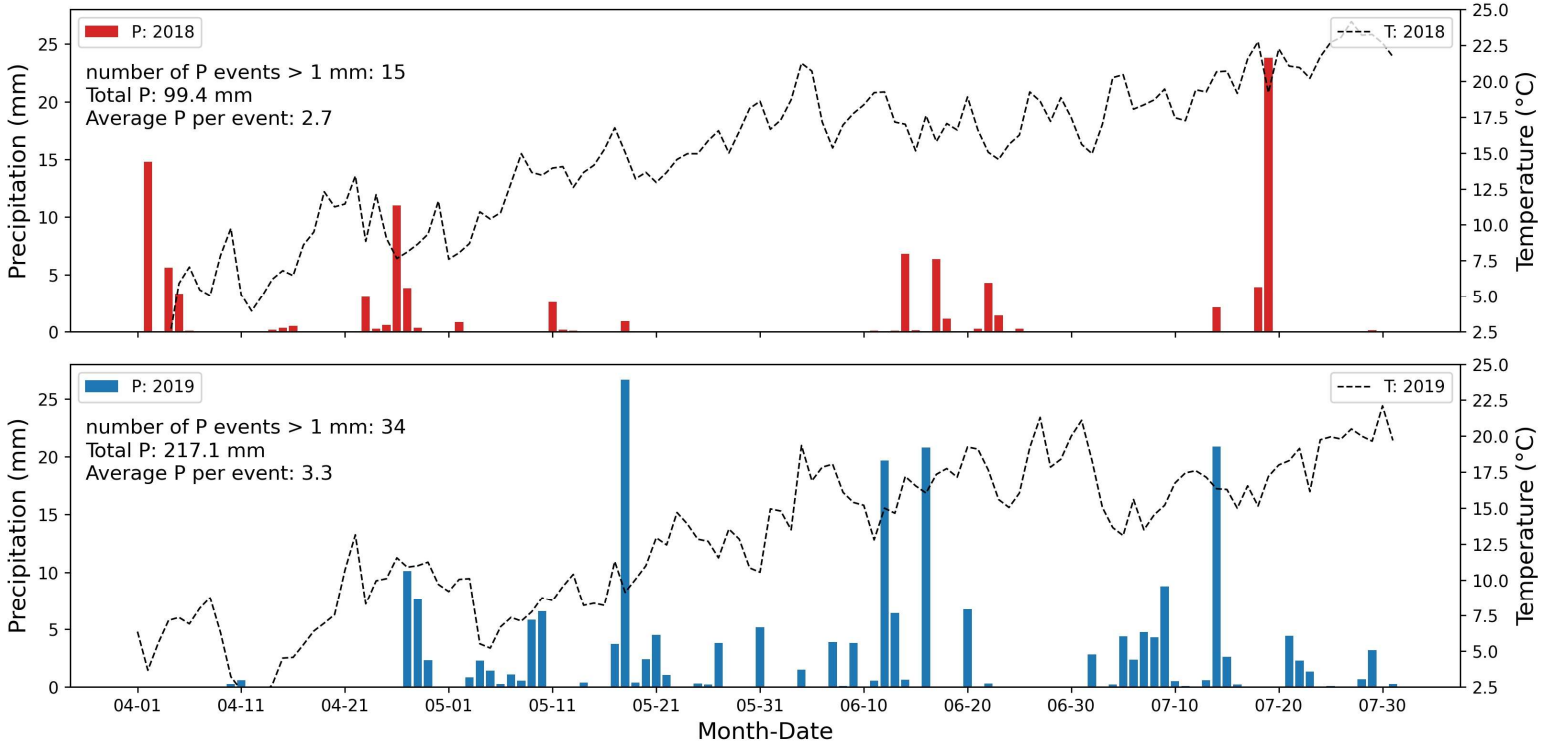

Fig. 17. Daily weighted average precipication (in mm) and temperature (in °C) over the whole study area, for the period April–July of 2018 and 2019.

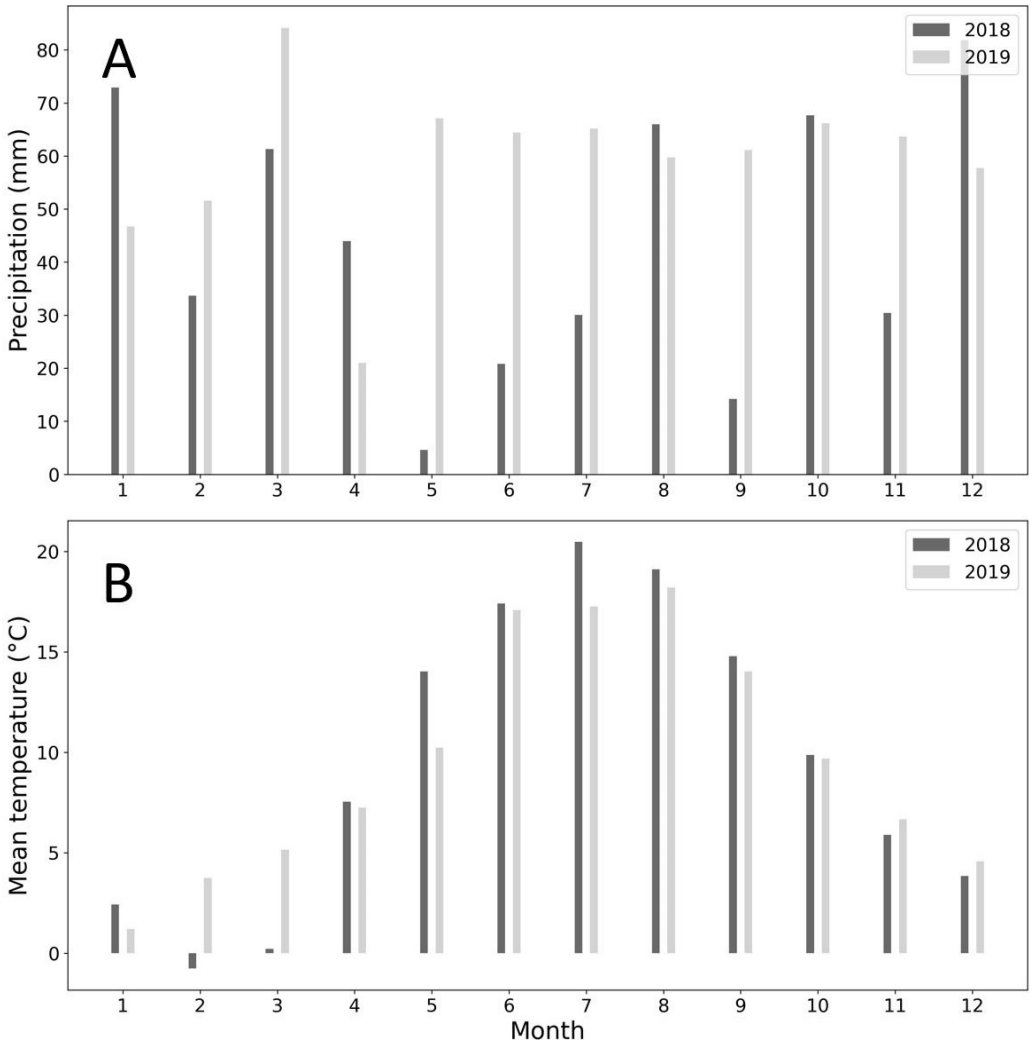

Fig. 18. A: weighted monthly average precipitation (n = 8) in 2018 and 2019. B: monthly average temperature (n = 2).

4.2. Slope, soil texture and field size

The obtained average field slope of all arable fields in the study area was 4.2 ± 3.5 % (n = 19,020). Within the study area the average field size was 4.0 ± 5.8 ha (n = 19,020). Soil texture is mainly dominated by sand, with an average sand content of 60 ± 14 %; average clay content is 12 ± 6 %; average silt content is 28 ± 6 %, see Fig. 19.

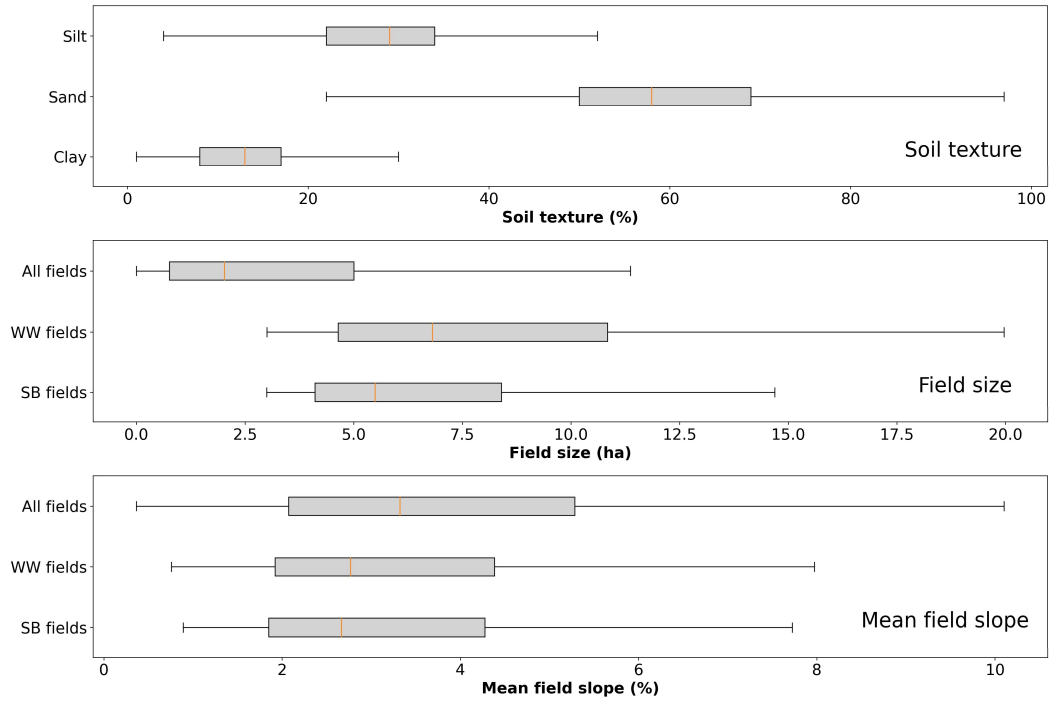

Fig. 19. Boxplots of soil texture in %, field size in ha and average field slope in %, for all fields in the study area as well as for fields cultivated successively with winter wheat (WW) and spring barley (SB) in 2018 and 2019.

Overall, about 40 % of the total arable land in the study area had an average field slope ranging from 2 – 4 % (Fig. 20, A). About 50 % of the total arable land was covered by fields with a size ranging from 4 – 15 ha (see Fig. 20, B).

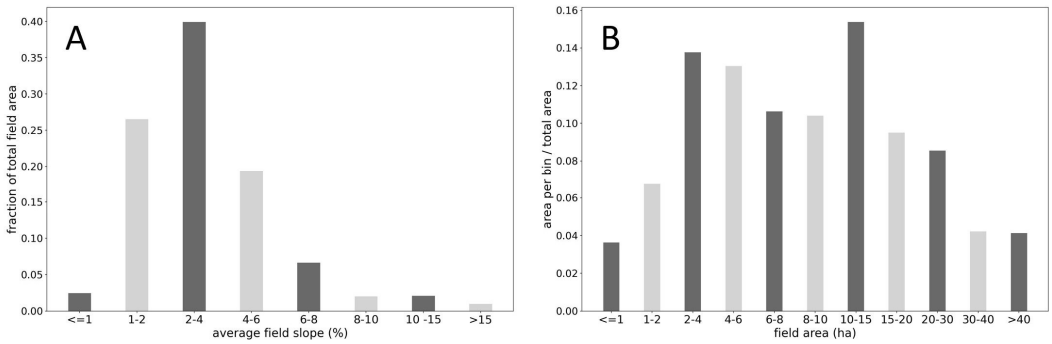

Fig. 20. A: Categorizing all fields as a fraction of total fields area, based on the average field slopes (A) and the field size (B).

4.3. Crop growth development

This part of the analysis was carried out on all fields cultivated with WW/SB in 2018 and 2019. The aim of was to assess the effect of drought on crop growth development during the crop development stages DC31-DC75, considering NDVI, NDRE and NDWI. In 2018, crop growth development was noticeable affected by drought when considering NDVI, NDRE and NDWI, with a mean reduction over the total time series of 36 % for the NDVI, 69 % for the NDWI and 43 % for the NDRE in comparison to 2019 for SB, and 25 % for the NDVI, 58 % for the NDWI and 32 % for the NDRE in comparison to 2019 for WW. Hence, when comparing between WW and SB, the negative effect in 2018 was 6 % - 11 % higher for SB in comparison to WW. As a result, both WW and SB were negatively affected by drought, with a noticeable higher drought-resilience of WW in comparison to SB. Furthermore, the results provided evidence that the negative effect severity of drought varied between fields of the same crop type. Overall, some fields seemed to be more resilient in response to drought - performing equally good under dry conditions in comparison to non-dry conditions.

NDVI:

For both crops the NDVI MoM values were on average 25 % (WW) and 36 % (SB) lower over the study period (April–July) in 2018 in comparison to 2019. For WW, the maximum of NDVI MoM value of the time series was reached at 24 of May with a value equal to 0.77 ± 0.07 (n = 1,230); while in 2019 the maximum value was reached 20 days later at 13 of June with a value equal to 0.91 ± 0.02 (n = 761). Hence, MoM NDVI time series maximum for WW was 18 ± 10 % higher in 2019 in comparison to 2018. For SB the maximum NDVI MoM value of the time series was reached at 3rd of June in 2018 with a value equal to 0.68 ± 0.02 (n = 1,142); while in 2019 the maximum value was reached 20 days later at 23 of June with a value equal to 0.91 ± 0.04 (n = 935). As a result, for SB, the MoM NDVI time series maximum was 33 ± 2.7 % higher in 2019 compared to 2018.

However, in 2018 the maximum NDVI was 0.09 higher for WW in comparison to SB. Furthermore, the mid-season was shorter, and the crop started to turn yellow earlier in 2018 than in 2019 for WW. This indicated a longer phase of maturation under non-dry conditions. Despite the offset between 2018 and 2019, the mid-season length was similar for SB in both years. Visually inspecting the range of the boxplots of the NDVI MoM time series revealed a very narrow range in 2019 compared to 2018 for WW and SB. This difference was especially noticeable in the mid-season. Hence, during non-dry conditions a homogeneous crop growth among fields was observed. During dry conditions a higher variation of crop growth in response to drought was noticed. Interestingly, some fields indicated a relatively

high crop growth during dry conditions in 2018, being equally high as the MoM in 2019 (see Fig. 21).

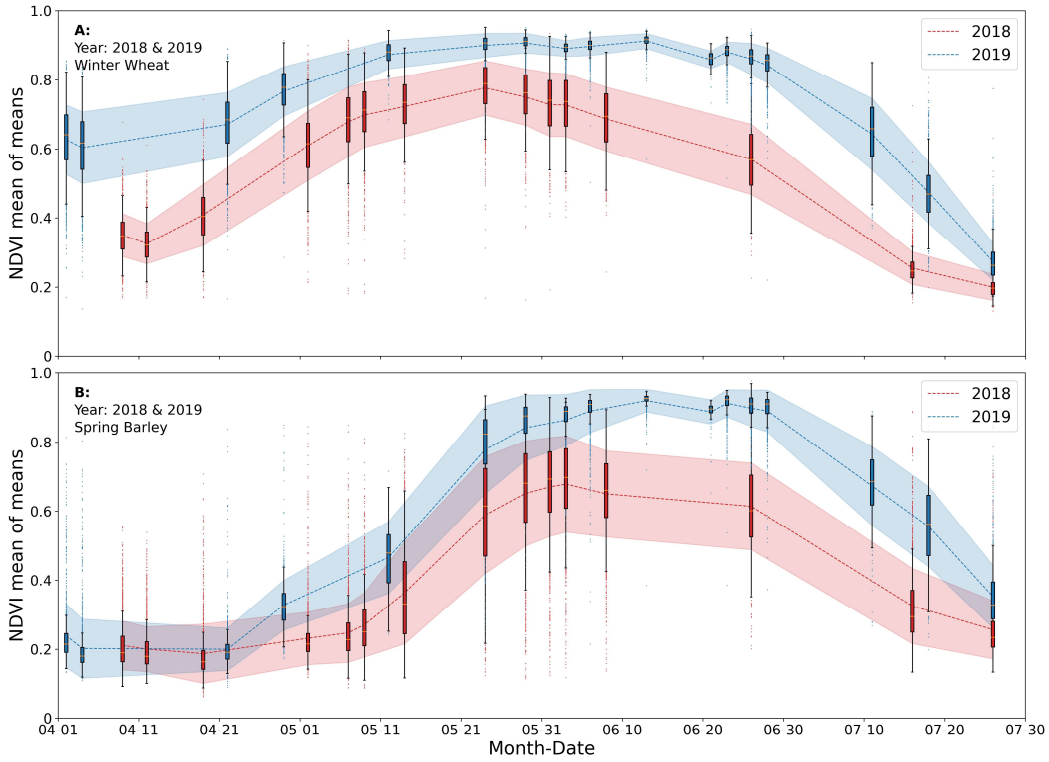

Fig. 21. A: Winter Wheat. B: Spring Barley. Time series of MoM values of NDVI (dashed line, 2018 in red, 2019 in blue). The blurred area is delineated by the standard deviation, the boxplot and outliers are visualized in the respective colours.

NDRE:

Generally, the MoM NDRE time series pattern was very similar to NDVI. MoM maximum NDRE was reached at the same dates as NDVI for SB and WW in both years as shown in Fig. 22. Nonetheless, NDRE had a noticeable offset of 0.18 (n = 4) in comparison to NDVI when considering the difference between NDVI and NDRE over the total time series (April–July) and between 2018 and 2019 for WW and SB. In keeping with that, the offset between NDRE and NDVI comparing the time series of MoM maximum values between the same years was 0.19 in 2018 and 0.16 in 2019 for WW and 0.23 in 2018 and 0.21 in 2019 for SB. This offset indicated a lower level of saturation of NDRE in comparison to NDVI. For both crops, the MoM NDRE values were on average 32 % and 43 % lower over the total study period in 2018 when compared to 2019.

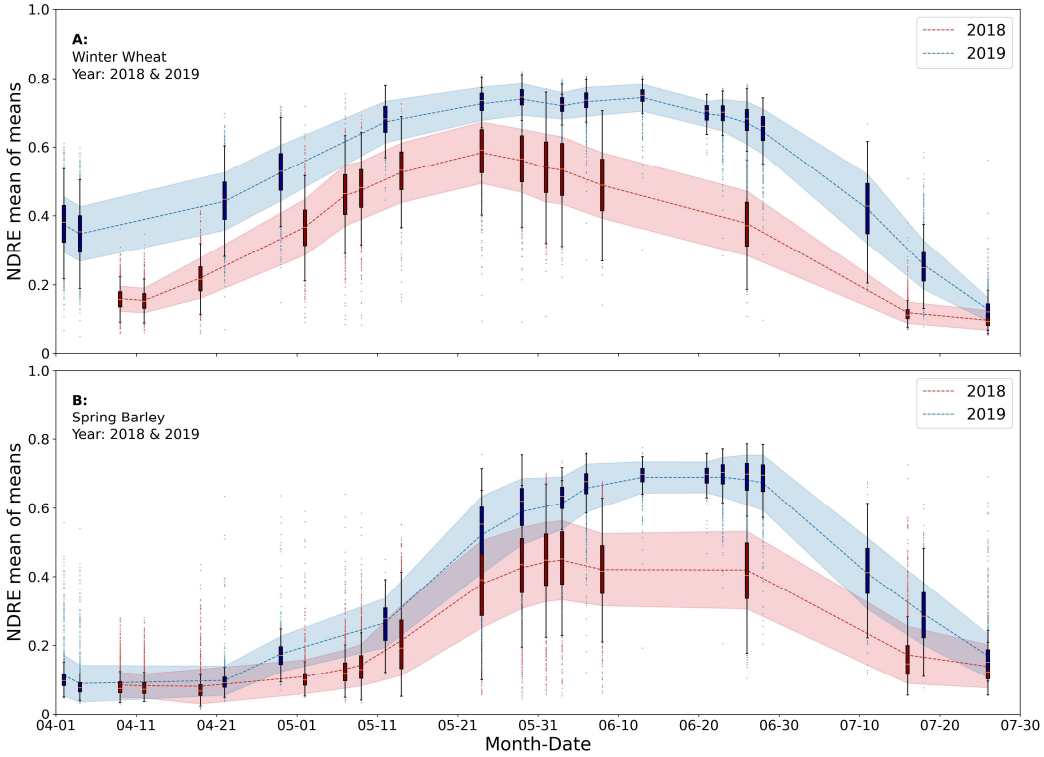

Fig. 22. A: Winter Wheat. B: Spring Barley. Time series of MoM values of NDRE (dashed line, 2018 in red, 2019 in blue). The blurred area is delineated by the standard deviation, the boxplot and outliers are visualized in the respective colours.

NDWI:

For WW, the MoM NDWI time series maximum values correspond to the same dates obtained from the NDVI time series with values of 0.36 ± 0.09 (24 of May 2018, n = 1,230) and 0.57 ± 0.03 (13 of June 2019, n = 761). For SB, the maximum NDWI MoM time series values were reached on 1st of June in 2018 with NDWI equal to 0.23 ± 0.13 (n = 1,142) and 20 days later on 21 of June in 2019 with NDWI equal to 0.56 ± 0.13 (n = 935), slightly earlier than NDVI. The MoM maximum values of NDWI were 58 % and 143 % higher in 2019 when compared to 2018 for WW and SB respectively. The MoM values of NDWI were below zero until mid of May for SB, indicating that the vegetation canopy had not significantly developed yet. This indicated that the reflectance was mainly dominated by soil before May. For WW, the MoM NDWI values, including all fields within one standard deviation from the mean, stayed above zero from the beginning of April in 2019, indicating a higher and earlier crop growth development. While at second of May in 2018, 90.9 % (n =1,119) of all WW fields had a mean field NDWI above zero. Hence, in the beginning of April, WW crops had a higher biomass and vegetation water content when compared to SB. Between end of May until mid of July the MoM value of the NDWI time series was 69 % lower in 2018 (NDWI = 0.2 ± 0.12, n = 6)

compared to 2019 (NDWI = 0.48 ± 0.12, n = 10) for SB. Considering the total study period from April to July, the MoM value of the NDWI time series was on average 58 % lower in 2018 (NDWI = 0.16 ± 0.07, n = 15) compared to 2019 (NDWI = 0.38 ± 0.06, n = 17) for WW. The time-series plot is presented in Fig. 23 below. In conclusion, these results indicated a higher level of drought stress for both crops in 2018 comparing to 2019, as the NDWI reflects upon the crop water content beside crop density.

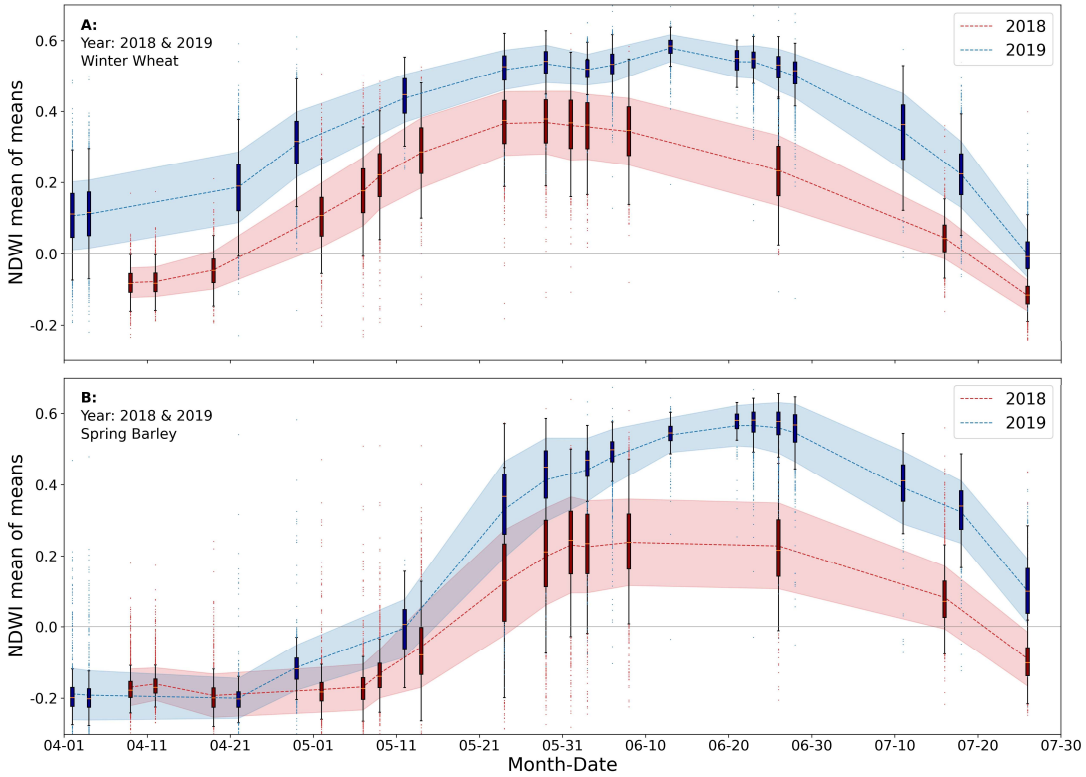

Fig. 23. A: Winter Wheat. B: Spring Barley. Time series of MoM values of NDWI (dashed line, 2018 in red, 2019 in blue). The blurred area is delineated by the standard deviation, the boxplot and outliers are visualized in the respective colours.

4.4. Crop growth development versus mean field slope

To assess a possible relation between mean field slope (in %) and crop growth development in response to drought, fields cultivated successively with WW (n = 363) and SB (n = 230) were selected, and then classified in three groups according to the quartiles of the mean field slope values (<=Q1, Q1–Q3, >Q3). The curves for NDVI, NDRE, NDWI and NDDI, were developed for the three slope groups separately. The curves represent the vegetation indices MoM values in each slope class. The crop growth development was than compared between the three slope classes (Fig. 24 and 25).

Winter wheat:

The differences between the vegetation indices MoM values in the different slope classes were quite small in both years. The standard deviation overlapped when considering the whole study period of all three slope classes for NDVI, NDRE and NDWI by >= 92 % in 2018 and 2019. Therefore, no consistent link between mean field slope classes and crop growth development, considering NDVI, NDRE, NDWI and NDDI was noticed in 2018 or in 2019.

Spring barley:

SB fields of the class <= Q1 (i.e., fields with a rather small topographic within-field variation in terms of slope) had a higher average field NDVI, NDRE, NDWI and lower NDDI, towards the end of June in 2018 in comparison to SB fields of the two other classes (Q1 – Q3 and > Q3). At the time series peak on 26 of June in 2018 MoM values of NDVI, NDRE, NDWI of the fields of class <= Q1 was 15 %, 16 %, 62 % higher compared to the fields of the slope class > Q3. Hence, the average (over study period) NDDI value was 30 % lower for the fields of class <= Q1 compared to the fields of class > Q3 in 2018. This indicated that during 2018, SB fields with a smaller mean field slope were more resilient in response to drought, compared to fields with a higher mean field slope. Generally, NDVI, NDRE, NDWI and NDDI values differed slightly between fields of the three slope classes in 2019 and much less when compared to 2018. Furthermore, in both years MoM values of NDVI, NDRE, NDWI for the slope classes Q1 – Q3 and >Q3 never exceeded the values of the slope class <= Q1. Nonetheless, the standard deviation overlap, considering the study period was on average >= 69 % when considering all three slope classes, both years and all vegetation indices.

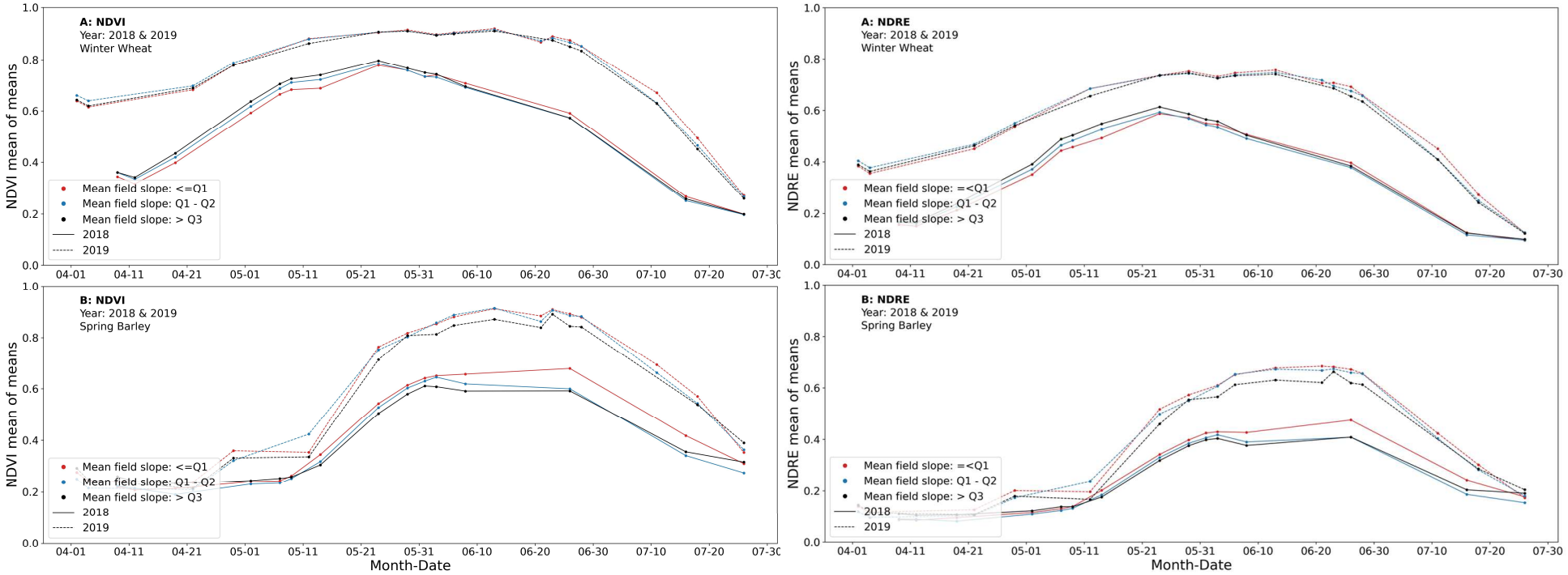

Fig. 24. NDVI (left) and NDRE (right), time series in the three slope classes for winter wheat (A) and spring barley (B) in 2018 and 2019.

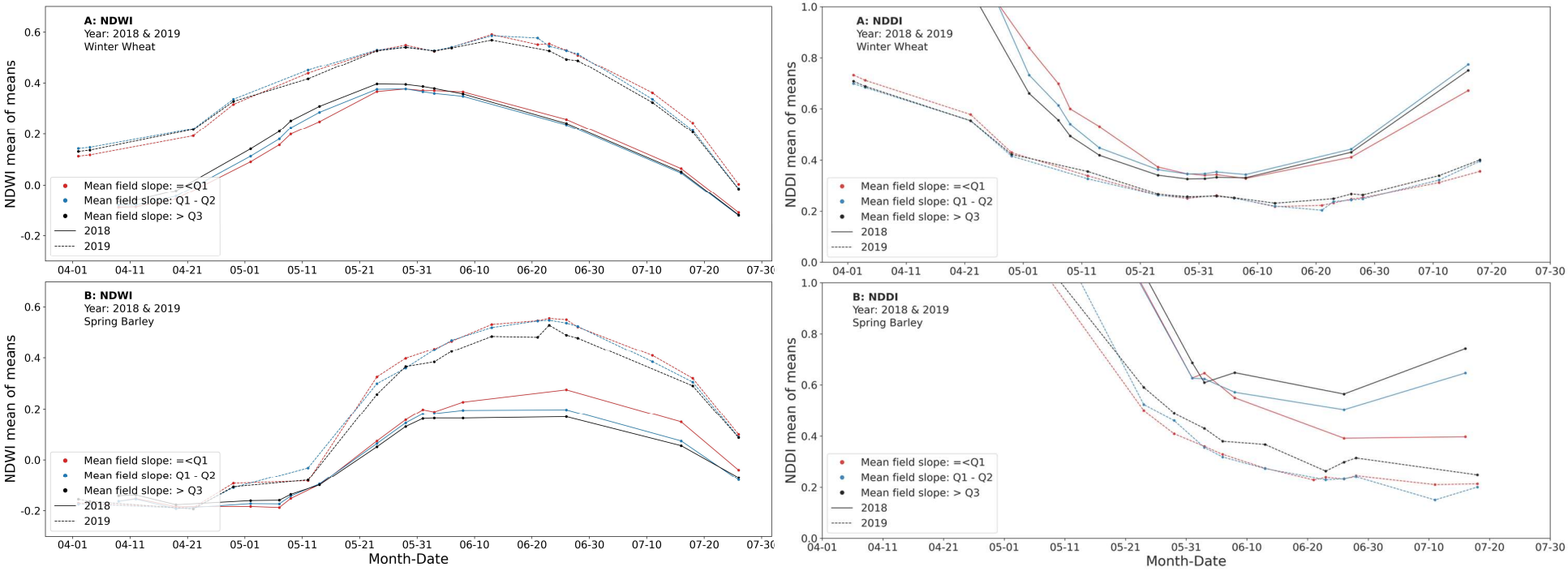

Fig. 25. NDWI (left) and NDDI (right), time series in the three slope classes for winter wheat (A) and spring barley (B) in 2018 and 2019.

4.5. Crop growth development versus slope, clay-content, field-size and location

In this section the results and the figures obtained from section 3.3 of the NDVI index, only for 2018 were used. WW and SB fields were classified based on the NDVI boxplot quartiles (>=Q1, Q1–Q3, >Q3) at the time-series maximum MoM. The aim of this analysis was to assess the effect of different field characteristics (i.e., slope, clay-content, field-size and location in the study area) on crop growth, under drought conditions. The analysis was carried on at the field scale, meaning calculation were based on mean field values (i.e., mean field slope, mean field NDVI etc.). In the dry year 2018, the maximum MoM NDVI value was reached at 24 of May for WW and at 3rd of June for SB (see Fig. 14). The MoM maximum NDVI value of WW was 14.5 % higher compared to SB, with 0.77 ± 0.07 (n = 1,230) and 0.68 ± 0.02 (n = 1,142) for WW and SB respectively. In this analysis special attention was paid to the two extreme classes (<=Q1 and >Q3). WW and SB fields of the two extremes classes were than related to the before mentioned site-specific field characteristics (see Fig. 26). The results showed that 25 % of all SB fields had a mean field NDVI below 0.6 and 25 % a mean field NDVI above 0.78; for WW 25 % of all fields had a mean field NDVI below 0.73 and 25 % had a mean NDVI above 0.83. In summary the results of this analysis provided no clear indication of a relation between field size, spatial location, mean field clay content and mean field NDVI. Nevertheless, a weak link for WW and a stronger relation for SB between mean field slope and mean field NDVI was revealed. This implied, the potential of a lower mean field slope contributing to a higher crop growth. Whereas in fields with a high mean field slope crop growth tended to be inhibited when considering the drought conditions in 2018.

Field slope versus NDVI:

For WW, the two extreme groups had a MoM slope value of 3.2 % for the group NDVI <= Q1 and 2.8 % for the group NDVI > Q3 (see red dots in the Fig. 26 B1). Overall, the mean slope distributions were ranging from 0.6 % – 6.4 % for the group NDVI <= Q1, and from 0.6 % – 7.9 % for the group NDVI > Q3. Therefore, no well-elaborated relation was identified between mean field slope and mean field NDVI. Similarly results, were obtained for SB, but with a stronger relation of mean field slop and mean field NDVI. The MoM field slope values were 3.4 % for NDVI <= Q1 in comparison to 2.2 % for NDVI > Q3 (white dots in the Fig. 26 B2). The range of the mean slope distribution for NDVI > Q3 was noticeably narrower for SB fields. This indicated that, fields with gentle slopes had an increased crop growth compared to fields with steeper slopes. For SB fields of the group NDVI <= Q1,

75 % of fields had a mean field slope values ranging from 0.7 % – 4.6 %; while for fields with NDVI > Q3, 75 % of fields had mean field slope values ranging from 0.6 – 2.6 % (Fig. 26 B2).

Field clay content versus NDVI:

For WW, the two NDVI groups had a MoM clay content values of 16 % for the group NDVI <= Q1 and 13 % for the group NDVI > Q3, red dots in the Fig. 26 C1. For SB, the results were almost equal (white dots Fig. 26 C2). Subsequently, the response of mean field NDVI in relation to mean field clay content was weak for both WW and SB. Overall, no indication of a higher mean field NDVI in relation to a higher mean clay content was provided by both NDVI groups, see Fig. 26 C below.

Field size versus NDVI:

For both NDVI groups and crops the range of the field size distribution was almost equally wide. Therefore, no relation between field size and crop growth was found for both cereals (Fig. 26 D1 & D2).

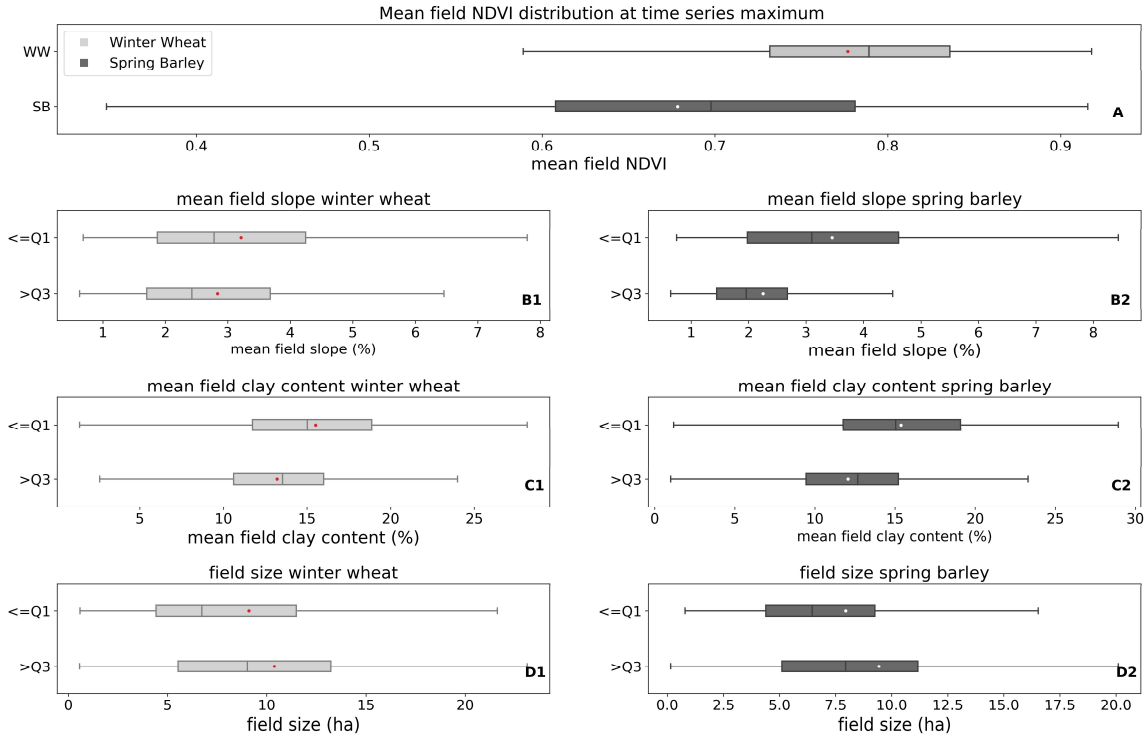

Fig. 26. Assessment of the field characteristics on drought resilience for both winter wheat (WW) and spring barley (SB). A: mean field NDVI boxplot at 24 of May for WW and 3rd of June for SB. B1, B2: Mean field slope. C1, C2: mean field clay content. D1, D2: Field size. MoM values are presented in red and white dotes.

Geographical location versus NDVI:

Mean field NDVI linked to field location revealed no definite spatial patterns for both cereals. However, there seemed to be a tendency of WW fields with NDVI > Q3 being located in the south-east of the study area (see Fig. 27).

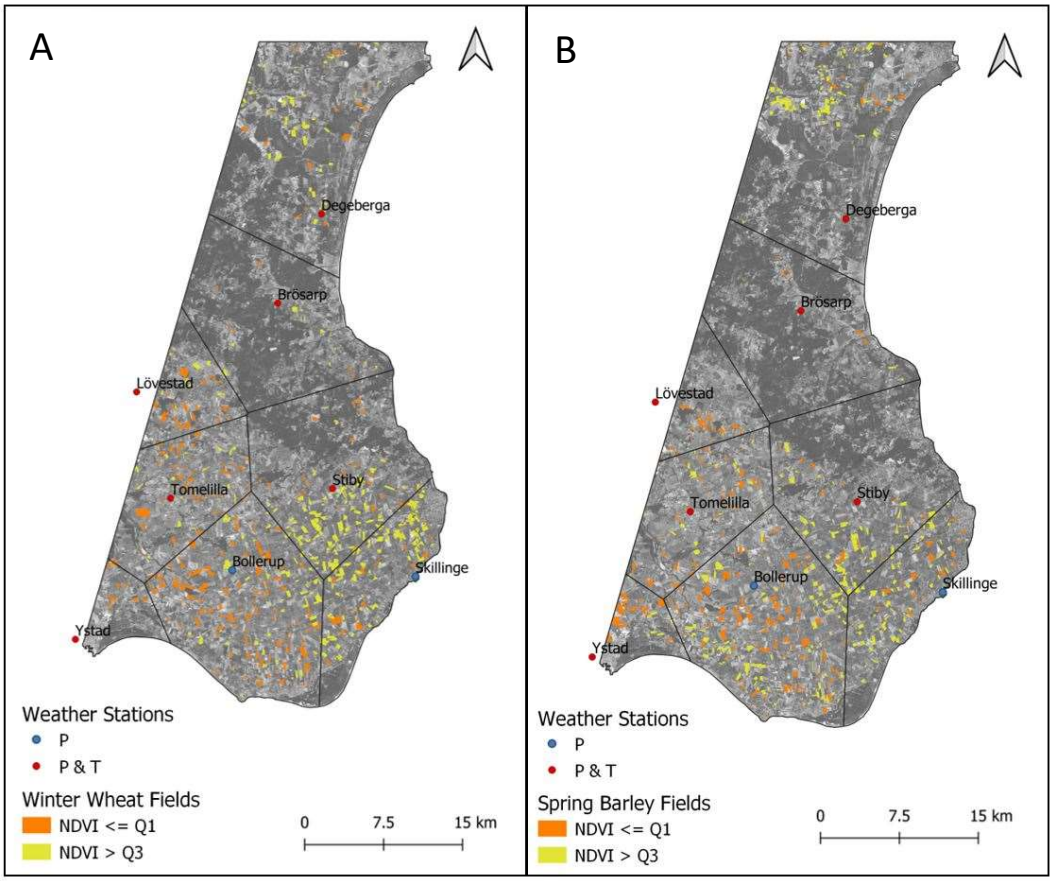

Fig. 27. Spatial field location in relation to mean NDVI performance (NDVI <= Q1 and NDVI > Q3). A: winter wheat fields. B: spring barley fields.

4.6. Crop growth development of nine fields

To better understand the effect of drought on crop growth development, nine fields were selected for WW and nine for SB. The selection was based on the three quartiles of the mean fields slope values of all WW/SB field successively cultivated in 2018 and 2019 (<=Q1, Q1–Q3, >Q3). The location of the nine WW and SB fields is presented in Fig. 12 in the methods section. The field size (ha) and mean field slopes (%) are presented in Tab. 6. The crop growth time series, for each field and both years, were drawn for the different indices (NDVI, NDWI, NDRE and NDDI) to visualize the effect of drought on crop growth.

Tab. 6. Mean field slope and field size of nine winter wheat and nine spring barley fields.

	Winter Wheat			Spring Barley		
Quartile	ID	Slope (%)	Size (ha)	ID	Slope (%)	Size (ha)
<=Q1	169	1.23	29.48	45	1.78	13.41
	275	1.84	21.24	243	1.59	19.59
	385	1.38	16.30	919	1.53	28.90
Q1-Q2	86	3.93	29.42	119	3.16	28.08
	239	3.03	36.62	121	3.13	44.10
	344	3.91	31.76	909	2.46	20.07
>Q3	47	7.86	12.10	138	6.25	8.91
	292	6.69	14.72	183	8.29	8.41
	389	4.63	31.54	885	8.80	9.16

4.6.1. Winter Wheat

In general, and for all the indices, there was a shift between index values in 2018 compared to 2019. The shift was negative for NDVI, NDRE and NDWI, while it was positive for NDDI. The minimum NDDI time-series values between Mai–June was on average 35 %, 52 % and 43 % higher in 2018 in comparison to 2019 for the slope classes <=Q1, Q1-Q3 and >Q3, respectively (Fig. 31). From the figures, it is noticeable that the time series maximum variability was much smaller in 2019 compared to 2018, for NDVI, NDRE and NDWI. This indicated an increased crop growth variability in response to drought in 2018. Hence, this confirmed the before stated effect of a higher crop growth variation in in response to drought. Crop growth tended to be homogeneous between fields under non-dry conditions, however. The standard deviation of the time series maximum of all nine fields was 5.0, 4.5 and 2.1 times lower in 2019 when compared to 2018 for NDVI, NDRE, NDWI respectively, see Fig. 28, 29, 30. Overall, the differences in crop growth development in response to drought could not be explained by mean field slope from the nine fields.

4.6.2. Spring Barley

The same results obtained for WW were obtained for SB. However, for SB the differences between 2018 and 2019 were much higher compared to WW. Subsequently, this indicated a higher effect of drought on SB in comparison to WW. The time series minimum NDDI values in June were on average 150 %, 146 % and 431 % higher in 2018 in comparison to 2019 for the slope classes <=Q1, Q1-Q3 and >Q3, respectively (Fig. 31). In comparison to WW the NDDI minimum differences of SB were much higher i.e., 4.2, 2.8 and 10 times. Hence, a higher drought-stress vulnerability of SB when compared to WW was obtained from these results. The standard deviation of the maximum time series value of all nine fields was 7.8, 3.75 and 4.5 times lower in 2019 in comparison to 2018 for NDVI, NDRE, NDWI respectively, see Fig. 28, 29, 30. The same remark noticed for WW, on crop growth homogeneity between fields under non-dry conditions was noticed for SB. Under dry conditions fields responded to drought with a higher degree of variation.

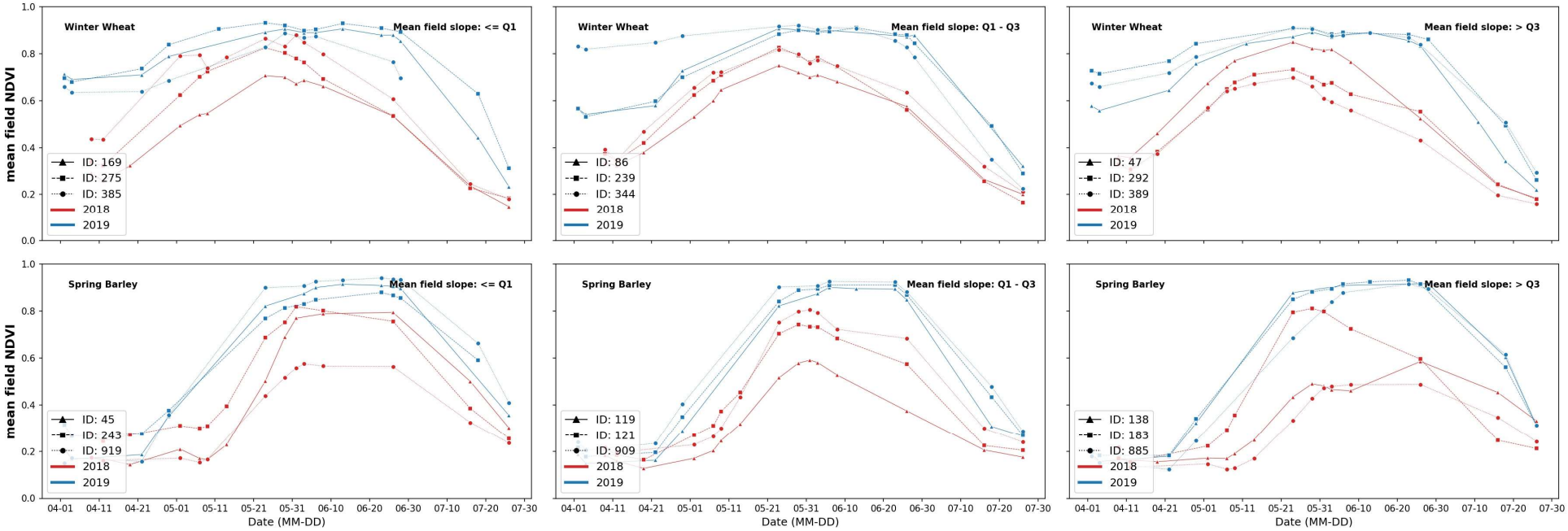

Fig. 28. Mean field NDVI time series for winter wheat (top row) and spring barley (bottom row) fields. First column: mean field slope <= Q. Second column: mean field slope Q1-Q3. Third column: mean field slope > Q3

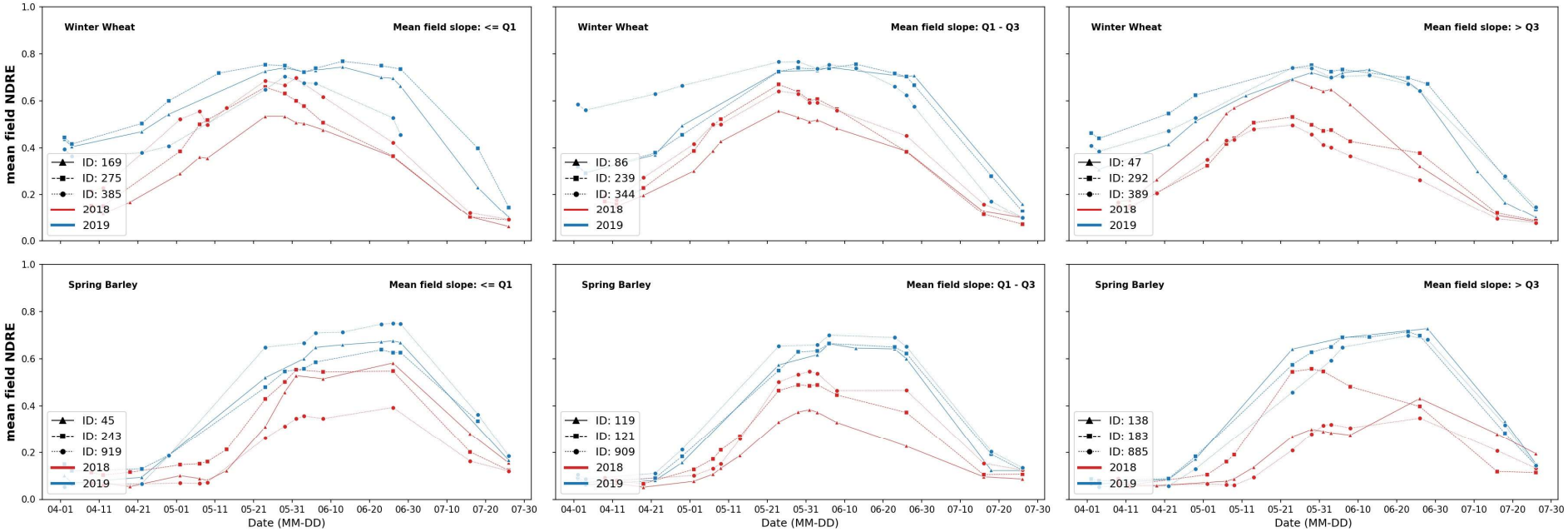

Fig. 29. Mean field NDRE time series for winter wheat (top row) and spring barley (bottom row) fields. First column: mean field slope <= Q. Second column: mean field slope Q1-Q3. Third column: mean field slope > Q3.

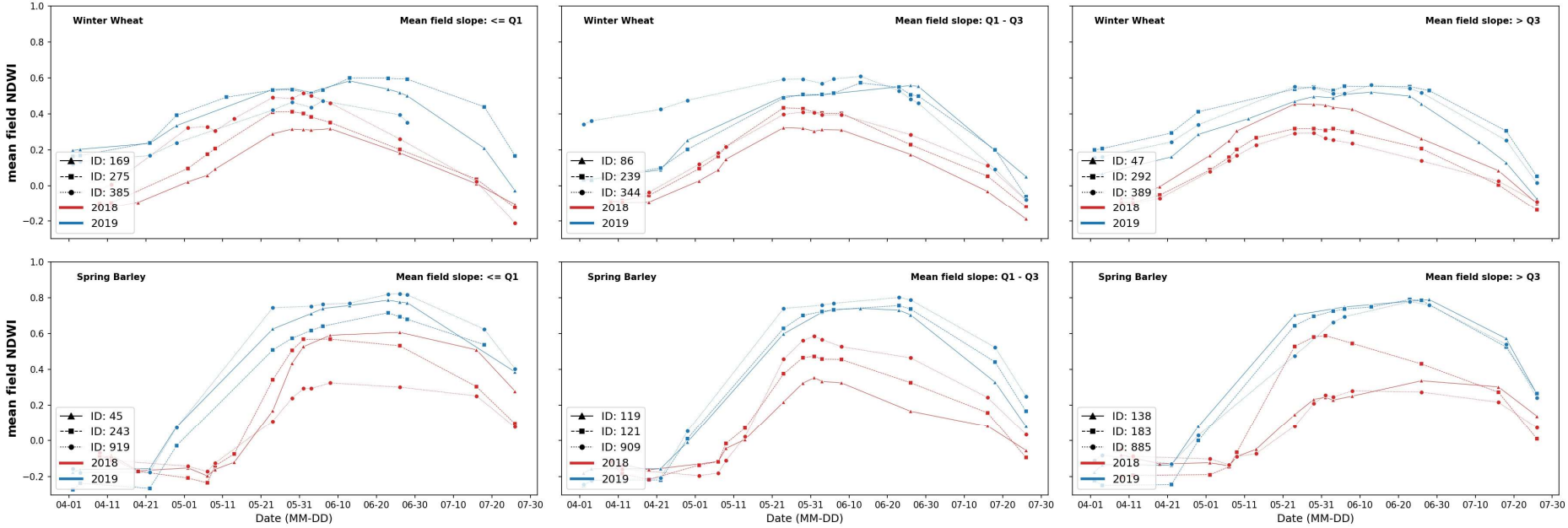

Fig. 30. Mean field NDWI time series for winter wheat (top row) and spring barley (bottom row) fields. First column: mean field slope <= Q. Second column: mean field slope Q1-Q3. Third column: mean field slope > Q3.

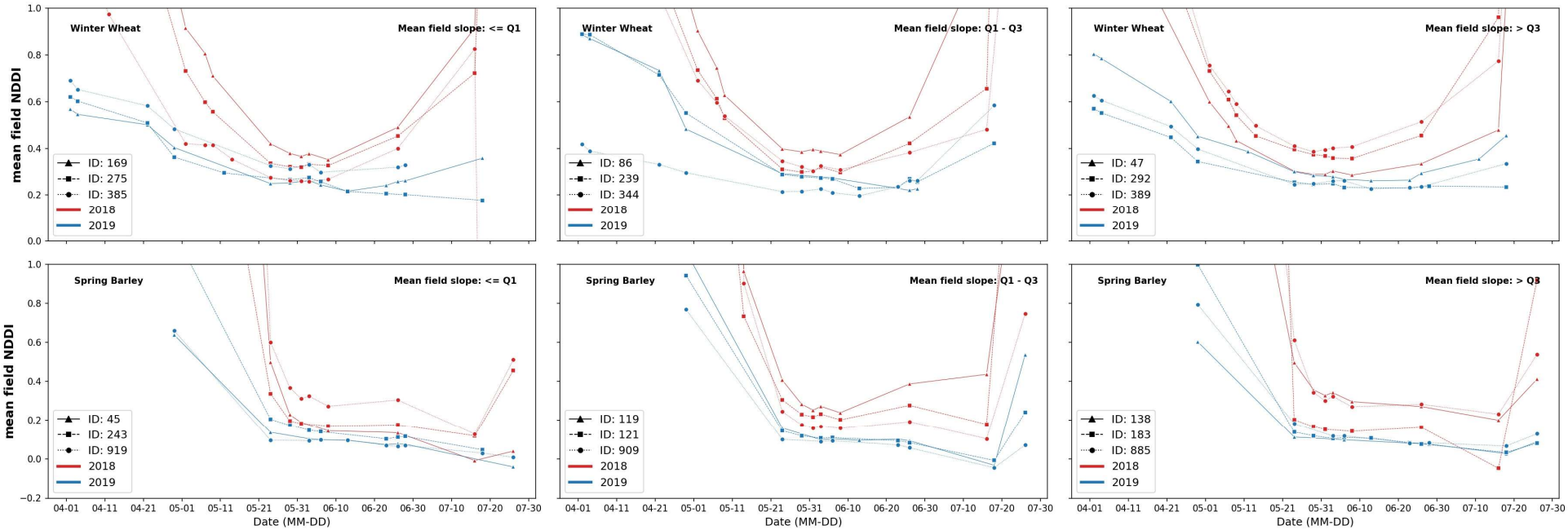

Fig. 31. Mean field NDDI time series for winter wheat (top row) and spring barley (bottom row) fields. First column: mean field slope <= Q. Second column: mean field slope Q1-Q3. Third column: mean field slope > Q3.

.

4.7. Within-field crop growth development

To evaluate possible crop growth variations related to topography, fields were divided into three zones, based on different topographic indices. Fields were divided based on RE, Slope and TWI maps. The within-field drought response was studied in those zones separately (section 3.5.3). Crop growth development was observed using NDVI and NDDI. This part of analysis was carried on the nine fields also used in the previous section 4.6. The results showed that within-field zonal variations of NDVI and NDDI were very small in the non-dry year 2019 for both SB and WW. While, in 2018, those variations were higher for both crops, and even higher for SB when compared to WW. Furthermore, fields zoning based on TWI showed the best results consistency (i.e., crop growth resilience improved in the same zonal order for all nine fields, lower zones were less resilient than upper) comparing to zoning based on RE and slope. The TWI zonal NDVI and NDDI crop growth development for the nine fields are presented in Fig. 32-35. Figures of zonal crop growth development based on RE and slope maps are appended.

4.7.1. Winter wheat

The difference between zones in terms of NDVI and NDDI development was quite small in 2019 regardless of the zoning method. In 2018 WW fields had a higher NDVI and NDDI variation considering the different zones, except for fields with a low mean field slope <= Q1. The highest consistency in NDVI and NDDI variations resulted from fields zoning based on TWI. Field zones with low TWI (steeper areas) were more vulnerable to drought in 2018. Results from zoning based on RE and slope were less consistent - meaning that sometimes, lower zones were more vulnerable to drought and sometime less, and vice versa.

4.7.2. Spring barley

For SB as for WW, the within-field crop growth development variations were quite small for NDVI and NDDI in 2019 and higher in 2018. Similarly, when compared to WW the highest consistency in NDVI and NDDI variations resulted from fields zoning based on TWI (zones with low TWI were more vulnerable to drought when compared to zones with medium to high TWI). The results from zoning based on RE and Slope were less consistent.

4.7.3. Quantitative assessment of within-field crop growth variations

To quantitatively assess the degree of within-field variations, the same approach applied on the nine fields, was applied on the three slope quartiles (<=Q1, Q1-Q3, >Q3) of all WW (n = 363) and SB (n = 230) fields cultivated successively in 2018 and 2019. From the results of the nine fields, zoning based on TWI and the NDVI index were chosen to carry out this analysis. The mean NDVI value in each zone was calculated at the time series maximum for each field separately. The date of the time-series maximum varied on the individual field level. The mean NDVI values were than aggregated by computing the MoM NDVI for each zone and all fields of the same slope quartiles (<=Q1, Q1-Q3, >Q3). The results and comparisons for WW and SB are presented in Tab. 7 an 8. Overall, the results showed that the influence of topography on crop growth development was negligible in the non-dry year 2019. In 2018, crop growth in high TWI zones was higher when compared to low TWI zones. This relation increased with an increase in mean field slope. Furthermore, within-field NDVI variations were smaller for WW in comparison to SB.

Winter Wheat:

The within-field MoM NDVI variations between the different zones for WW based on time series maximum values were quite small in 2019 for all slope quartiles (<=Q1, Q1-Q3, >Q3) (Tab. 7). In 2018, the within-field variation was on average negligible for fields with a low mean field slope(<=Q1). Whereas for fields with a medium to high mean field slope (Q1-Q3 and >Q3) the NDVI mean difference at the maximum value of the time-series, between zone three (higher TWI) and zone one (lower TWI) was 0.018 and between zone two (medium TWI) and zone one was 0.012 (Tab. 7).

Spring Barley:

For SB the same results as for WW were obtained. No NDVI variations between the different within-field zones were noticed in 2019 for all slope quartiles (<=Q1, Q1-Q3, >Q3) (Tab. 8). However, in 2018 within field variations, between the three zones, were noticeable for all slope quartiles (<=Q1, Q1-Q3, >Q3) with a tendency to increase with an increase in mean fields slopes. For example, the MoM of the NDVI differences between TWI zone three and zone one was 142 % higher between fields of the slope quantiles >Q3 compared to <=Q1 and was 92 % higher between fields of the slope quantiles Q1-Q3 compared to <=Q1 (Tab. 8). Furthermore, the results showed that in dry years, zones with a higher TWI had a higher NDVI compared to zones with a lower TWI. This indicated a higher resilience of zones with a higher TWI in response to drought.

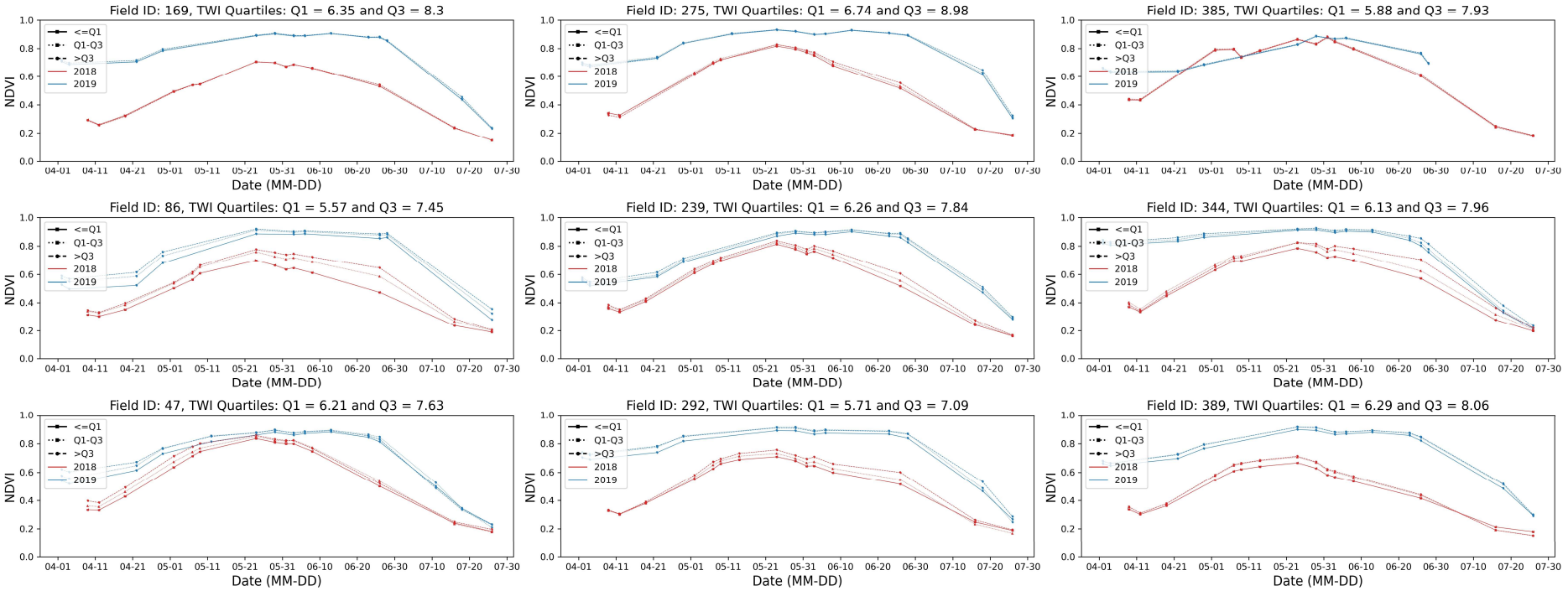

Fig. 32. Winter wheat-within field NDVI crop growth development variations for the nine fields, zoning method based on TWI maps.

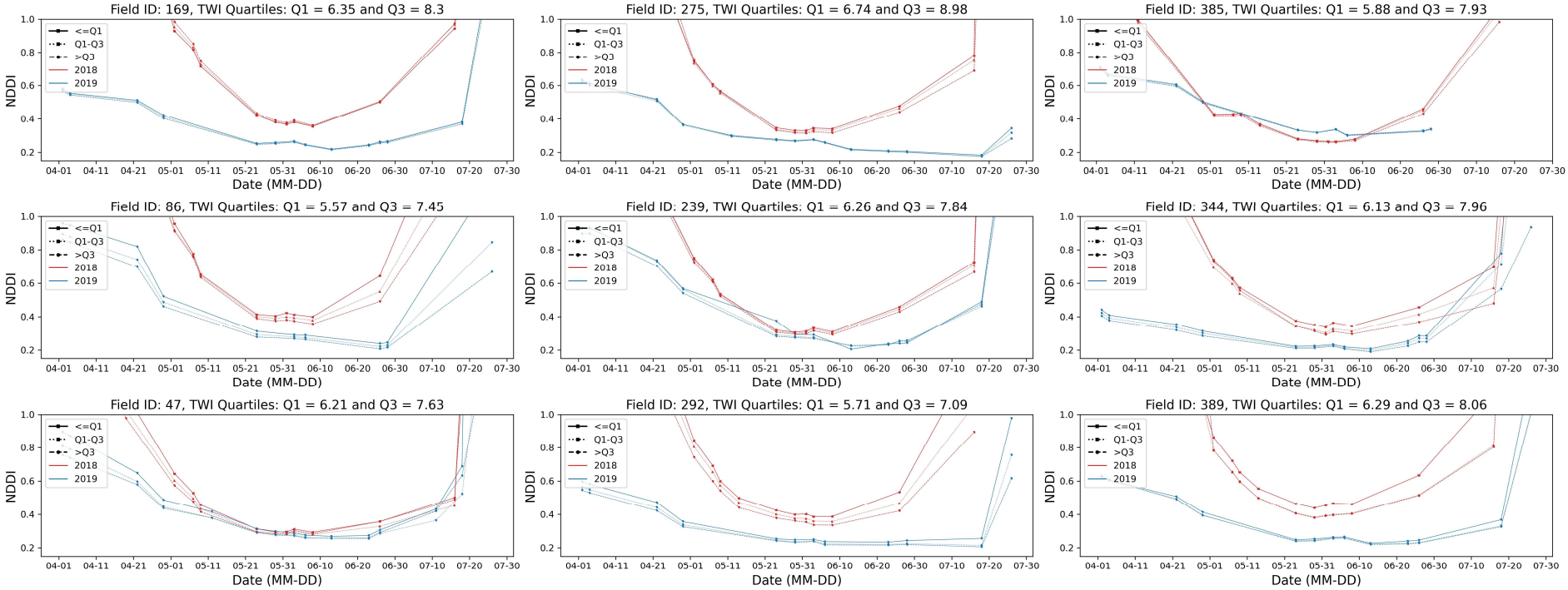

Fig. 33. Winter wheat-within field NDDI crop growth development variations for the nine fields, zoning method based on TWI maps.

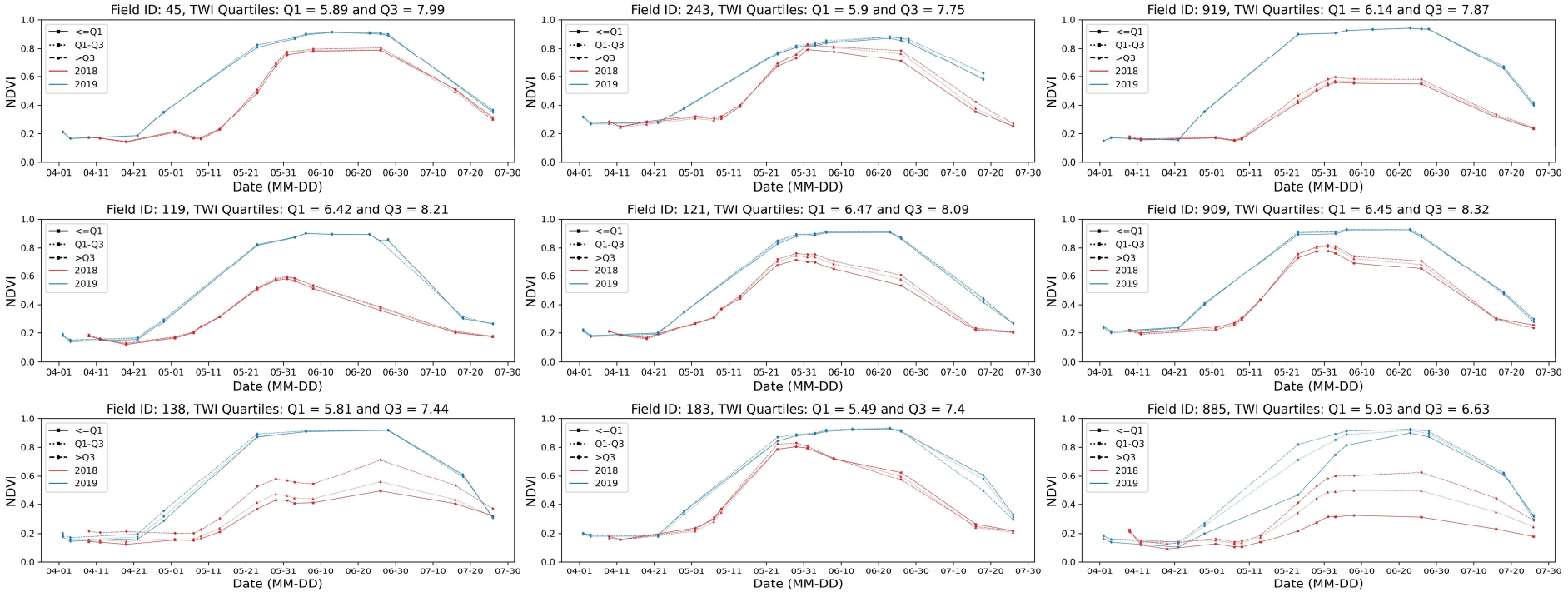

Fig. 34. Spring barley within-field NDVI crop growth development variations for the nine fields, zoning method based on TWI maps.

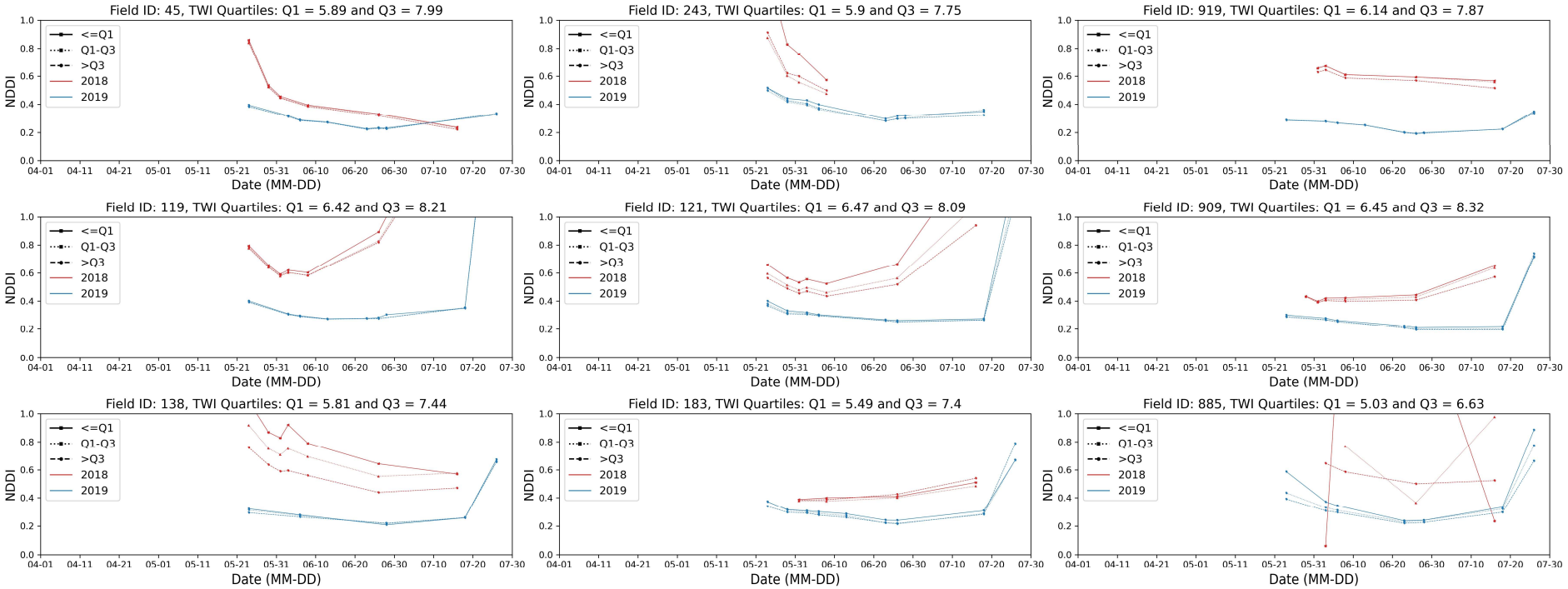

Fig. 35. Spring barley within-field NDDI crop growth development variations for the nine fields, zoning method based on TWI maps.

Tab. 7. Winter wheat, NDVI (MoM) values (based on the time series maximum of the individual fields), in the three different TWI zones (1, 2, 3) in 2018 and 2019 in relation to the mean field slope categories (1 = low TWI, 2 = medium TWI, 3 = high TWI).

Slope Category	n	1 NDVI	2 NDVI	3 NDVI	Δ (2 – 1)	Δ (3 – 1)	Δ (3 – 2)	Year
<=Q1	91	0.781	0.783	0.787	0.002	**0.006**	0.004	2018
Q1-Q3	181	0.778	0.787	0.791	0.009	**0.012**	0.004	
>Q3	91	0.778	0.791	0.796	0.013	**0.018**	0.005	
<=Q1	91	0.914	0.916	0.917	0.002	0.003	0.001	2019
Q1-Q3	181	0.913	0.917	0.918	0.004	0.005	0.002	
>Q3	91	0.912	0.916	0.918	0.004	0.006	0.002	

Tab. 8. Spring barely, NDVI (MoM) values (based on the time series maximum of the individual fields), in the three different TWI zones (1, 2, 3) in 2018 and 2019 in relation to the mean field slope categories (1 = low TWI, 2 = medium TWI, 3 = high TWI).

Slope Category	n	1 NDVI	2 NDVI	3 NDVI	Δ (2 – 1)	Δ (3 – 1)	Δ (3 – 2)	Year
<=Q1	58	0.736	0.742	0.749	0.006	**0.014**	0.008	2018
Q1-Q3	114	0.689	0.702	0.716	0.014	**0.027**	0.014	
>Q3	58	0.682	0.700	0.716	0.018	**0.034**	0.016	
<=Q1	58	0.911	0.913	0.914	0.003	0.003	0.000	2019
Q1-Q3	114	0.908	0.911	0.913	0.003	0.004	0.001	
>Q3	58	0.901	0.906	0.907	0.005	0.006	0.001	

4.7.4. NDDI maps

The NDDI reflects upon the crop drought status. Therefore, NDDI maps can reveal different levels of drought-stress within the field. The aim of this section is to present NDDI maps to show the spatial-temporal variation of drought stress of three WW fields and three SB fields for both years 2018 and 2019. These three fields were selected based on the mean field slope quartiles (<=Q1, Q1-Q3, >Q3) - one field out of each slope category. The results are presented in Fig 36-41. RE, Slope and TWI and clay content maps, are presented besides NDDI maps. In summary, NDDI maps revealed a non-uniform drought response of both WW and SB within the field in 2018. Drought-stress in SB fields was higher in comparison to WW fields. The below listed points can serve as interpretation guidelines when visually inspecting the presented NDDI maps by eye:

- The fields reached higher NDDI values in 2018 in comparison 2019.
- The NDDI variability range within the field was higher in 2018 with NDDI distributed as patches. In 2019, the NDDI distribution within the field was more uniform. Hence, a non-uniform drought response for all selected fields in 2018 was indicated.
- On average, the NDDI standard deviation of all three WW and SB fields was 11.4 times higher in 2018 compared to 2019 when considering all available maps in June.
- As described above, the drought affected SB fields more than WW fields in 2018. Higher values of NDDI were noticed for SB fields in comparison to WW fields. Subsequently, WW showed a higher drought resilience compared to SB in response to drought in 2018.

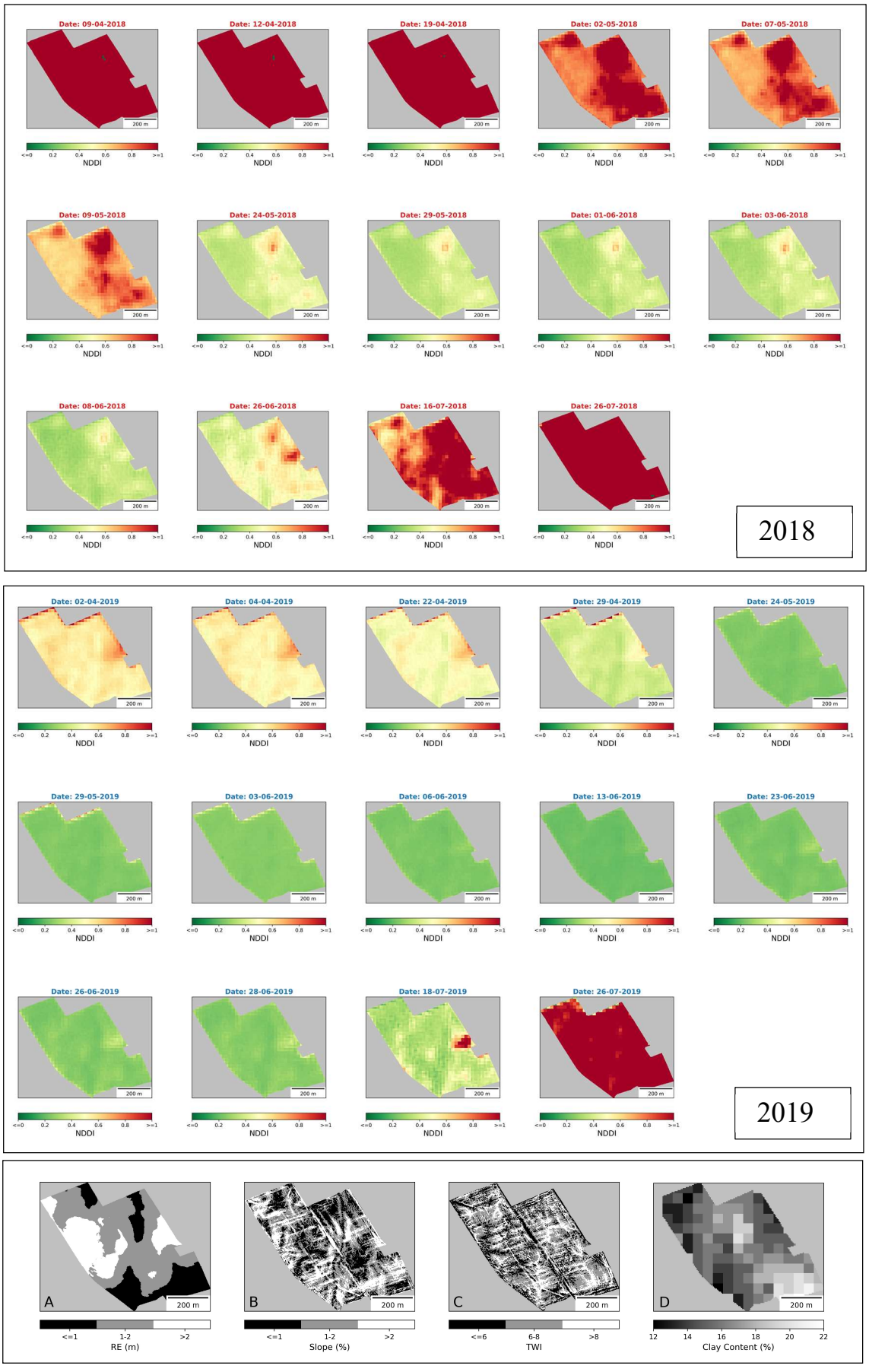

Fig. 36. NDDI maps of winter wheat field: ID 169. Spatiotemporal NDDI development in 2018 and 2019. Field topography (RE, Slope and TWI) maps and clay content are presented at the bottom.

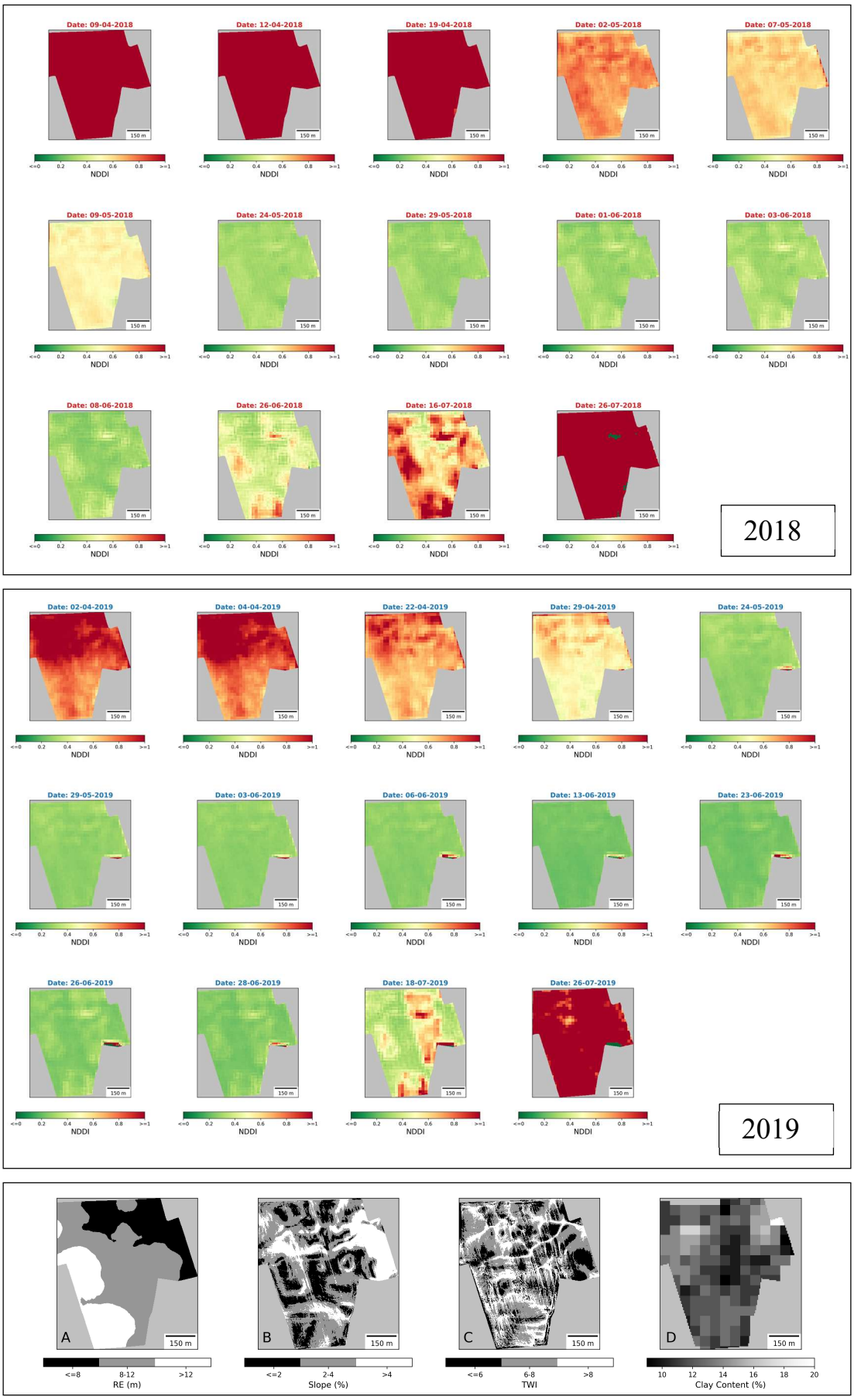

Fig. 37. NDDI maps of winter wheat field: ID 239. Spatiotemporal NDDI development in 2018 and 2019. Field topography (RE, Slope and TWI) maps and clay content are presented at the bottom.

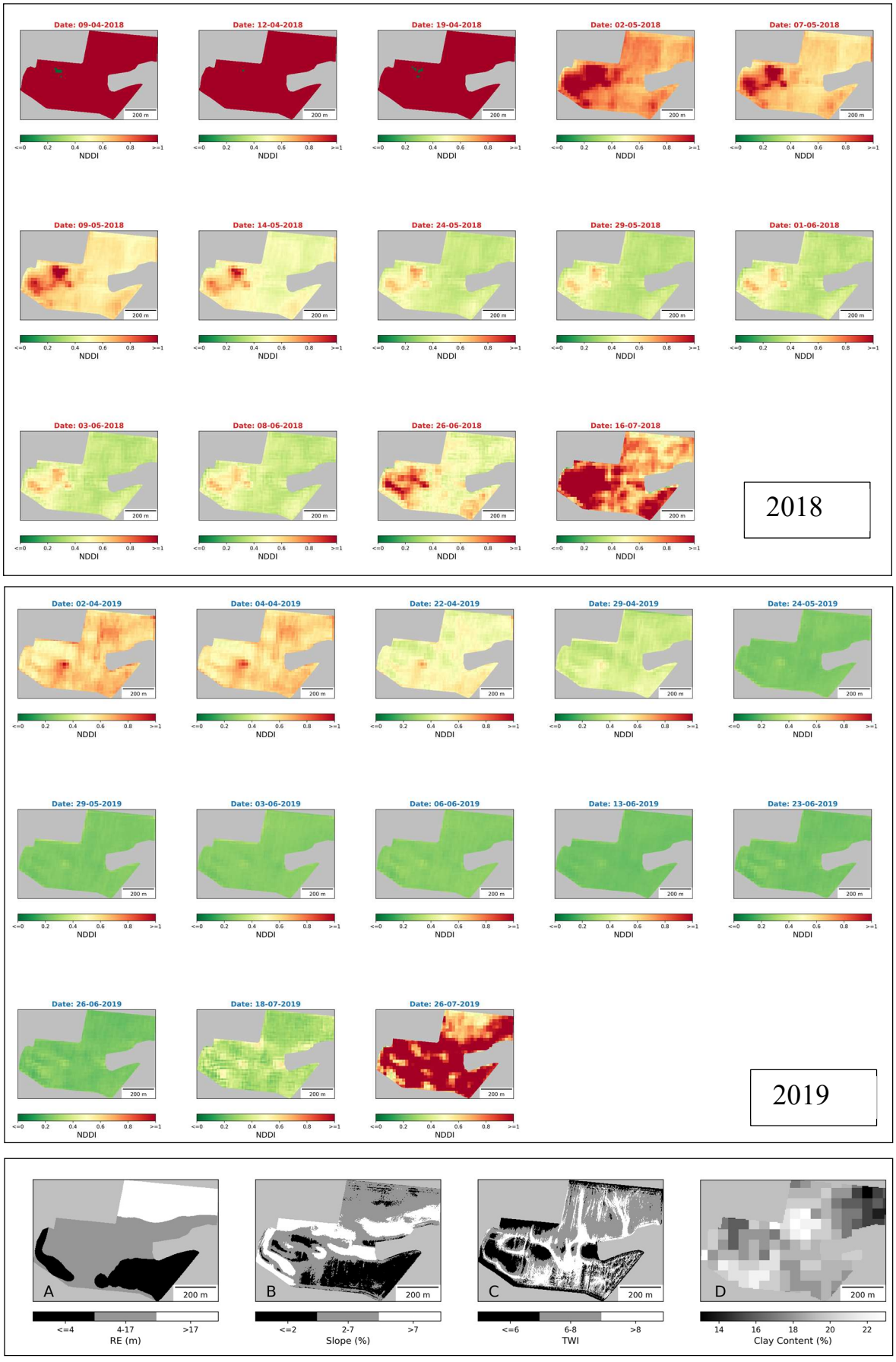

Fig. 38. NDDI maps of winter wheat field: ID 389. Spatiotemporal NDDI development in 2018 and 2019. Field topography (RE, Slope and TWI) maps and clay content are presented at the bottom.

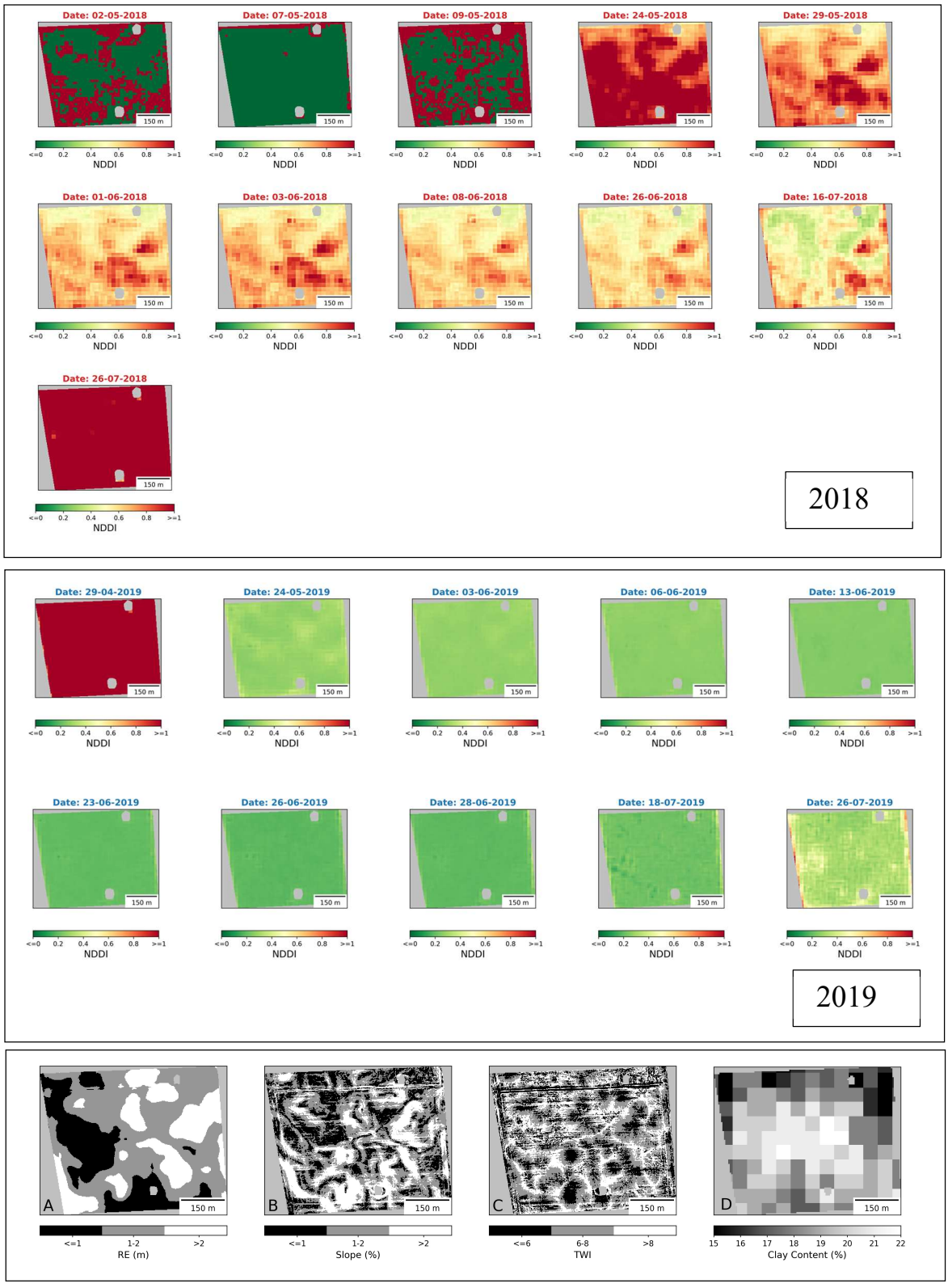

Fig. 39. NDDI maps of spring barley field: ID 919. Spatiotemporal NDDI development in 2018 and 2019. Field topography (RE, Slope and TWI) maps and clay content are presented at the bottom.

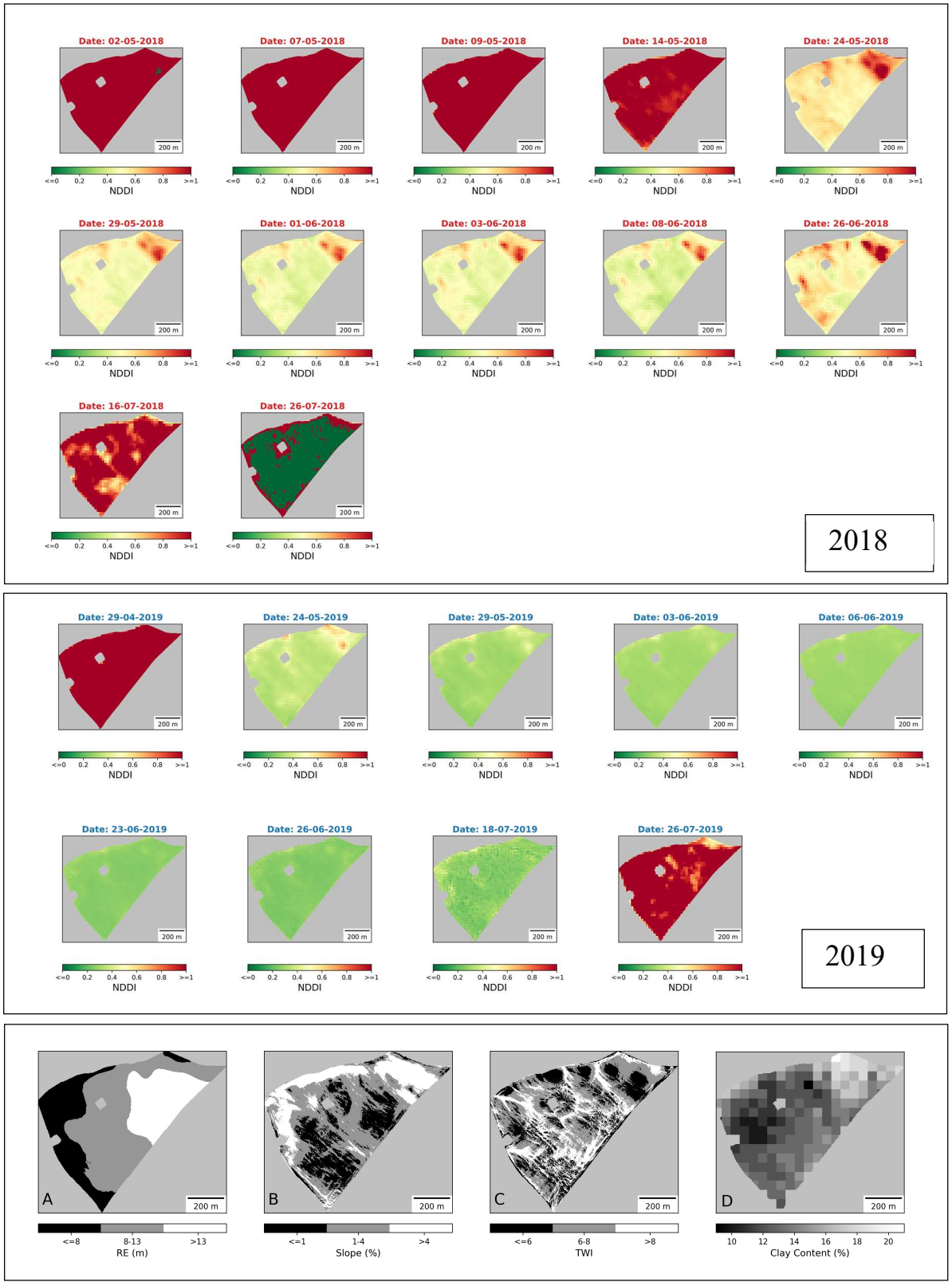

Fig. 40. NDDI maps of spring barley field: ID 121. Spatiotemporal NDDI development in 2018 and 2019. Field topography (RE, Slope and TWI) maps and clay content are presented at the bottom.

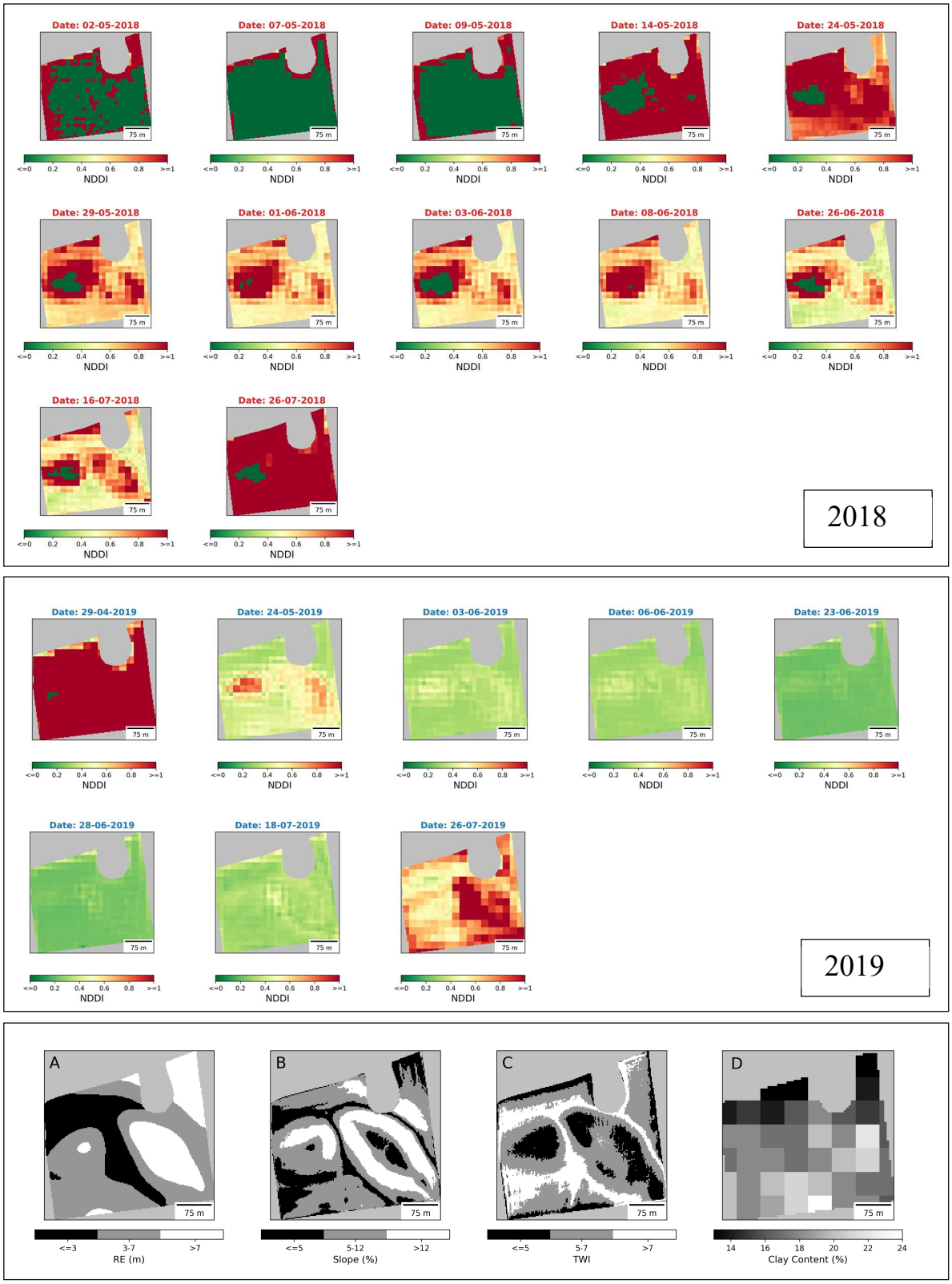

Fig. 41. NDDI maps of spring barley field: ID 885. Spatiotemporal NDDI development in 2018 and 2019. Field topography (RE, Slope and TWI) maps and clay content are presented at the bottom.

5. Discussion

The aim of this study was to assess the effect of topography in relation to drought of two field crops (WW, SB). A multi-scale analysis using satellite images was carried out from within-field to the total study area. Several indices related to vegetation growth and drought stress were utilized in this analysis (NDVI, NDRE, NDWI and NDDI). Topographic indies i.e., slope, RE and TWI maps were elaborated from a high-resolution DEM. In the following sections the results are discussed, and general conclusions are retrieved.

5.1. Drought response of WW and SB

Considering all vegetation indices used in this study, the results indicated that both WW and SB production were negatively affected by the extreme dry summer of 2018. The degree of the drought effect varied, with WW production being less affected compared to SB. This was supported by average yield (in kg/ha) data for the region of Skåne. In 2018, WW and SB yields were 43.2 % and 51.5 % lower in comparison to 2019, confirming that SB production was more affected by dry conditions compared to WW (SCB 2018, 2019). Similar results were found by a study from Czech Republic, where SB compared to winter crops was significantly more affected by dry conditions (Hlavinka et al. 2009).

The different response of SB and WW to drought can possibly be explained by the root-depth, which is of fundamental importance for water uptake, especially during dry conditions (Richards et al. 2002). Furthermore, Richards et al. pointed out, that an earlier sowing time is the easiest way to increase the overall root-depth. Thorup-Kristensen et al. (2009) showed a root-depth twice as high for winter wheat (2.2 m) in comparison to spring wheat (1.1 m). In another study by Djanaguiraman et al. (2019) a difference in depth of WW in comparison to spring wheat roots, penetrating soils 1.5 times deeper was elaborated. Although, these results are for wheat, the general principles are supposed to be applicable for spring and winter barley cultivars. In summary, the observed difference in drought resilience between WW and SB can possibly be linked to a higher root-depth of WW compared to SB.

5.2. Within-field variation

The results showed that within-field variation, considering NDVI and NDDI, was prominent in 2018 and not indicated in 2019. TWI seemed to be the most consistent topographic index in explaining this variation when compared to RE or Slope. An high influence of topography linked to within-field variation in dry years compared to non-dry years is supported by Kumhálová et al. (2011), Chi et al. (2009) and Kaspar et al. (2003). Furthermore, a study by Pilesjö et al. (2005) showed that topography can potentially be used to delineate within-field agricultural management zones in central Sweden. Nevertheless, explaining within-field variation of NDVI and NDDI in dry years by topography only might be biased, enabling a risk to underestimate the actual within-field variability. Besides, topography other circumstances may contribute to within-field drought response variations. To name a few examples possibly relevant: soil texture, organic carbon content, compacted layers, or the presence of shallow ground water.

5.3. Implementation opportunities for precision agriculture in Sweden

Decision support systems (DSSs) for precision agriculture are mostly build and developed upon proximal and remote sensing data. Globally, many different web-service are available using remote sensing data for DSSs. To name a few examples from Europe, FieldSense and SatAgro provide DSSs based on Sentinel-2 and Landsat remote sensing data. Advantages of the mentioned DSSs and how they can be used for PAP are outlined in two case studies from Denmark and Poland, conducted by the European association of remote sensing companies (EARSC 2018, 2019). Some of the advantages pointed out in those studies were: reduced crop scouting time for farmers, irrigation timing and management, optimizing the application of fertilizers.

In Sweden, the web-based service CropSAT developed by SLU, owned by the company Dataväxt, provides free of charge global decision support maps based on Sentinel-2 data. Currently, CropSAT mainly operates as a DSS providing site-specific information for variable rate application (VRA) of nitrogen fertilizer, besides vegetation maps. A study by the federation of Swedish farmers showed that in 2020 about 100,000 – 200,000 hectares of arable land cultivated with wheat were managed using PAP for improved fertilizing (LRF 2020). As stated in the introduction, the drought frequency is expected to increase in the 21st century at the global scale (Cook et al. 2014). Hence, an increasing irrigation demand is expected for Sweden as outlined in a recent study (Grusson et al. 2021). In consequence, there is an increasing need for DSSs providing information on drought magnitude

as well as DSSs for advanced irrigation management at the field level, to better cope with drought induced water stress in the future.

5.3.1. Historical and near-real time monitoring of crop growth development

This study showed that crop growth development can be monitored at different scales (field scale and within-field scale) using vegetation and drought indices and using automatization tools like Python and GDAL. Studying historical data can improve the understanding of crop growth in response to drought. In turn historical data from past years is required when assessing the crop drought status near-real time. Furthermore, crop growth development monitoring can identify fields which are more vulnerable or resilient to drought, enabling to develop relevant site-specific management strategies. Such information can help to intervene at the right time and place to mitigate drought effects. Hence, to assess the effect of drought in the future in near-real time, a crop growth development monitoring system is needed.

In conclusion, a suggestion of this study is to develop a near-real time crop growth development monitoring system, at different scales from field to district level. Potentially, this could enable an improved drought response assessment within the field, within the district and between different districts to manage drought in a better way.

5.3.2. Topography as a site-specific drought management

Topography is one site-specific factor contributing to an enhanced understanding of the within-field drought response, enabling precision agriculture improvements. Subsequently, topography is a promising factor to evaluate the within-field drought risk prior to a drought event, potentially increasing the preparedness of farmers. The results of this study showed that topography is a main factor influencing within-field variability of NDVI and NDDI in dry years. It was further evaluated that within-field crop growth variability was less important in fields with a relatively low mean field slope. However, for SB the within-field crop growth variability was higher in fields with medium to high mean field slope. In general, topography is a factor among others controlling within-field crop growth in response to drought. Nonetheless, it remains uncertain how efficient the different topographical indices are to delineate within-field drought management zones.

5.3.3. NDDI maps for irrigation management

Considering, the presented NDDI maps, areas affected by drought did not necessarily correspond to field topography or clay content when visually inspected (Fig. 42). This indicated that variability of within-field crop growth development could not be explained by field topography only. Therefore, NDDI maps are necessary to investigate the within-field spatiotemporal development of the vegetation drought status. In a study from Sweden by Campana et al. (2018) the authors elaborated the potential benefit of irrigation in the context agricultural drought to counteract yield losses. The study showed that yields were reduced by up to 50 % if irrigation measures were not implemented. Grusson et al. (2021) outlined an increased need for irrigation especially in the early season (May – June) for cereal crops in Sweden, considering future climate changes. DSSs for irrigation requirement assessment and management are increasingly needed in Sweden to adapt to climate change. Therefore, NDDI maps could potentially be utilized as decision support for precision irrigation.

5.4. Future improvements

Automatization

Apart from masking of clouds and cloud shadows, most of the analytical parts of this study have been conducted by developing automatization algorithms. Nevertheless, to implement the suggested tools (i.e., NDDI maps and near-real time crop growth development monitoring) in the context of a DSSs for precision agriculture in Sweden, an automated detection and removal of clouds will be necessary. For Sentinel-2 data several algorithms for the detection of clouds are available. In a study by Tarrio et al. (2020) the authors achieved the best cloud cover detection, by using an ensemble of approach, combining the results of several algorithms. In this study, clouds were masked manually for the total study area (see Fig. 4). In order, to improve the efficiency of the developed algorithms, instead of masking clouds manually, a quality control for the input satellite images at the field level is suggested, irrespectively to the original cloud coverage percentage. Detecting clouds and cloud shadows at the field level might most likely increase the accuracy of any used detection algorithm. Deciding automatically, instead of manually, if a satellite image could be used versus discarded (cloud free field versus cloud covered) in the analysis will make the algorithm applicable for DSSs development.

Which resolution to use?

In this study, the resolution of the input datasets varied: DEM (2m), Sentinel-2 (10 - 20m), soil texture maps (50m). For, example one 20 m Sentinel-2 pixel incorporates 100 DEM pixels. Hence, the resolution of Sentinal-2 data was virtually increased to 2 m to optimize clipping and thus to prevent information losses at the field boundaries. Nevertheless, future studies should evaluate which resolution is optimal while preserving the result quality. This question should especially be evaluated for the DEM. Since topographic indices maps for fields with a low mean field slope were very scattered, it made it difficult to split the field in zones manageable for precision agriculture.

Sentinel-2 offset

In a recent study by Rufin et al. (2021) the authors elaborated a spatial offset between Sentinel-2A/B with a mean shift of 14 m in x direction and 13.4 m in y-direction. In this study, this offset was generally ignored. Nevertheless, when displaying the spatiotemporal crop growth development at the field level using the graphics interchange format (GIF) in motion, the described offset was visible at the field level. Therefore, future studies should elaborate how relevant this offset is when describing within-field crop growth development for PAP in Sweden. Therefore, the *operational coregistration* approach suggested by Rufin et al. (2021) could possibly be used to improve the overall result quality of this study.

Deductive versus inductive data analysis and within field variability

A deductive approach was used to investigate within-field crop growth development variability based on field topography in this study. The results indicated that field topography seemed to influence crop drought response in fields with medium to high mean field slope. The variability of within-field crop growth development was however not detected in fields with low mean field slope (rather flat fields). However, from this perspective it cannot be concluded that the variability of within-field crop growth development does not occur in flat fields. The results rather indicated that within-field variability was not detected when splitting the fields based on RE, slope or TWI maps into zones, especially in flat fields. In Fig. 42 below it is clearly noticeable that within-field crop growth variability of the presented WW field (ID 169) did not correspond to the field topography. Subsequently, it is very important to mention that variations in crop growth are also caused by variations in other environmental factors except drought. Such factors can be nutrient deficiencies, poor crop establishment or disease etc. Subsequently, using an inductive approach to delineate zones of elevated and reduced crop growth within the field in response to drought or possibly other factors, might be useful. An increased accuracy in detecting within-field crop growth variability is associated with an inductive approach since it is unbiased.

Potentially, using an inductive approach for data analysis could help to develop an advanced splitting base to delineate drought management zones at the field level.

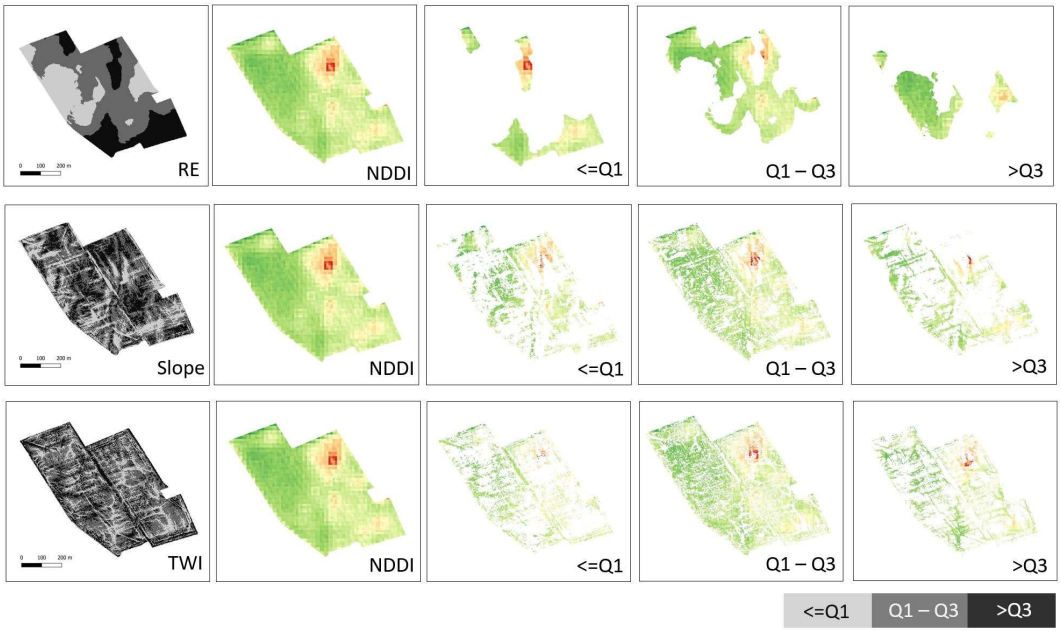

Fig. 42. Showing the inaccuracy in zoning the field based on topographical indices maps, to visualize the drought response within the field.

6. Conclusion

This study assessed the usage of NDVI, NDRE, NDWI and NDDI to evaluate the effect of drought on two cereal crops (winter wheat and spring barley) in the south of Sweden. Therefore, the drought effect along the study period (crop development stages DC31-DC75) on crop growth development was related to field topography and was assessed in a dry year (2018) and compared to a non-dry year (2019). The results showed that winter wheat and spring barley were both affected in the dry year of 2018 but by a different degree - winter wheat was less affected compared to spring barley. An average reduction over the study period of NDVI, NDRE and NDWI in 2018 compared to 2019 of about 25 %, 32 % and 58 % for winter wheat and about 36 %, 43 % and 69 % for spring barley was observed. Furthermore, the results clearly indicated that field topography is an important site-specific factor when reasoning within-field drought stress and crop growth variations. Topographic related within-field crop growth variability increased with an increase in mean field slope. The topographic wetness index (TWI) was the most efficient index in explaining crop growth variations within the field. Topography related crop growth variability was negligible in fields with a low mean field slope as well as during non-dry conditions in 2019. Overall, topography proved to be a major factor when explaining crop growth development variations within the field under dry conditions. Subsequently, topography as a site-specific field characteristic can help farmers to adapt to climate change, mitigating droughts in the future. However, further work is required to use topography as a site-specific factor for precision agriculture practices in an appropriate way. Therefore, a more accurate field zoning for drought monitoring and assessment is crucial to enable an advanced site-specific drought management.

Acknowledgements

Very special thanks are dedicated to my supervisor Omran Alshihabi - thank you for the high-quality support, being available online via E-mail and zoom answering and discussing my questions and results as well as giving valuable feedback on the written part of this study. Furthermore, I would like to thank Kristin Piikki acting as my co-supervisor, providing very valuable feedback and remarks, answering my questions, and helping me to improve the overall quality of this work. This work was part of the "Baby Grain Passport" project which is funded by Formas national research programme for food (contract: 2019-02280). I would like to thank my study friends Neerajaa and Sheryl. We always stayed connected online motivating each other, sharing our experiences throughout the process. I also would like to take the opportunity to thank my friends Jana and Therese for proofreading this work. Further, I would like to thank SLU's department of soil water and environment research staff in Uppsala and Skara as well as SLU's non-scientific staff. Studying at SLU was an amazing experience!

I would like to thank my parents making it is possible to go and study abroad.

References

Anaconda (2021). *Anaconda Software Distribution*. Version: Vers. 2-2.4.0. https://anaconda.com

Beven, K.J. (2011). *Rainfall-Runoff Modelling: The Primer*. John Wiley & Sons.

Campana, P.E., Zhang, J., Yao, T., Andersson, S., Landelius, T., Melton, F. & Yan, J. (2018). Managing agricultural drought in Sweden using a novel spatially-explicit model from the perspective of water-food-energy nexus. *Journal of Cleaner Production*, 197, 1382–1393. https://doi.org/10.1016/j.jclepro.2018.06.096

Campbell, B.M., Beare, D.J., Bennett, E.M., Hall-Spencer, J.M., Ingram, J.S.I., Jaramillo, F., Ortiz, R., Ramankutty, N., Sayer, J.A. & Shindell, D. (2017). Agriculture production as a major driver of the Earth system exceeding planetary boundaries. *Ecology and Society*, 22 (4). https://www.jstor.org/stable/26798991 [2021-07-18]

Chi, B.-L., Bing, C.-S., Walley, F. & Yates, T. (2009). Topographic Indices and Yield Variability in a Rolling Landscape of Western Canada. *Pedosphere*, 19 (3), 362–370. https://doi.org/10.1016/S1002-0160(09)60127-2

Cook, B.I., Smerdon, J.E., Seager, R. & Coats, S. (2014). Global warming and 21st century drying. *Climate Dynamics*, 43 (9), 2607–2627. https://doi.org/10.1007/s00382-014-2075-y

Delin, S. & Berglund, K. (2005). Management Zones Classified With Respect to Drought and Waterlogging. *Precision Agriculture*, 6 (4), 321–340. https://doi.org/10.1007/s11119-005-2325-4

Djamai, N. & Fernandes, R. (2018). Comparison of SNAP-Derived Sentinel-2A L2A Product to ESA Product over Europe. *Remote Sensing*, 10 (6), 926. https://doi.org/10.3390/rs10060926

Djanaguiraman, M., Prasad, P.V.V., Kumari, J. & Rengel, Z. (2019). Root length and root lipid composition contribute to drought tolerance of winter and spring wheat. *Plant and Soil*, 439 (1), 57–73. https://doi.org/10.1007/s11104-018-3794-3

Du, T.L.T., Bui, D.D., Nguyen, M.D. & Lee, H. (2018). Satellite-Based, Multi-Indices for Evaluation of Agricultural Droughts in a Highly Dynamic Tropical Catchment, Central Vietnam. *Water*, 10 (5), 659. https://doi.org/10.3390/w10050659

EARSC (2018). Sentinels Benefits Study (SeBS) - A Case StudyFarmManagement Supportin Denmark. https://earsc.org/sebs/wp-content/uploads/2019/03/Farm-management-in-Denmark-Full-case.pdf [2021-07-26]

EARSC (2019). Sentinels Benefits Study (SeBS) - A Case StudyFarm Management Support in Poland. https://earsc.org/sebs/wp-content/uploads/2020/02/SeBS-Case-Agriculture-in-Poland.pdf [2021-07-26]

ESA (2021). *MSI Instrument – Sentinel-2 MSI Technical Guide – Sentinel Online - Sentinel Online*. https://sentinels.copernicus.eu/web/sentinel/technical-guides/sentinel-2-msi/msi-instrument [2021-08-12]

ESA (2021). *Open Access Hub*. https://scihub.copernicus.eu/ [2021-05-12]

ESA (2021). *Sentinel-2 - Missions - Sentinel Online - Sentinel*. https://sentinel.esa.int/web/sentinel/missions/sentinel-2 [2021-05-12]
Gao, B. (1996). NDWI—A normalized difference water index for remote sensing of vegetation liquid water from space. *Remote Sensing of Environment*, 58 (3), 257–266. https://doi.org/10.1016/S0034-4257(96)00067-3
GDAL/OGR contributors (2021). *GDAL/OGR Geospatial Data Abstraction software Library*. Open Source Geospatial Foundation. https://gdal.org
Gebbers, R. & Adamchuk, V.I. (2010). Precision Agriculture and Food Security. *Science*, 327 (5967), 828–831. https://doi.org/10.1126/science.1183899
GET (2021). *Geodata Extraction Tool*. https://zeus.slu.se/get [2021-05-12]
Godfray, H.C.J., Beddington, J.R., Crute, I.R., Haddad, L., Lawrence, D., Muir, J.F., Pretty, J., Robinson, S., Thomas, S.M. & Toulmin, C. (2010). Food Security: The Challenge of Feeding 9 Billion People. *Science*, 327 (5967), 812–818. https://doi.org/10.1126/science.1185383
GRASS Development Team (2020). *Geographic Resources Analysis Support System (GRASS GIS) Software, Version 7.2*. Open Source Geospatial Foundation. http://grass.osgeo.org
Grusson, Y., Wesström, I. & Joel, A. (2021). Impact of climate change on Swedish agriculture: Growing season rain deficit and irrigation need. *Agricultural Water Management*, 251, 106858. https://doi.org/10.1016/j.agwat.2021.106858
Gu, Y., Brown, J.F., Verdin, J.P. & Wardlow, B. (2007). A five-year analysis of MODIS NDVI and NDWI for grassland drought assessment over the central Great Plains of the United States. *Geophysical Research Letters*, 34 (6). https://doi.org/10.1029/2006GL029127
Hlavinka, P., Trnka, M., Semerádová, D., Dubrovský, M., Žalud, Z. & Možný, M. (2009). Effect of drought on yield variability of key crops in Czech Republic. *Agricultural and Forest Meteorology*, 149 (3), 431–442. https://doi.org/10.1016/j.agrformet.2008.09.004
Howden, S.M., Soussana, J.-F., Tubiello, F.N., Chhetri, N., Dunlop, M. & Meinke, H. (2007). Adapting agriculture to climate change. *Proceedings of the National Academy of Sciences*, 104 (50), 19691–19696. https://doi.org/10.1073/pnas.0701890104
IPCC (2018). *Summary for Policymakers. In: Global warming of 1.5°C. AnIPCC Special Report on the impacts of global warming of 1.5°C above pre-industrial levels and related global greenhouse gas emission pathways, in the context of strengthening the global response to the threat of climate change, sustainable development, and efforts to eradicate poverty [V. Masson-Delmotte, P. Zhai, H. O. Pörtner, D. Roberts, J. Skea, P.R.Shukla,A. Pirani, W. Moufouma-Okia, C.Péan, R. Pidcock, S. Connors, J. B. R. Matthews, Y. Chen, X. Zhou, M. I. Gomis, E. Lonnoy, T. Maycock, M. Tignor, T. Waterfield(eds.)]*. In Press.
Iqbal, J., Read, J.J., Thomasson, A.J. & Jenkins, J.N. (2005). Relationships between Soil–Landscape and Dryland Cotton Lint Yield. *Soil Science Society of America Journal*, 69 (3), 872–882. https://doi.org/10.2136/sssaj2004.0178
Kaspar, T.C., Colvin, T.S., Jaynes, D.B., Karlen, D.L., James, D.E., Meek, D.W., Pulido, D. & Butler, H. (2003). Relationship Between Six Years of Corn Yields and Terrain Attributes. *Precision Agriculture*, 4 (1), 87–101. https://doi.org/10.1023/A:1021867123125
Knipling, E.B. (1970). Physical and physiological basis for the reflectance of visible and near-infrared radiation from vegetation. *Remote Sensing of Environment*, 1 (3), 155–159. https://doi.org/10.1016/S0034-4257(70)80021-9

Kriegler, F.J., Malila, W.A., Nalepka, R.F. & Richardson, W. (1969). Preprocessing Transformations and Their Effects on Multispectral Recognition. *Remote Sensing of Environment, VI*, 97

Kumhálová, J., Kumhála, F., Kroulík, M. & Matějková, Š. (2011). The impact of topography on soil properties and yield and the effects of weather conditions. *Precision Agriculture*, 12 (6), 813–830. https://doi.org/10.1007/s11119-011-9221-x

Kumhálová, J. & Moudrý, V. (2014). Topographical characteristics for precision agriculture in conditions of the Czech Republic. *Applied Geography*, 50, 90–98. https://doi.org/10.1016/j.apgeog.2014.02.012

Lantmäteriet (2021). KVALITETSBESKRIVNING: Laserdata. https://www.lantmateriet.se/globalassets/kartor-och-geografisk-information/hojddata/kvalitetsbeskrivning_laserdata.pdf

Li, F., Miao, Y., Feng, G., Yuan, F., Yue, S., Gao, X., Liu, Y., Liu, B., Ustin, S.L. & Chen, X. (2014). Improving estimation of summer maize nitrogen status with red edge-based spectral vegetation indices. *Field Crops Research*, 157, 111–123. https://doi.org/10.1016/j.fcr.2013.12.018

Lipper, L., Thornton, P., Campbell, B.M., Baedeker, T., Braimoh, A., Bwalya, M., Caron, P., Cattaneo, A., Garrity, D., Henry, K., Hottle, R., Jackson, L., Jarvis, A., Kossam, F., Mann, W., McCarthy, N., Meybeck, A., Neufeldt, H., Remington, T., Sen, P.T., Sessa, R., Shula, R., Tibu, A. & Torquebiau, E.F. (2014). Climate-smart agriculture for food security. *Nature Climate Change*, 4 (12), 1068–1072. https://doi.org/10.1038/nclimate2437

LRF (2020). *5 klimatsmarta saker Sveriges bönder gör – som ingen vet om - LRF*. *Lantbrukarnas Riksförbund*. https://www.lrf.se/mitt-lrf/nyheter/riks/2020/10/sveriges-bonders-miljoatgarder/ [2021-07-26]

Maestrini, B. & Basso, B. (2018). Drivers of within-field spatial and temporal variability of crop yield across the US Midwest. *Scientific Reports*, 8 (1), 14833. https://doi.org/10.1038/s41598-018-32779-3

Marques da Silva, J.R. & Silva, L.L. (2008). Evaluation of the relationship between maize yield spatial and temporal variability and different topographic attributes. *Biosystems Engineering*, 101 (2), 183–190. https://doi.org/10.1016/j.biosystemseng.2008.07.003

Mattivi, P., Franci, F., Lambertini, A. & Bitelli, G. (2019). TWI computation: a comparison of different open source GISs. *Open Geospatial Data, Software and Standards*, 4 (1), 6. https://doi.org/10.1186/s40965-019-0066-y

Meier, T. (2017). Planetary boundaries of agriculture and nutrition – an Anthropocene approach. http://www.nutrition-impacts.org/media/2017_TMeier_planetary_boundaries_agriculture_nutrition.pdf [2017-12-07]

Murphy, P.N.C., Ogilvie, J. & Arp, P. (2009). Topographic modelling of soil moisture conditions: a comparison and verification of two models. *European Journal of Soil Science*, 60 (1), 94–109. https://doi.org/10.1111/j.1365-2389.2008.01094.x

Pierce, F.J. & Nowak, P. (1999). Aspects of Precision Agriculture. In: Sparks, D.L. (ed.) *Advances in Agronomy*. Academic Press, 1–85. https://doi.org/10.1016/S0065-2113(08)60513-1

Piikki, K. & Söderström, M. (2019). Digital soil mapping of arable land in Sweden – Validation of performance at multiple scales. *Geoderma*, 352, 342–350. https://doi.org/10.1016/j.geoderma.2017.10.049

Pilesjö, P., Thylén, L. & Persson, A. (2005). Topographical data for delineation of agricultural management zones. 819–826

QGIS Development Team (2021). *QGIS Geographic Information System*. QGIS Association. http://www.qgis.org

Quinn, P.F., Beven, K.J. & Lamb, R. (1995). The in(a/tan/β) index: How to calculate it and how to use it within the topmodel framework. *Hydrological Processes*, 9 (2), 161–182. https://doi.org/10.1002/hyp.3360090204

Richards, R.A., Rebetzke, G.J., Condon, A.G. & Herwaarden, A.F. van (2002). Breeding Opportunities for Increasing the Efficiency of Water Use and Crop Yield in Temperate Cereals. *Crop Science*, 42 (1), 111–121. https://doi.org/10.2135/cropsci2002.1110

Rockström, J., Steffen, W., Noone, K., Persson, Å., Chapin, F.S.I., Lambin, E., Lenton, T., Scheffer, M., Folke, C., Schellnhuber, H.J., Nykvist, B., de Wit, C., Hughes, T., van der Leeuw, S., Rodhe, H., Sörlin, S., Snyder, P., Costanza, R., Svedin, U., Falkenmark, M., Karlberg, L., Corell, R., Fabry, V., Hansen, J., Walker, B., Liverman, D., Richardson, K., Crutzen, P. & Foley, J. (2009). Planetary Boundaries: Exploring the Safe Operating Space for Humanity. *Ecology and Society*, 14 (2). https://doi.org/10.5751/ES-03180-140232

Rouse, J.W., Jr., Haas, R.H., Schell, J.A. & Deering, D.W. (1974). Monitoring Vegetation Systems in the Great Plains with Erts. *NASA Special Publication*, 351, 309

Rufin, P., Frantz, D., Yan, L. & Hostert, P. (2021). Operational Coregistration of the Sentinel-2A/B Image Archive Using Multitemporal Landsat Spectral Averages. *IEEE Geoscience and Remote Sensing Letters*, 18 (4), 712–716. https://doi.org/10.1109/LGRS.2020.2982245

Santos Valle, S. & Kienzle, J. (2020). *Agriculture 4.0 – Agricultural robotics and automated equipment for sustainable crop production*. Rome, Italy: FAO. http://www.fao.org/publications/card/en/c/CB2186EN/ [2021-07-19]

SCB (2018). Production of cereals, dried pulses and oilseed crops in 2018 Preliminary statistics for counties and the whole country. https://www.scb.se/contentassets/660c1fe2e98a41a3aa7a2a9d047cf715/jo0601_2018a01_sm_jo19sm1801.pdf

SCB (2019). Production of cereals, dried pulses and oilseed crops in 2019 Preliminary statistics for counties and the whole country. https://www.scb.se/contentassets/da4d13a440bf48238dc7f8a4e33de7ba/jo0601_2019a01_sm_jo19sm1902.pdf

Schmidt, F. & Persson, A. (2003). Comparison of DEM data capture and topographic wetness indices. *Precision Agriculture*, 4 (2), 179–192. https://doi.org/10.1023/A:1024509322709

Segarra, J., Buchaillot, M.L., Araus, J.L. & Kefauver, S.C. (2020). Remote Sensing for Precision Agriculture: Sentinel-2 Improved Features and Applications. *Agronomy*, 10 (5), 641. https://doi.org/10.3390/agronomy10050641

Sims, D.A. & Gamon, J.A. (2002). Relationships between leaf pigment content and spectral reflectance across a wide range of species, leaf structures and developmental stages. *Remote Sensing of Environment*, 81 (2), 337–354. https://doi.org/10.1016/S0034-4257(02)00010-X

Sinclair, V.A., Mikkola, J.W., Rantanen, M. & Raisanen, J. (2019). The summer 2018 heatwave in Finland. *Weather*, 74 (11), 403–409. https://doi.org/10.1002/wea.3525

SMHI (2019). Climate extrems for Sweden. Authors: Danijel Belusic, Peter Berg, Denica Bozhinova, Lars Bärring, Ralf Döscher, Anna Eronn, Erik Kjellström, Katharina Klehmet, Helena Martins, Carin Nilsson , Jonas Olsson, Christiana Photiadou, David Segersson, Gustav Strandberg. https://doi.org/10.17200/Climate_Extremes_Sweden

SMHI (2020-09-16). *Ladda ner meteorologiska observationer | SMHI*. https://www.smhi.se/data/meteorologi/ladda-ner-meteorologiska-observationer/#param=precipitation24HourSum,stations=all,stationid=98210 [2020-09-16]

Söderström, M., Piikki, K. & Stadig, H. (2021). 109. Yield maps for everyone - scaling drone models for satellite-based decision support. *Precision agriculture ?21*. Wageningen Academic Publishers, 911–918. https://doi.org/10.3920/978-90-8686-916-9_109

Spear, M.E. (1952). *Charting statistics.* New York: McGraw-Hill.

Sugarbaker, L.J. & Carswell, Jr., W.J. (2016). *The 3D elevation program - Precision agriculture and other farm practices*. (Fact Sheet, 2016–3088). Reston, VA: U.S. Geological Survey. https://doi.org/10.3133/fs20163088

Swedish Board of Agriculture (2009). *Facts about Swedish agriculture*. https://www2.jordbruksverket.se/webdav/files/SJV/trycksaker/Pdf_ovrigt/ovr2gb.pdf [2021-07-14]

Swedish Board of Agriculture (2018-2020). *Startsida jordbruksverket.se*. [text]. https://jordbruksverket.se/ [2021-05-12]

Taesombat, W. & Sriwongsitanon, N. (2009). Areal rainfall estimation using spatial interpolationtechniques. *ScienceAsia*, 35 (3), 268. https://doi.org/10.2306/scienceasia1513-1874.2009.35.268

Tarrio, K., Tang, X., Masek, J.G., Claverie, M., Ju, J., Qiu, S., Zhu, Z. & Woodcock, C.E. (2020). Comparison of cloud detection algorithms for Sentinel-2 imagery. *Science of Remote Sensing*, 2, 100010. https://doi.org/10.1016/j.srs.2020.100010

Thilakarathna, M.S. & Raizada, M.N. (2018). Challenges in Using Precision Agriculture to Optimize Symbiotic Nitrogen Fixation in Legumes: Progress, Limitations, and Future Improvements Needed in Diagnostic Testing. *Agronomy*, 8 (5), 78. https://doi.org/10.3390/agronomy8050078

Thorup-Kristensen, K., Salmerón Cortasa, M. & Loges, R. (2009). Winter wheat roots grow twice as deep as spring wheat roots, is this important for N uptake and N leaching losses? *Plant and Soil*, 322 (1), 101–114. https://doi.org/10.1007/s11104-009-9898-z

Tilman, D. (1999). Global environmental impacts of agricultural expansion: The need for sustainable and efficient practices. *Proceedings of the National Academy of Sciences*, 96 (11), 5995–6000. https://doi.org/10.1073/pnas.96.11.5995

USGS (2021). *What is a digital elevation model (DEM)?* https://www.usgs.gov/faqs/what-a-digital-elevation-model-dem?qt-news_science_products=0#qt-news_science_products [2021-08-26]

Weiss, M., Jacob, F. & Duveiller, G. (2020). Remote sensing for agricultural applications: A meta-review. *Remote Sensing of Environment*, 236, 111402. https://doi.org/10.1016/j.rse.2019.111402

Wheeler, T. & Braun, J. von (2013). Climate Change Impacts on Global Food Security. *Science*, 341 (6145), 508–513. https://doi.org/10.1126/science.1239402

Wilcke, R.A.I., Kjellström, E., Lin, C., Matei, D., Moberg, A. & Tyrlis, E. (2020). The extremely warm summer of 2018 in Sweden – set in a historical context. *Earth System Dynamics*, 11 (4), 1107–1121. https://doi.org/10.5194/esd-11-1107-2020

WMO (2015). *New Two-Tier approach on "climate normals". World Meteorological Organization*. https://public.wmo.int/en/media/news/new-two-tier-approach-%E2%80%9Cclimate-normals%E2%80%9D [2021-06-15]

Wolters, S., Söderström, M., Piikki, K., Reese, H. & Stenberg, M. (2021). Upscaling proximal sensor N-uptake predictions in winter wheat (Triticum aestivum L.) with Sentinel-2 satellite data for use in a decision support system. *Precision Agriculture*,. https://doi.org/10.1007/s11119-020-09783-7

Zadoks, J.C., Chang, T.T. & Konzak, C.F. (1974). A decimal code for the growth stages of cereals. *Weed Research*, 14 (6), 415–421. https://doi.org/10.1111/j.1365-3180.1974.tb01084.x

Zhang, T., Su, J., Liu, C., Chen, W., Liu, H. & Liu, G. (2017). Band selection in sentinel-2 satellite for agriculture applications. *Proceedings of 2017 23rd International Conference on Automation and Computing (ICAC)*, September 2017. 1–6. https://doi.org/10.23919/IConAC.2017.8081990

Appendix

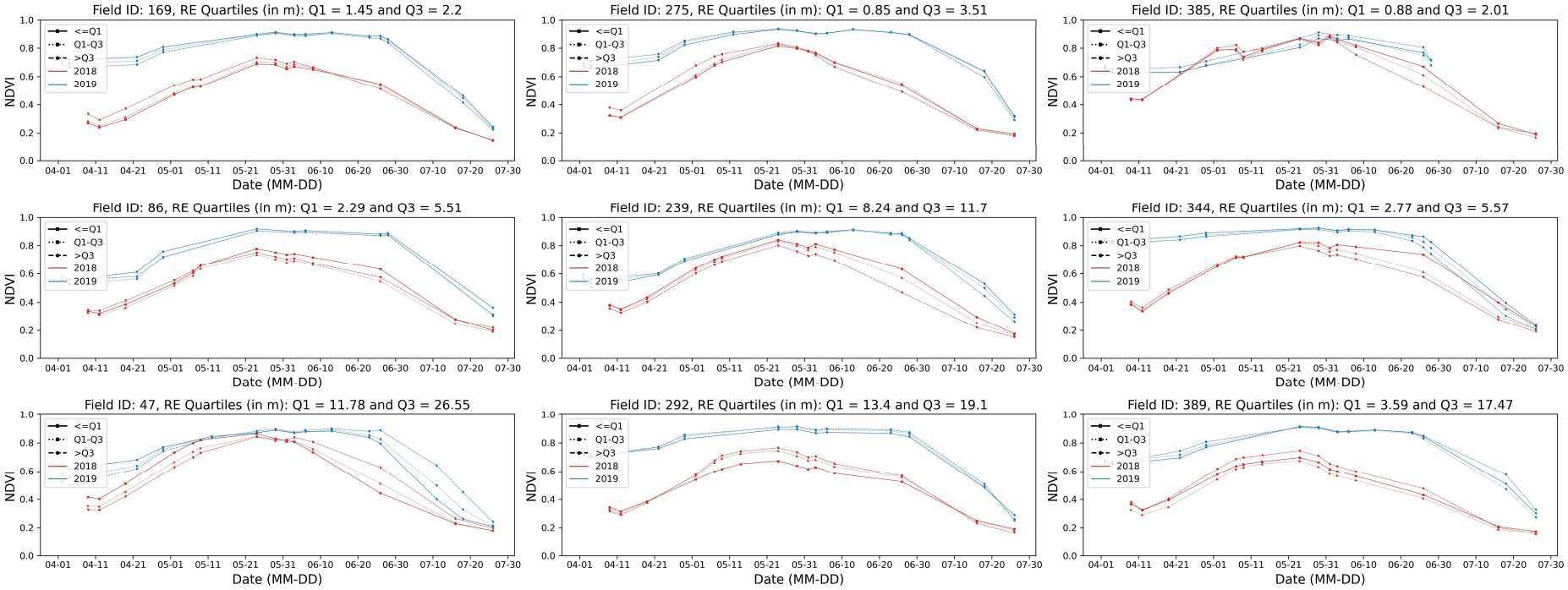

Fig. 43. Winter-wheat within field NDVI crop growth development variations for the nine fields, zoning method based on RE maps.

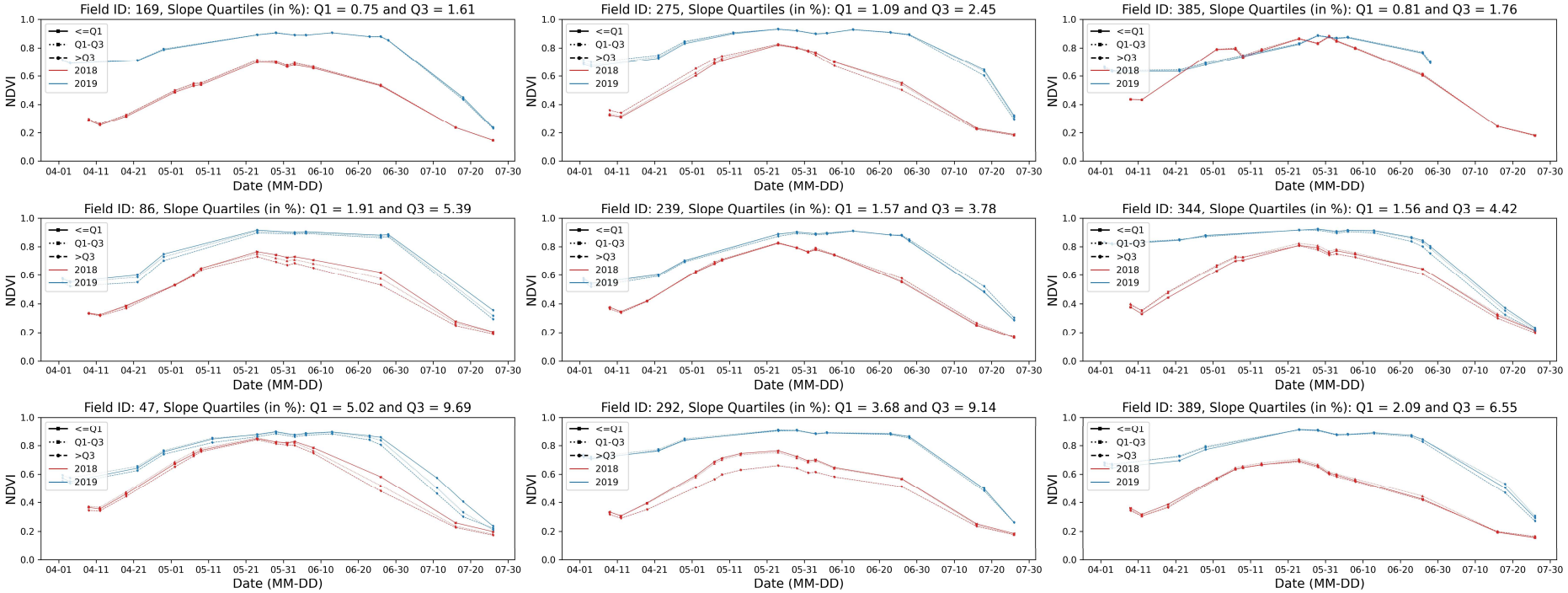

Fig. 44. Winter wheat within-field NDVI crop growth development variations for the nine fields, zoning method based on slope maps.

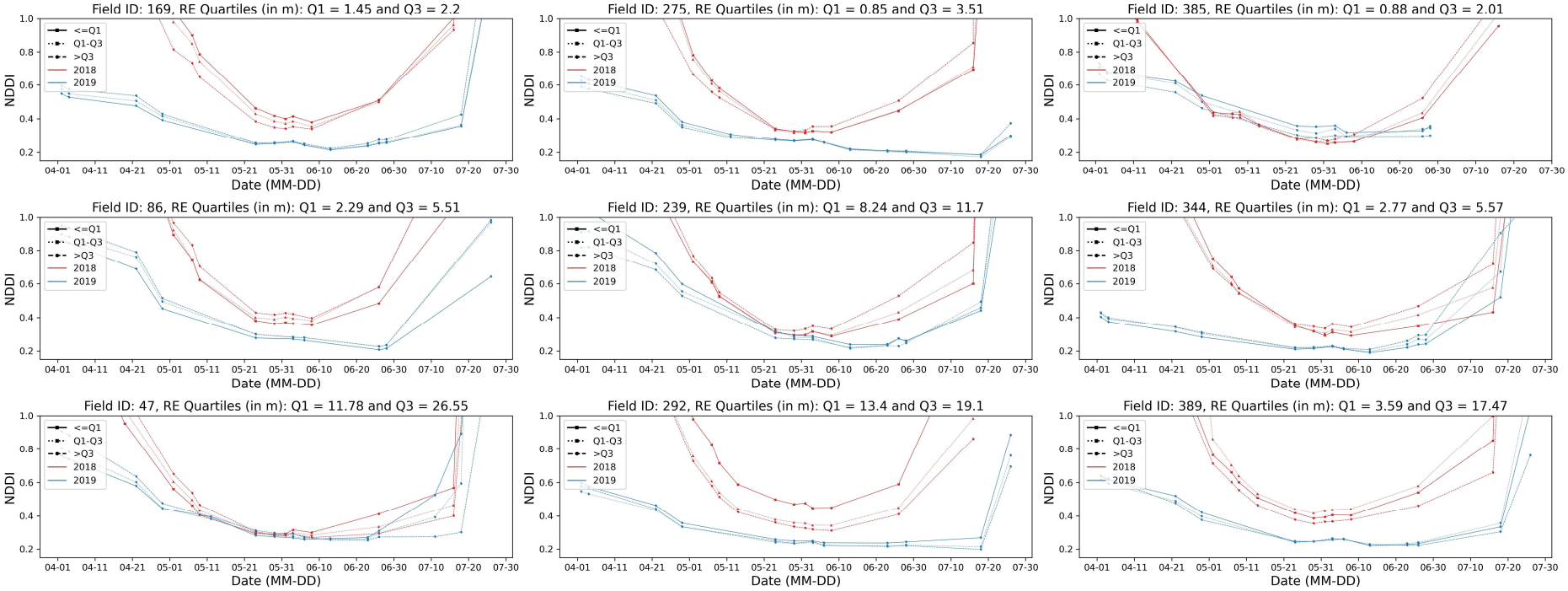

Fig. 45. Winter wheat within-field NDDI crop growth development variations for the nine fields, zoning method based on RE maps.

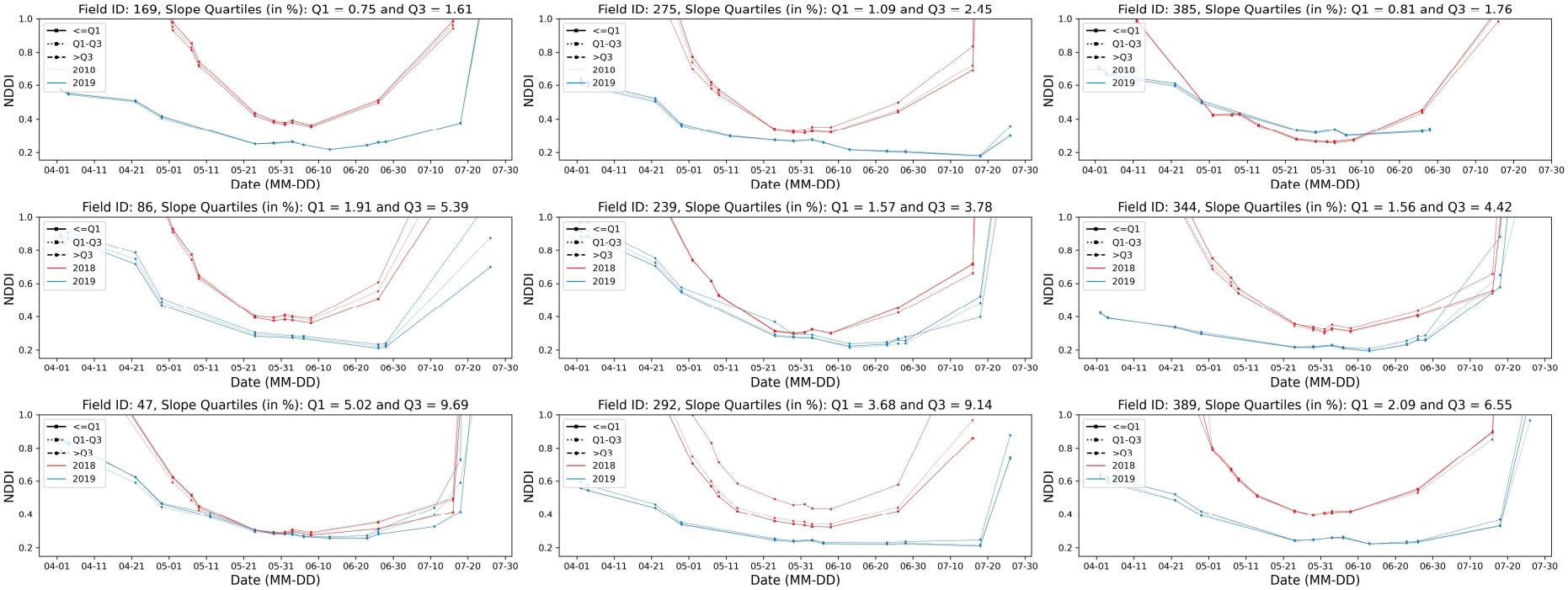

Fig. 46. Winter wheat within-field NDDI crop development growth variations for the nine fields, zoning method based on slope maps.

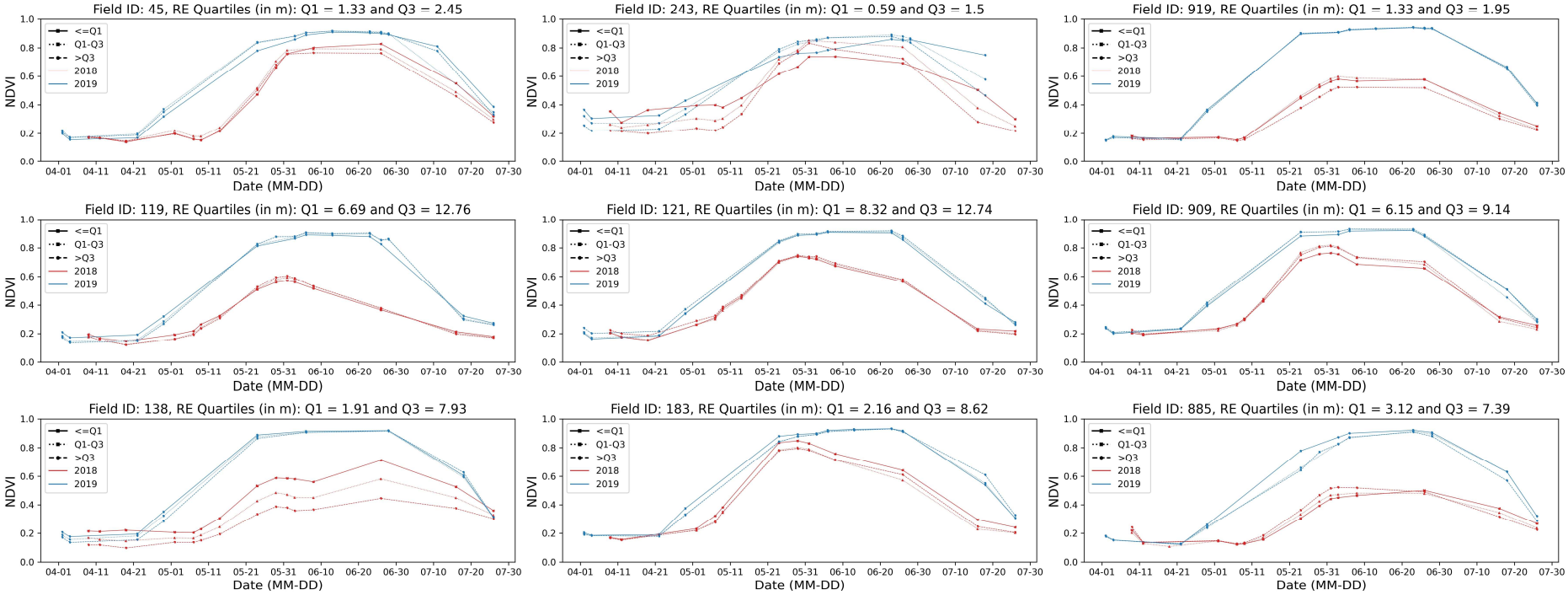

Fig. 47. Spring barely within-field NDVI crop growth development variations for the nine fields, zoning method based on RE maps.

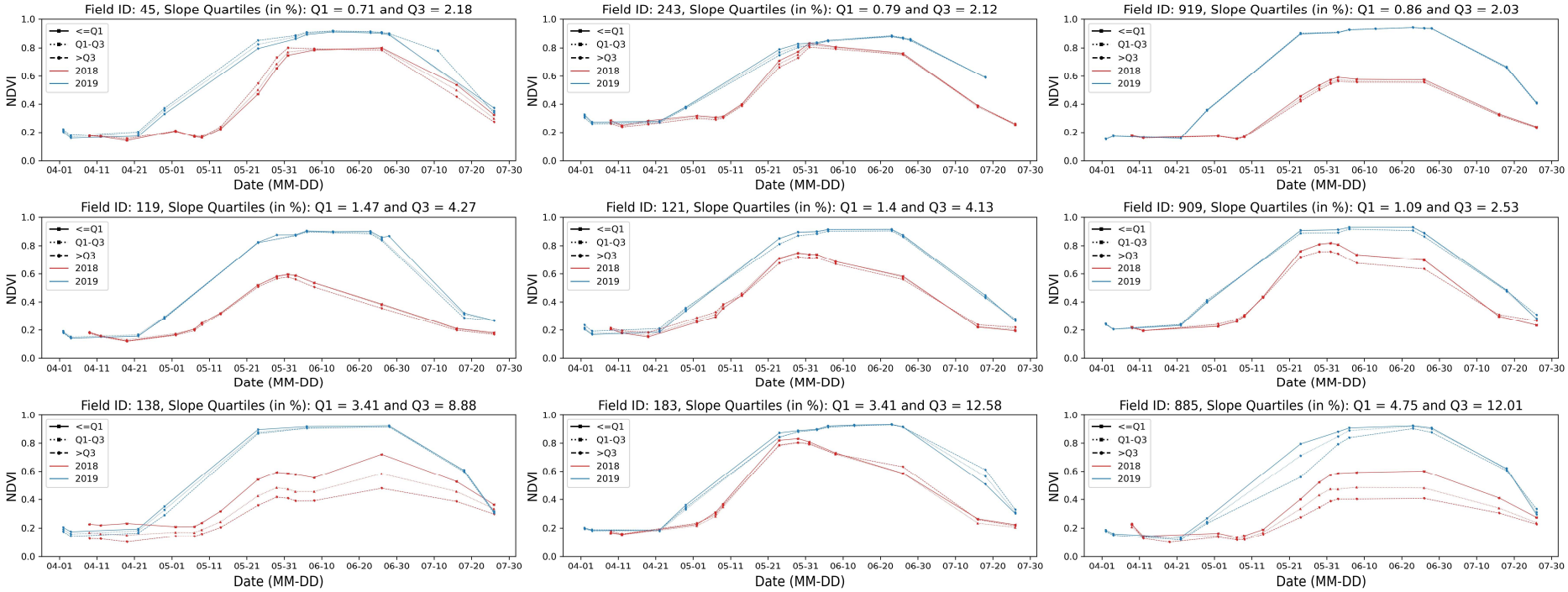

Fig. 48. Spring barley within-field NDVI crop growth development variations for the nine fields, zoning method based on Slope maps.

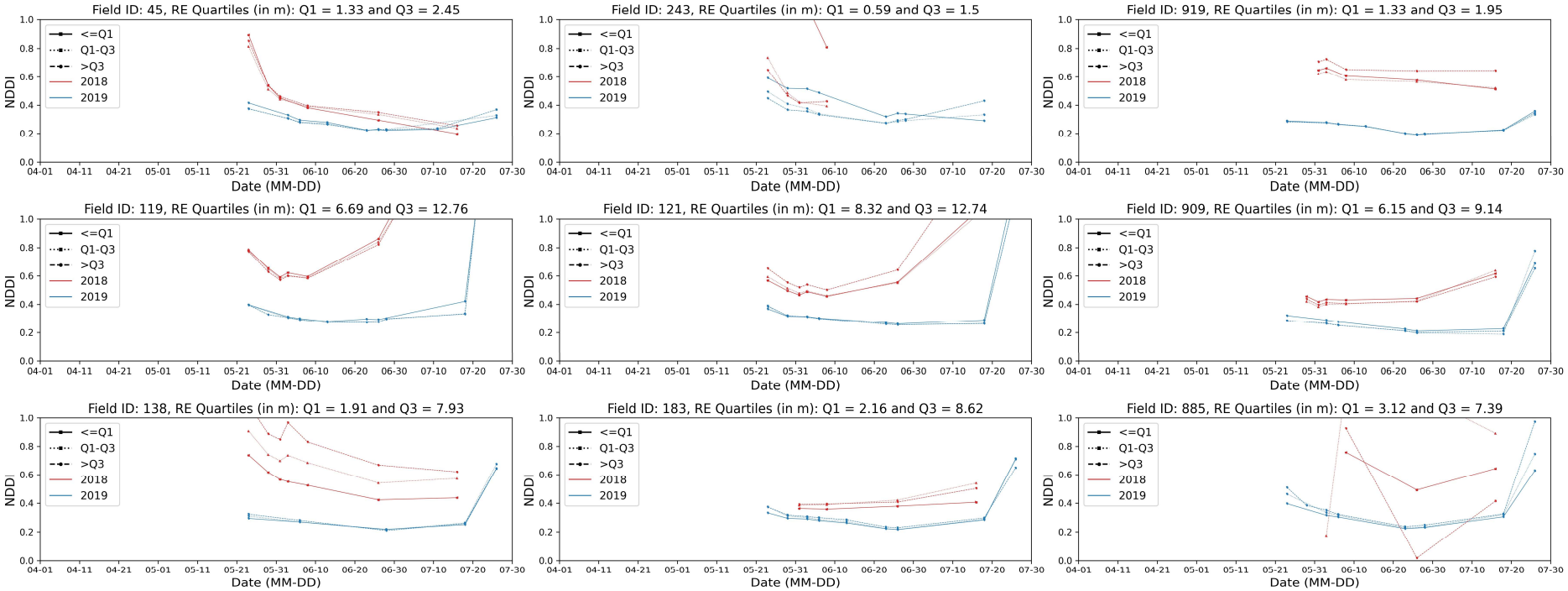

Fig. 49. Spring barley within-field NDDI crop growth development variations for the nine fields, zoning method based on RE maps.

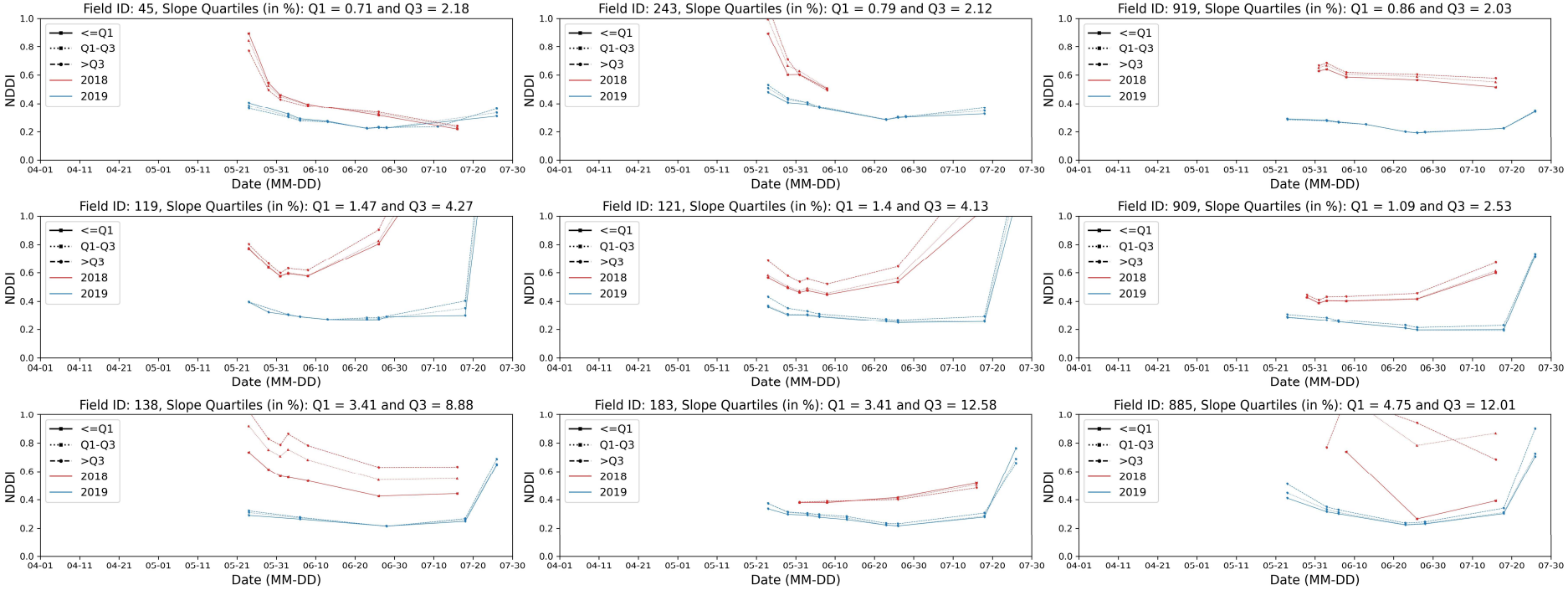

Fig. 50. Spring barley within-field NDDI crop growth development variations for the nine fields, zoning method based on slope maps.